THE ELECTRICAL PROPERTIES OF PURE MANGANESE AND MANGANESE/MAGNESIUM FLUORIDE CERMET THIN FILM RESISTORS

A Thesis Submitted by

LOUIS OLUMEKOR

for the Degree of Doctor of Philosophy

BRUNEL UNIVERSITY

1977

To My Parents

ACKNOWLEDGEMENT

I would like to express my thanks to the following: Dr. J. Beynon for acting as Supervisor; Professor C.A. Hogarth for valuable discussions and suggestions; Dr. A.W. Whitaker for advice on the structural analysis of the films; Mr R.H. Creamer for discussions on the electrical properties of the films and for permission to work in the Solid State Physics Laboratory; Mr D.J. Pacey for permission to use the High Vacuum Physics Laboratory; Dr. B.P. Betts for allowing the use of certain special equipments; Mr R. Banerjee for operating the electron microscope; and the Mid-West State Govt. for providing a grant for the research programme.

I also wish to thank all the work-shop and laboratory technicians who advised and helped with various aspects of the work, viz: Mr. S. Woodise, Mr L. Lightowler, Mr K. Schlacter, Mr M. Varga, Mr T. Davies, Mr M. Krasso, Mr S. Stephens, and Mr Chandrasekera; Mrs A. Olumekor for encouragement and loss of leisure hours and lastly to Mrs E. Ackah for typing the thesis.

ABSTRACT

Pure Mn and Mn/MgF_2 cermet films (50 to 1500A thick) containing between 10 and 100 Wt % Mn have been prepared by single-boat evaporation *in vacuo* $\leq 10^{-5}$ torr. All films studied are ohmic, and the resistivity lying between 100 $\mu\Omega$ - cm and 10 m Ω - cm. Within this range, the resistivity decreases non-linearly with increase in film thickness and increase in Mn content. The effect on the film resistivity of other deposition parameters, viz substrate temperature, residual gas pressure, annealing and aging are investigated. The structure of the films was investigated using X-ray diffraction and transmission electron microscopy. Films with negative TCR have low activation energies ($\sim$ 1 to 100 meV) in the temperature range 110 to 720K, and the electronic conduction mechanism in these films is probably electron tunnelling and/or percolation depending on film composition, thickness and annealing temperature.

CONTENTS

i ACKNOWLEDGEMENTS

ii ABSTRACT

CHAPTER 1

1 INTRODUCTION

1.1 Scope of Thesis

1.1.1 Film Fabrication and Resistivity Measurement

1.1.2 Results and Discussions

1.1.2.1 Review of Conduction Mechanisms in Thin Films

1.1.2.2 Resistivity Parameters

1.1.2.3 Experimental Results

1.1.2.4 Interpretation of Results/Discussions.

CHAPTER 2

2 CONDENSATION, NUCLEATION AND GROWTH OF THIN FILMS

2.1 Introduction

2.2 Condensation

2.3 Nucleation

2.3.1 Capillarity Model

2.3.2 Atomistic Model

2.4 Growth

CHAPTER 3

3 REVIEW OF ELECTRONIC CONDUCTION MECHANISMS IN THIN FILMS

3.1 Introduction

3.2 Conduction in Thin Continuous Metallic Films

3.2.1 Thomson Theory

3.2.2 Fuchs Theory
3.3 Conduction in Discontinuous Metallic Films
3.3.1 Neugebauer and Webb Theory
3.3.2 Hartman Theory
3.3.3 Substrate Effect on Electronic Conduction in Discontinuous Metallic Films
3.3.3.1 Hill Theory (A)
3.3.3.2 Herman and Rhodin Theory
3.3.3.3 Thermionic Emission
3.3.3.3.1 van Steensel Theory
3.3.3.3.2 Hill Theory (B)
3.4 Conduction in Cermet Films
3.4.1 Coutts Theory
3.4.2 Christen and Hewitt Theory
3.4.3 Abeles et al Theory
3.4.4 Gasperick and Navinsek Theory

CHAPTER 4

4 EXPERIMENTAL APPARATUS

4.1 Deposition Equipment
4.1.1 The Coating Plant
4.1.1.1 Resistive Heating
4.1.1.1.1 Boat Filaments
4.1.1.1.2 Wire Filaments
4.1.1.2 Film Thickness Monitor
4.2 Equipment Associated with The Measurement of Electrical Resistivity
4.2.1 Auxiliar Vacuum Plant
4.2.2 d.c. Potentiometer

CHAPTER 5

5 EXPERIMENTAL TECHNIQUE

5.1 Pre-deposition Preparation

5.1.1 Cermet Material
5.1.2 Substrates and Substrate Cleaning
5.1.3 Calibration of the Monitor Crystal
5.1.4 Conversion Factors
5.2 Film Deposition and Resistivity Measurement
5.2.1 Temperature Coefficient of Resistance
5.2.2 Initial Investigation
5.2.3 Subsequent Investigation
5.2.3.1 Substrate Temperature
5.2.3.2 Deposition Rate
5.2.3.3 Deposition Pressure
5.2.3.4 Annealing
5.2.4 Structural Analysis
5.2.4.1 X-Ray Diffraction
5.2.4.2 Electron Microscopy

CHAPTER 6

6 RESULTS AND DISCUSSIONS

6.1 Introduction
6.2 Variation of Resistivity with Composition
6.3 Variation of Resistivity with Thickness
6.4 Variation of Resistivity with Substrate Temperature
6.5 Variation of Resistivity with Deposition Rate
6.6 Variation of Resistivity with Residual Gas Pressure
6.7 Heat-Treatment of Pure Mn and Mn/MgF_2 Cermet Films
6.7.1 Annealing
6.7.1.1 Vand's Theory of the Effect of Annealing on Resistivity
6.7.1.1.1 Estimation of the Lattice Distortion Energy in Pure Mn Films
6.7.2 Post-Annealing Heat-Treatment

6.7.2.1 Activation Energy of Unannealed Mn/MgF_2 Cermets
6.7.2.2 Activation Energy of Films Annealed at 620, 690 and 720K
6.7.2.3 Electronic Conduction Mechanism in Annealed Mn/MgF_2 Cermets
6.7.2.4 Temperature Coefficient of Resistivity
6.8 Reliability of Mn/MgF_2 Cermets
6.8.1 Performance
6.8.2 Stability

CHAPTER 7

7 CONCLUSION

7.1 Proposals for Further Work.

CHAPTER ONE

1. INTRODUCTION

This thesis contains the result of a systematic investigation into the electrical resistive properties of manganese (Mn) and manganese/magnesium fluoride (Mn/MgF_2) cermet thin films, evaporated onto Corning 7059 Borosilicate glass substrates *in vacuo*.

Thin metallic films prepared *in vacuo* have been used for the construction of resistors for over half a century [68]. Initially their development was slow due to:

(i) poor reproducibility, because the films were fabricated in rough vacuum conditions. Hence, the resistors often suffer from a high and varying degree of contamination;

(ii) lack of a developed theory to explain the observed high resistivity of the films;

(iii) little industrial demand for high value resistors. The lower values required ($\sim k\Omega$) being adequately provided by wire wound resistors, composition resistors, carbon resistors etc.

However, the industrial demand for high value resistors ($\sim M\Omega$) increased considerably after the advent of radio broadcasting (e.g. the high input impedance of the triode valve.) The development of the electron microscope, of the high and ultra-high vacuum pumps, coupled with higher industrial demand for miniaturized electronic components, accelerated the development of thin film resistors after the second world war.

The main requirements for miniaturized resistor components are:

(i) High resistivity;

(ii) Small size;

(iii) Low temperature coefficient of resistance;

(iv) High thermal, mechanical, and aging stability;

(v) Small 'high frequency' losses;

(vi) Compatible support for the resistor and its connecting leads; and

(vii) Low cost.

Thin films prepared by vacuum evaporation excel all other types of resistors in that they can fulfil almost all these requirements. Marsten [71] has made a detailed survey of the evolutionary steps leading to the present state of resistors.

The resistivity of a thin metallic film is always higher than that of its bulk counterpart. The higher resistivity is due mainly to an increase in the number of structural defects, such as impurity atoms, vacancies and interstitials, dislocations and grain boundaries. The use of structural defects to increase the film resistivity is not feasible in vacuum-evaporated films because the nature of the defects is unpredictable and the number is difficult to control.

A reduction in film thickness will also increase the resistivity of a metallic film in a more controlled way. When pure metallic films are less than 100A, they are usually discontinuous. Discontinuous films have a higher resistivity than continuous films but they are also less stable. High resistivity and good stability can be achieved by introducing an insulator phase into the film to form a cermet system.

1.1. SCOPE OF THESIS

The investigation into the resistive properties of Mn and Mn/MgF_2 cermet thin films may be divided into two sections for convenience:

(i) Film fabrication and resistivity measurement; and

(ii) Results and discussions.

1.1.1. FILM FABRICATION AND RESISTIVITY MEASUREMENT

Film fabrication in this context includes pre-deposition preparation, such as substrate cleaning and cermet mixing, instrumentation and instrument calibration, experimental techniques and a review of the events occurring during film deposition.

The results on instrument calibration are presented under "Experimental Techniques" (Chapter 5) as they bear no direct relation to the main result section which deals mainly with Resistivity.

Events occurring during film deposition consist of three distinct stages:

(i) Transforming the solid evaporant (Mn or Mn/MgF_2) into a vapour phase;

(ii) The movement of the vapour from source to substrate *in vacuo*; and

(iii) The formation of a thin film by vapour condensation on the substrate.

Stage (i), solid-vapour phase transformation is purely a thermodynamic process. Such transformations have not been discussed as they are well treated in any standard thermodynamic text book. Similarly, stage (ii) has not been discussed as it is a gas flow

problem which has been covered adequately by a number of authors [69, 70, 84]. However, stage (iii) was considered relevant to this investigation since the resistive properties of a thin film (for a given thickness, substrate and cermet system) is controlled mainly by the events occurring at the substrate during deposition, provided the deposition pressure is sufficiently low (high to ultra-high vacuum range) and the vacuum system is clean. Hence a review of the process involved (condensation, nucleation and growth) is given in Chapter 2.

1.1.2 RESULTS AND DISCUSSIONS

Results and discussions in this context mean:

(i) review of electronic conduction mechanisms in thin films;

(ii) definition of commonly measured thin film resistivity parameters;

(iii) experimental results; and

(iv) interpretation of results/discussions.

1.1.2.1 REVIEW OF CONDUCTION MECHANISMS IN THIN FILMS

The origin of resistivity in thin films is discussed in Chapter 3 in the form of a review of the electronic conduction mechanisms of thin films under the influence of a low dc electric field (≤ 500 V cm^{-1}). The review is also limited to the conduction processes in planar metallic and cermet thin film resistors in the temperature range 50 to 1000K.

1.1.2.2. RESISTIVITY PARAMETERS

The various parameters used to express thin film resistivity are defined in Section 5.2.1. An attempt has been made to keep to a

unified system of units throughout this thesis. For this reason, the reader may find that some units in the thesis are different from those in the original reference manuscripts. For example, all weights % and atomic % have been converted into volume %; temperature and activation energy are expressed in K and eV respectively.

1.1.2.3 EXPERIMENTAL RESULTS

The experiments were limited to resistivity measurements obtained with a low electric field ($< 85 \, Vcm^{-1}$) except in one experiment in which an ac field of less than $2.5 \, Vcm^{-1}$ was applied, in order to investigate the frequency response of the resistors. 100V dc was the highest break-down voltage observed in the test films. All resistivity measurements were made in the direction of the applied field along the length of the resistor and in the absence of a magnetic field. The factors affecting the resistivity of the films such as percentage composition of the metal, film thickness, annealing, substrate temperature, deposition rate, deposition pressure, and the aging stability were investigated.

1.1.2.4 INTERPRETATION OF RESULTS/DISCUSSIONS

Manganese has certain peculiar properties [25, 72, 73]. It exists in four physical forms having a large variation in bulk resistivity and structural properties. The results from electron microscopic investigations enabled comparisons to be made between film structure and its resistivity.

As there were no available data for the Mn/MgF_2 cermets, experimental results were compared extensively with results of other cermet systems. For this reason emphasis was laid on the form (shape of graphs) and the relative order of magnitude of Mn and Mn/MgF_2 cermets. Whenever possible experimental results were also fitted to known theories.

CHAPTER TWO

2 CONDENSATION, NUCLEATION AND GROWTH OF THIN FILMS

2.1. INTRODUCTION

Due to differences in structure, the electrical properties of a thin film may be quite different from its bulk counterpart. The structure of a thin film is dictated by a combination of factors present during the process of film formation. In the case of films prepared by thermal evaporation in vacuo, the most important of these factors are:

(i) substrate temperature;

(ii) deposition rate;

(iii) pressure and nature of the residual gases;

(iv) surface mobility of adsorbed atoms on the substrate;

(v) type of substrate (amorphous, monocrystalline or polycrystalline);

(vi) chemical reaction between substrate and film;

(vii) chemical reaction at the vapour source; and

(viii) presence of an electric or a magnetic field at the substrate.

In the fabrication of Mn/MgF_2 cermet films factors (vi) to (viii) are not applicable as the substrates used were inert, no chemical reaction was observed at the source* and no electric or magnetic field was applied to the substrate during film deposition. The other factors are most important at the initial stages of film growth (Nucleation) which is a problem of vapour-solid phase transformation (condensation). Although the effect of factors (i) to (v) on the

* information taken from X-ray powder diffraction

resistivity of completed Mn and Mn/MgF_2 cermets, 100 to 2500 Å thick was studied (Chapter 6), the condensation and nucleation processes in these films were not investigated but an understanding of the processes and theory involved is necessary for the proper interpretation of the structural information.

2.2. CONDENSATION

Thin film condensation from the vapour phase is governed by the interaction of the impinging atoms on the substrate. An arriving atom usually has velocity components parallel and perpendicular to the surface. If the substrate is inert, the atom may either be adsorbed or reflected back into the gas phase. The adsorbed atom may execute a random motion over the surface of the substrate, due to thermal activation energy from the substrate and/or due to its kinetic energy component parallel to the substrate surface. After a relaxation time, the absorbed atom can re-evaporate (desorption) or becomes chemisorbed (condensation). Therefore condensation is a net result of an equilibrium between the adsorption and desorption processes. The degree of thermal equilibrium is described by the accomodation coefficient γ_T which is defined as:

$$\gamma_T = \frac{E_v - E_r}{E_v - E} = \frac{T_v - T_r}{T_v - T} \qquad (2-1)$$

where E_v is the incident kinetic energy of a vapour atom, E_r the energy of an adsorbed atom before equilibrium with the substrate and E the energy of a desorbed atom after it has equilibrated with the substrate. T_v, T_r and T are the corresponding temperatures. The probability that an impinging atom be condensed on the substrate

is called the sticking coefficient and it is the ratio of the amount of material condensed to the total amount impinging.

Many investigators [1, 2, 3] have indicated that in the case of "hot" atoms impinging on a one dimensional lattice γ_T is less than unity only if the incident kinetic energy is larger than 25 times the energy required for desorption after equilibration with the substrate. The probability of complete accomodation occurring $\gamma_T = 1$ increases as the ratio of the mass of an impinging atom to the mass of a substrate atom increases. In the case of a 3-dimensional lattice, Goodman [4] has estimated that γ_T becomes unity if E_v is smaller than the energy necessary for desorption after equilibration with the substrate. Thus if the activation energy for desorption is 0.5eV for example, the incident atom would have to arrive at the substrate with an energy of 0.775 eV corresponding to a temperature excess of 6000K before thermal accomodation would become incomplete. Therefore it appears that except in the case of either very light atoms or very high kinetic energies, the incident vapour atoms equilibrate thermally with the substrate very rapidly.

The mean relaxation time required for an incident atom to equilibrate thermally with the substrate has been estimated by Lennard-Jones [5] to be less than $\frac{2}{\nu}$, where ν is the vibrational frequency of the lattice. According to McCarrol and Ehrlich [6] the adsorbed atoms will lose all but a few percent of E_v within three lattice oscillations.

2.3. NUCLEATION

It is generally agreed that for a thin film to condense into a permanent deposit, a small number of adsorbed atoms must form clusters (nuclei) at nucleation sites on the substrate. These clusters grow by depleting the surrounding regions (capture zones) of adsorbed atoms so that further nucleation is not possible in the capture zone. Two models are frequently used to explain nucleation in thin films, viz (i) the capillarity model and (ii) the atomistic model.

2.3.1 CAPILLARITY MODEL

The capillarity model [7, 8] is based on the classical capillarity theory for homogeneous nucleation of single droplets of liquid from the vapour phase, as postulated by Volmer and Webb [9], and Becker and Doring [10]. The model assumes that clusters are formed from a supersaturated vapour by the sequential addition of single atoms from the vapour phase. A condensed phase will be formed if a stable nucleus is first formed and this will require a positive free energy. The model also assumes that bulk thermodynamic quantities are applicable to the properties of clusters. The treatment below essentially follows that of Neugebauer [102]

The Gibbs free energy ΔG for forming a spherical cluster of radius r is given by the sum of the surface energy and the volume energy of condensation , i.e.

$$\Delta G = 4\pi r^2 \delta + \frac{4}{3}\pi r^3 \Delta G_v \quad \text{——} \quad (2 - 2)$$

where $\Delta G_v = \frac{-kT}{V} \ln P/P_e$

is the Gibbs free energy difference per unit volume. V is the molecular volume condensed from the supersaturated vapour at a pressure P and P_e

is the equilibrium pressure. P/P_e is defined as supersaturation and δ is the interfacial energy.
Differentiating equation (2 - 2) with respect to r gives the radius $r_\times$ of the critical nucleus as:

$$r_\times = -2\delta / \Delta G_v \quad \text{———} \quad (2-3)$$

$r_\times$ is the minimum size of a cluster required for the formation of a stable nucleus and the nucleation rate I_r (at a pressure P) under homogeneous nucleation is given by:

$$I_r = \frac{4\pi r^2 \gamma P}{(2\pi mkT)^{\frac{1}{2}}} \cdot n_* \quad \text{———} \quad (2-4)$$

where γ is the condensation coefficient and n_* is the equilibrium concentration of nuclei.

The capillarity model was extended by Hirth and Pound [11] to include the effect of desorption and of surface diffusion of adsorbed atoms. They assumed that the surface of a substrate possesses a density n_o of adsorption sites for which the free energy for desorption is Q_{des} and that surface diffusion is a "jump" process between adsorption sites, characterised by a free energy of diffusion Q_{diff}. In this case the nucleation rate is given by:

$$I_r = \frac{2\pi a P Z r_\times n_o \sin\theta}{(2\pi mkT)^{\frac{1}{2}}} \exp\left(\frac{Q_{des} - Q_{diff} - \Delta G_m'}{-\ kT}\right) \quad \text{———} \quad (2-5)$$

and

$$\Delta G_m' = \Delta G_m \; \phi(\theta) \quad \text{———} \quad (2-6)$$

where $\phi(\theta)$ is a geometric factor involving the angle of contact

θ of the deposit on the surface, Z is a correction factor allowing for the departure from equilibrium which occurs among the clusters and ΔG_m is the maximum free energy and a is the "jump" distance.

In the capillarity model r_x in equation (2 - 3) is usually of atomic dimensions. For example if we use the bulk value of for silver [12] and deposition rate of 1 A s^{-1} at 300K, r_x is equal to 2.2 A . However the application of the model is restricted to situations in which the number of atoms in the critical nucleus is large enough for macroscopic parameters, such as interfacial energies and angle of contact, to be realistic.

Hirth and Pound[11] have suggested that the capillarity model is valid only for nuclei containing more than about 100 atoms. Experimental investigations by many workers, among them Walton[13a,13b], Hirth and Pound [11], and Rhodin and Walton [14] have shown that the critical nucleus for metals is often less than 10 atoms. This is far below the critical number of atoms $\sim$100 mentioned above.

2.3.2 ATOMISTIC MODEL

Walton [13a, 13b], and Rhodin and Walton [14] have suggested that the difficulties encountered in applying the capillarity model to a cluster containing a small number of atoms may be overcome by using the atomistic model. Here they treated small clusters of atoms as individual molecules and expressed the concentration n_{i_*} of clusters of i_* atoms in terms of the concentration n_o of adsorption sites and the potential energy E_i of decomposition of such clusters into i

adsorbed atoms at absolute temperature T, n_{i_x} is given by:

$$\frac{n_{i_x}}{n_o} = \left(\frac{n_i}{n_o}\right)^{i_x} \exp\left(\frac{-E_i}{kT}\right) \qquad (2 - 7)$$

where n_i is the surface density of adsorbed atoms and the nucleation rate is given by:

$$I_r = D_r n_o a^2 \left(\frac{D_r}{\nu n_o}\right)^{i_x} \exp\left[\frac{(i_x + 1)\, Q_{des} - Q_{diff} + E_i}{kT}\right] \qquad (2 - 8)$$

where D_r is the deposition rate, a the separation between adsorption sites and ν the frequency of desorption.

Thus for a very high degree of supersaturation, the critical cluster may be one atom only ($i_x = 1$) which means that a two-atom cluster is the smallest stable aggregate. At a lower supersaturation $i_x = 2$, a three-atom cluster is now the smallest stable aggregate, etc.

The atomistic model predicts:

(i) a linear relation between ln I_r and $^1/T$ (see equation (2-8));

(ii) that the nucleation rate is proportional to the deposition rate for a constant substrate temperature;

(iii) the nucleation rate is very sensitive to changes in supersaturation (i.e. substrate temperature); and

(iv) if the size of the critical nucleus changes by even one atom as the degree of supersaturation alters, a discontinuity will be found in the nucleation rate Vs supersaturation curve. Lewis and Campbell [15] have shown that such a discontinuity exists in gold films deposited on rock salt.

The disadvantage of the atomistic model is that it contains parameters which are difficult to estimate.

2.4 GROWTH

The nucleation theories in Section 2.3 indicate that there is a nucleation barrier which adsorbed atoms have to overcome before they can form a permanent deposit. If there is a nucleation barrier, then the film will show an island structure in the initial stages of growth (which is indeed the usual case). For a very large nucleation barrier, i.e. large critical nucleus as in the capillarity model (large $r_{\times}$), with a high positive energy of formation E_i, the film should consist of a small number of relatively large aggregates after a film of a few monolayers thick has been deposited. The aggregates are large because their minimum stable size is large and there are relatively few of them because the nucleation frequency is relatively small. In the case of a small nucleation barrier (atomistic model) the film should be composed of a relatively large number of small aggregates as the minimum stable size is small and the nucleation frequency is relatively large.

A film consisting of a large number of small islands will become continuous at a relatively low average thickness. This is because neighbouring islands grow and touch to form a continuous film matrix early in the deposition process. On the other hand a film of only a few big islands will attain continuity at a relatively higher film thickness on account of the large inter-island separations.

Pashley et al [16] have distinguished four stages of thin film growth processes, viz:

(i) Nucleation and island-structure;

(ii) Coalescence of islands;

(iii) Channel formation and

(iv) The formation of the continuous film.

These stages of film growth are shown schematically in Figure 2.1.

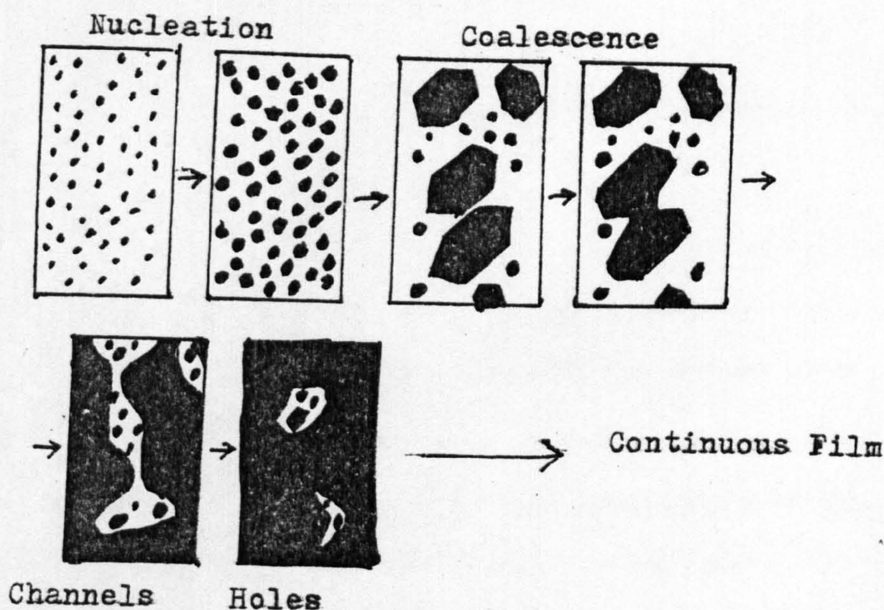

Fig. 2.1. The stages of thin film growth (Pashley [16])

When thin film deposition starts, the first evidence of condensation on the substrate is a sudden appearance of nuclei of fairly uniform size (Fig. 2.1). The growth of the nuclei is three-dimensional but the growth parallel to the substrate is greater than that normal to it because growth occurs largely by surface diffusion of adsorbed atoms on the substrate, rather than

by direct impingment from the vapour phase.

Coalescence is assumed to occur only when islands physically touch each other, the mechanism being analogous to that of sintering of two spheres [17, 18] as shown in

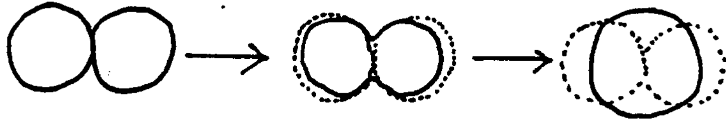

Fig. 2.2. Shape changes during Coalescence (Pashley [16])

Figure 2.2. Kingery and Berg [17] have suggested that, during sintering, transport of material may occur by evaporation and condensation, volume diffusion and surface diffusion.

Coalescence leads to the formation of larger islands separated by regions with a much lower density of small islands than were present at the earlier stage. The smaller islands are incorporated very quickly into the larger islands which, as a result become elongated to form a continuous network structure; the islands are separated by long irregular and narrow channels (Fig. 2.1).

With further deposition, secondary nucleation occurs in the channels and the nuclei coalesce with the elongated islands as soon as they touch . Eventually, as most of the channels continue to be filled, the film becomes largely continuous but contain many small irregular holes (non-filled areas) as shown in Figure 2.1. Further secondary nucleation occurs within these holes, as we saw above, until the holes are completely filled.

Pashley et al [16] have also observed that some recrystallization occurs during coalescence even with the substrate held at room temperature. Recrystallization causes large grain sizes in the completed film compared with the average separation of the initial nuclei. In polycrystalline films, recrystallization is randomly distributed and orientated.

In the condensation, nucleation and growth theories of thin films given above, it is assumed that a vapour-solid transformation occurred only during film formation. Semenoff, [19] Palatnik [20] and Palatnik et al [21] have questioned the validity of this assumption. They observed the presence of spherical islands in metallic films of Bi, Sn, Pb, Au, Cu and Al deposited on amorphous substrates at a temperature $T_s > T_m$ (T_m is the bulk melting point of the evaporant)

Palatnik [20, 21] postulated that film condensation occurs via a vapour-liquid-solid transformation. For $T_s < \frac{2}{3} T_m$, the transformation occurs directly from vapour to solid. However, in some cases (such as S_b) the mechanism reverts to vapour-liquid-amorphous solid for $T_s < \frac{1}{3} T_m$. Support for the vapour-liquid-solid transformation is provided by the "frozen in" high-temperature metastable phases of some solids. This is expected on the basis of Ostwald's rule [22] which states that a system undergoing a reaction proceeds from a less stable state through a series of increasingly more stable intermediate states to reach a final equilibrium state. If we assume that the liquid (or liquid-like) phase is formed as a first step during condensation (Semenoff [19]) and is stabilized by quenching, then Ostwald's rule suggests that on annealing, we would observe various

metastable high-temperature phases of the material. The metastable amorphous phases observed in Buckel's vapour-quenched films of Bi, Ga and Sb were accounted for in this way.

CHAPTER THREE

3. REVIEW OF ELECTRONIC CONDUCTION MECHANISMS IN THIN FILMS

3.1. INTRODUCTION

Metals are good conductors of electricity and according to the modern theories of metals [24, 28] (quantum mechanics), conduction is due to electron motion through the metal lattice. From a quantum mechanical view point, an electron will move through a perfect lattice whose potential is perfectly periodic without loss of energy, resulting in zero resistivity [24]. However in practice, the electron loses some energy resulting in a finite (bulk) resistivity. These losses can occur through:

(i) thermal vibration of lattice ions. This is responsible for a major contribution to bulk resistivity. This component of resistivity is usually referred to as thermal, ideal, intrinsic, lattice or phonon resistivity; it is temperature dependent;

(ii) physical and chemical imperfections caused by localised lattice damage or the presence of foreign atoms. These contribute a temperature independent component to the resistivity, and

(iii) size effect and localised spin. These make a negligible contribution to the bulk resistivity, and are temperature independent except near liquid helium temperatures.

The total contribution to the bulk resistivity ρ_o of the various components are contained in Mathiessen's rule, which states that ρ_o is the sum of two resistivity terms, one due to lattice scattering ρ_s which is temperature dependent and the other due

to impurities ρ_i which is temperature independent i.e.:

$$\rho_o = \rho_s + \rho_i \qquad \text{—— (3 - 1)}$$

The variation of ρ_s with temperature depends on the type of metal and its relation to the Debye temperature θ_D, where θ_D is given by:

$$k\theta_D = h\nu_{max} \qquad \text{—— (3 - 2)}$$

ν_{max} is the characteristic maximum vibrational frequency of an atom, h is Plank's constant and k is Boltzmann's constant. At a given temperature T, $\rho_s \propto T$ for $T > \theta_D$ and $\rho_s \propto T^5$ for $T << \theta_D$. Bulk metals have resistivities at 295K lying in the range [25] 1.5 to 150$\mu\Omega$ -cm.

The resistivity of a vacuum-deposited non-contaminated thin metallic film is generally considerably higher than that of its bulk counterpart if the film thickness is of the same order as the electron mean free path (m.f.p.). This is because electron collisions with the film surfaces and the grain boundaries are no longer negligible. The thickness at which surface scattering becomes important varies from metal to metal and it is strongly temperature dependent. Maissel [26] has shown that the electron m.f.p. for bulk gold is ~1530 A at 73K, 406 A at 273K and 290 A at 373K whilst the corresponding value for silver are 2425 ,575 and 405 A at the same temperatures. Metallic films with thicknesses of the same order as these m.f.p. are usually continuous in structure.

Deposition parameters also contribute to the resistivity of thin films condensed from the vapour phase. Matthiessen's

rule for thin films is given by:

$$\rho = \rho_o + \rho_a + \rho_b \quad \text{———} \quad (3-3)$$

where ρ_a and ρ_b are resistivity components due, respectively, to size effects and deposition parameters. When the films are prepared in a clean vacuum system at a low residual pressure ($\ll 10^{-4}$ torr) and at deposition temperatures above 273K, ρ_a becomes the dominant part of ρ. Thus as the thickness falls, ρ increases. However when the thickness becomes extremely small and the film structure is discontinuous, the increase in ρ becomes too large to be explained by thickness effects alone. A number of theories based on electronic conduction have been proposed to explain this difference. The development of these theories and their practical limitations are discussed in the following sections.

3.2. CONDUCTION IN THIN CONTINUOUS METALLIC FILMS

3.2.1. THOMSON [27] THEORY

Thomson proposed that electronic conduction in thin continuous metallic films may be due to diffuse internal scattering of electrons at the upper and lower surfaces of the film. As a starting point he used the Drude-Lorentz free electron gas model, which says that the bulk resistivity is inversely proportional to the electron m.f.p., but made the following assumptions:

(i) all electrons start their motion at the centre of the film, (Fig. 3.1.);

(ii) the scattering of electrons at the film surface is non-specular, (i.e. the direction of motion after collision is independent of its motion before collision); and

(iii) the m.f.p. λ_o in bulk metals is a constant and its magnitude is greater than the film thickness t. (Fig. 3.1).

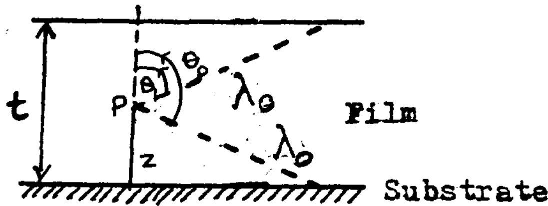

Fig. 3.1. Thin film showing the effect of surfaces on m.f.p. (Thomson [27])

He obtained an expression for the film resistivity ρ in the form:

$$\frac{\rho_o}{\rho} = {}^q/_2 \left[\log \left({}^1/_q\right) + {}^3/_2\right] \quad \text{—— (3 -4)}$$

where q is $\frac{t}{\lambda_o}$

3.2.2. <u>FUCHS[29] THEORY</u>

Fuchs pointed out that equation (3 - 4) cannot be valid because Thomson made the following incorrect assumptions:

(i) λ_o was taken as the mean of all the free paths in a given direction instead of considering electrons with a given momentum and using the average of their free paths; and

(ii) the free paths of electrons starting on the film surfaces were neglected and the statistical distribution of the free paths about λ_o was also neglected.

Fuchs[29] modified the Thomson theory by considering:

(i) electrons whose motion start at the film surfaces and

(ii) elastic and inelastic electron scattering at the film surfaces.

He assumed that in bulk metals the probability that an electron is scattered with an energy E in time ds is given by $\frac{ds}{d\tau}(E)$, where τ is the mean free time of scattered electrons and is taken for the highest occupied energy level in the metal. He applied Maxwell-Boltzmann statistics to those electrons whose motion begins on the film surfaces and obtained the following expression, viz:

$$\frac{\rho_o}{\rho} = 1 - (3/8q)(1 - p) \text{ for } q \gg 1 \quad —— (3 - 5)$$

where p represents the fraction of electrons that are scattered elastically. For complete diffuse scattering p = 1 and for complete specular reflection p = o. Equation (3 - 5) is valid for thick films only (i.e. films with $q \gg 1$ at room temperature).

Sondheimer [30] worked along the same lines as Fuchs and obtained an expression for the resistivity of very thin continuous films of the form:

$$\frac{\rho_o}{\rho} = \frac{3}{4} \left\{\frac{(1 + p)}{(1 - p)}\right\} q \log (1/q) \text{ for } q \ll 1 \quad —— (3 - 6)$$

The main objection to the use of the Fuch-Sondheimer resistivity equations is the use of a single parameter p to describe electron scattering from the upper and lower surfaces of a film.

Lucas[31] observed experimentally that the resistivity of a specular film of gold deposited on bismuth oxide substrates could be increased by roughening the upper surface. Specular films were made by annealing at 625K for a few minutes and non-specular films by depositing a small amount of gold (less than a monolayer) on top of the annealed film. Similar observations were made by Chopra and Randlett[33] with Au, Ag, Cu and Al films on SiO substrates.

Lucas[32] modified the Fuchs expression (equation (3 - 5) by letting p_1 be the fraction of electrons specularly reflected from the top surface and p_2 the corresponding fraction for the lower surface. He obtained:

$$\frac{\rho_0}{\rho} = 1 - \frac{3}{16q}(2 - p_1 - p_2) \text{ for } q \gg 1 \quad \text{—— (3 - 7)}$$

It can be seen that this reduces to equation (3 - 5) when p_1 is equal to p_2. Equation (3 - 7) gave a good fit to experimental result.

The Fuchs-Sondheimer-Lucas assumptions are inapplicable for discontinuous films as the electrons will now have to travel from one conducting metallic island to another through a dielectric region. Although there is good agreement between the various theories and experiment when $p_1 = p_2 = 0$, the use of the theories are limited as the values of p are difficult to estimate.

3.3. CONDUCTION IN DISCONTINUOUS METALLIC FILMS

There are two types of electrically discontinuous films prepared by vacuum evaporation: films consisting of metallic islands separated by free space (pure metallic films), and those having metallic islands separated by an insulating medium (cermets). We shall consider conduction in discontinuous metallic films next and return to cermet films in Section 3.4.

The resistivity of various ultra-thin metallic films, a few Angstroms thick, has been found [34 - 48] to be many decades (up to 10^6) higher than the bulk metal resistivity. The temperature coefficient of resistance (TCR) is negative in contrast to the positive values for both continuous thin metallic films and bulk metals. Electron micrographs of discontinuous metallic films [35, 45, 48] show that they possess an island-type structure. The film resistivity is therefore governed by the transfer of electrons across the gaps between islands and the negative TCR suggests a thermally-activated process. The origin of the activation energy is not clearly understood and many models based on quantum-mechanical tunnelling, substrate-assisted tunnelling and thermionic emission have been proposed to explain it.

3.3.1 NEUGEBAUER AND WEBB [38] THEORY

Neugebauer and Webb (N and W) investigated electronic conduction in ultra-thin metallic films of nickel, platinum and gold deposited on glass substrates. The films were ohmic at low applied fields and the film resistivity was found to depend exponentially on the reciprocal temperature.

They postulated that the conduction mechanism in a discontinuous (island structured) metallic film was due to electron tunnelling through the vacuum between neighbouring islands. They assumed that ultra-thin films consisted of identical spherical islands of radius r separated by a distance d in a planar array. Tunnelling is possible only between charged and uncharged micro-particles; an activation energy is needed to create the charge carriers. In the absence of an applied field N and W suggested that the only electrons which could be transferred were those lifted to an energy level of the order of E_b above the Fermi level of a neighbouring island. E_b is the work done in removing an electron from an island radius r to infinity. It is given by:

$$E_b = \frac{e^2}{4\pi \epsilon_o \epsilon . r} \quad \text{—— (3 - 8)}$$

Here e is the electronic charge, ϵ_o the permitivity of free space and ϵ the low frequency dielectric constant. N and W also pointed out that electrons are actually removed to a neighbouring island, distance d away and not to infinity. In this case the energy E_c required is of the form:

$$E_c = \frac{e^2}{4\pi\epsilon_o\epsilon}\left[\frac{1}{r} - \frac{1}{d + r}\right] \quad \text{—— (3 - 9)}$$

In the presence of an applied field F, the Schottky effect [24] should be included so that the energy E_d necessary to remove an electron to a distance d is:

$$E_d = E_c - deF \quad \text{—— (3 - 10)}$$

The activation energy E_a, under these conditions is obtained by maximizing equation (3 - 10). Then we have:

$$E_a = \frac{e^2}{4\pi\epsilon_o\epsilon r} - \left(\frac{e^3F}{\pi\epsilon_o\epsilon}\right)^{\frac{1}{2}} + reF \quad —— \quad (3 - 11)$$

At low fields and small r equation (3-11) becomes:

$$E_a = \frac{e^2}{4\pi\epsilon_o\epsilon r} - \left(\frac{e^3F}{\pi\epsilon_o\epsilon}\right)^{\frac{1}{2}} \quad —— \quad (3 - 12)$$

Neugebauer and Webb assumed a Boltzmann distribution for the number of charged islands present at a given temperature T and a transition coefficient D across all the tunnelling barriers in order to obtain the resistivity expression:

$$\rho \propto \frac{r}{d^2e^2D} \exp\left(\frac{E_a}{kT}\right) \quad —— \quad (3 - 13)$$

The model predicts that the resistivity of island-structured films (e.g. platinum and gold 150 Å thick) varies exponentially with inverse temperature and is independent of low electric fields (up to 500 V cm^{-1}). The model also predicts that the activation energy decreases with thickness since thicker films consist of bigger islands (large r) and smaller inter-island spacing (small d). (See Section 2.4).

The main objections to the N and W theory are:

(i) the model neglects the interaction between charged islands; the number of charged islands can be very high.

For example at room temperature, 25% of the total number of islands are charged in platinum films which have an activation energy of 50.6 meV. Thus interactions are extremely likely when the activation energy is $\sim kT$;

(ii) electron micrographs (of N and W) show that the islands are not of equal size, are not uniformly spaced and they are not spherical in shape. Therefore the assumption of a constant transition coefficient D is incorrect, as a large variation in d should lead to a large variation in D.

Neugebauer and Webb only considered electrons tunnelling from a charged particle to a neutral one but Swanson et al [39] have considered the contribution to activation energy from both positively and negatively charge carriers. (i.e. transitions between neutral and between charged particles as well as between charged-neutral particles). They assumed that an island receiving an electron will increase its charge by -e and the donor island will assume a positive charge. Allowing for image forces [25, 51] they calculated the energy required to charge an island, and obtained an expression for the activation energy E_a of the form:

$$E_a = \frac{e^2}{4\pi\epsilon_0\epsilon r}\left[1 - \frac{r}{2r + d}\right] \qquad (3 - 14)$$

Ni and Ni/Cr films, 50 to 100A thick (from Swanson et al[39]) gave activation energies 25 to 50% lower than those of N and W. The objections raised with the N and W theory apply here also because the same basic assumptions have been used.

3.3.2 HARTMAN [41] THEORY

Neugebauer and Webb did not discuss why a charging of the micro-particles is necessary nor why electron tunnelling in the neutral island cannot be the predominant conduction mechanism since this type of tunnelling would require no activation. Another possible origin of the activation energy was suggested by Hartman [41], who proposed that it arises from the need for electrons to be elevated to a higher energy level before tunnelling can take place when an electric field is applied.

Hartman assumed that the band structure of individual micro-particle was discrete because of their small size. He represented the islands by cubic potential wells in which electrons are only able to move from one excited state to another by quantum mechanical tunnelling through the gap between adjacent islands.

The energy level in a one dimensional potential well is given by:

$$E_n = \frac{\hbar^2 \pi^2 n^2}{2 m a^2} \qquad (3 - 15)$$

where n is the principal quantum number (= 1, 2, 3 - - - -), m is the mass of an electron and a is the width of the potential well (= 2 r). Tunnelling can only occur between the $(n + 1)^{th}$ levels (the highest occupied level at absolute zero temperature being the nth level). The activation energy in this case corresponds to the energy difference between the nth and the $(n + 1)^{th}$ levels.

It is given by:

$$E_a = \frac{\hbar^2 \pi^2}{2 m a^2} (2n + 1) \quad \text{——} \quad (3 - 16)$$

The main objections to the model are:

(i) it assumes the islands to be a uniform array of cubes. Electron micrographs [38, 45, 49] have shown that islands are neither uniform in size nor in their distribution, neither are they cubic;

(ii) it is a one-dimensional model and therefore ignores transitions in the y and z directions. Hence equation (3 - 16) over-estimates the energy level spacing;

(iii) the model assumes that the ground levels are always uncrossed by either the applied field or by the statistical distribution of island sizes. The probability of tunnelling between the nth levels would be high if the island size distribution caused the ground states to be crossed when a field is applied.

In all the models discussed in Section 3.3., the role of the substrate on the conduction process has not been considered. Let us now consider some theories that include the substrate in the overall mechanism.

3.3.3. SUBSTRATE EFFECT ON ELECTRONIC CONDUCTION IN DISCONTINUOUS METALLIC FILMS

3.3.3.1 HILL [49] THEORY A

Hill proposed that a dielectric substrate has a large number of trapping sites between its conduction and valence bands; most

traps are situated near the band edge and a few in the band gap as shown in Figure (3.2).

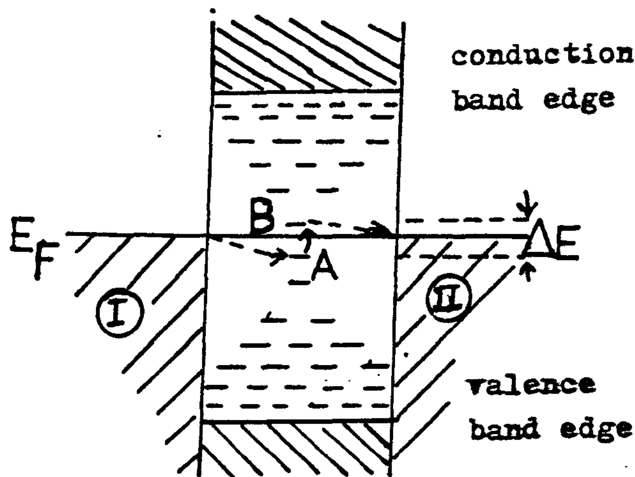

Fig. 3.2. Energy diagram for transfer of an electron from island I to II by means of a trap jump (Hill [49]).

When a discontinuous metallic film is deposited on the substrate, the Fermi level E_f in the substrate becomes aligned with those of the two neighbouring metallic islands I and II. Band bending effects were neglected because only the region just below the metal-substrate interface were considered.

If a trap is located at the Fermi level, direct electron-tunnelling between I and II should occur, via the trap and the process should be non-thermally activated. However, if there is no trap at the Fermi level, electron-tunnelling would occur in two stages:

(i) electrons in I with energy equivalent to E_f could first tunnel into trap A below the Fermi level in the substrate, with the energy difference lost to the substrate lattice. Transition from trap A into II cannot occur as there are no available energy levels below E_f;

(ii) the electron must be thermally activated into the next available trap B higher than E_f and tunnelling into II can then occur.

Hill[49] tested his theory on gold films prepared on soda-lime and borosilicate glasses. He measured the current through the films as a function of the voltage applied across the substrate normal to the direction of current. The results indicate that the film resistance varies with applied transverse voltage at a constant temperature. At a substrate temperature of 395K, the resistance of gold films having an average spacing of 52A decreased from 5.5.kΩ at - 75V to about 4.0kΩ at 100V for films deposited on soda-lime glass, but remained constant at 5.0kΩ from - 100V to -25V and thereafter rose steadily to a peak of 12.5kΩ at 50V before falling steadily to about 5.0kΩ at 100V for films deposited on Corning glass. The change in resistance was interpreted in terms of a shift in the position of the Fermi level in the substrate.

Although Hill[49] observed that the film resistance varied exponentially with inverse temperature, he did not obtain an expression for the activation energy.

3.3.3.2. HERMAN AND RHODIN [42] THEORY

Herman and Rhodin assumed that charge carriers are located beneath metallic islands and that electron-tunnelling occurs between neighbouring islands through the substrate surface. They postulated that a high density of unfilled electron traps or surface states exists on the substrate. When an island-structured metallic film is deposited on the surface, a flow of electrons will occur across the metal-insulator interface filling some of the traps until equilibrium is reached (i.e. their Fermi levels come into correspondence). No such regions are formed in the spaces between metallic islands and the traps in these spaces will remain empty.

A simplified energy band representation of the surface region of the insulator as a function of the position parallel to the surface is shown in Figure 3.3.

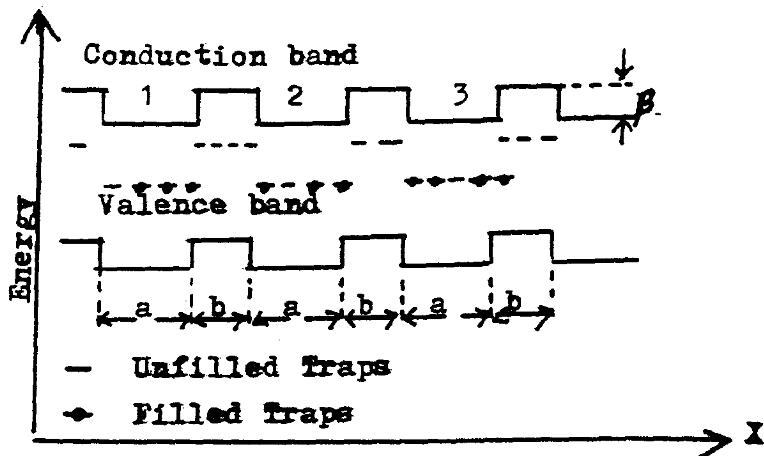

Fig. 3.3. Distribution of traps in the surface of an insulator between metallic islands (Herman and Rhodin [42])

Let the trap regions under the metallic island be designated a regions and the unfilled trap regions of the surface separating two adjacent metallic island, b regions. The energy bands are considered to be bent by an energy value which is unknown. It is designated β in Figure 3.3. The energy bands are also assumed to have a sharp discontinuity where regions a and b meet. At absolute zero temperature, the a regions are assumed to be electrostatically neutral. However, the filled traps in region a may not be at the same level as the unfilled traps due to image forces.

For tunnelling to occur between a filled and an unfilled trap, an activation energy must first be provided by the emission or absorption of a phonon. This energy is considered to be the electrostatic energy (N and W model) to move an electron out of a metallic region into an unfilled trap in region b, midway between two metallic islands. It is given by:

$$E_a = \frac{2\,e^2}{4\pi\epsilon_o\epsilon}\left[\frac{1}{a} - \frac{1}{a+b}\right] \qquad (3-17)$$

The Herman and Rhodin theory combined the Hill [49] and Neugebauer and Webb [38] models and the final resistivity expression was very similar to Neugebauer and Webb's equation (3 - 13). The main objections to the theory are:

(i) the resistivity expression contained two parameters: δ, the depth of the surface trap region and n the surface density which are difficult to estimate;

(ii) in the derivation of equation (3 - 17) Herman and Rhodin did not justify why an electron has to be moved to a distance midway between two metallic islands.

In the substrate-assisted tunnelling models, discussed above, the effect on the activation energy E_a from large and small island separations have not been considered. According to Niffontoff, [50], at 300K and negligible applied electric fields, the conduction process is dominated by thermionic emission, if the island separation is greater than 100A. Let us now look into this possible mechanism in a little more detail.

3.3.3.3. THERMIONIC EMISSION

3.3.3.3.1. VAN STEENSEL [45] THEORY

Van Steensel studied discontinuous films of gold and platinum, deposited on substrates of barium titanate and quartz, in the temeperature range 125 to 625K. He found that at low electric fields gold has an activation energy of 44 meV in the low temperature region ($<$250K) and 140 meV in the high temperature region ($>$250K). He interpreted his results by a thermionic emission mechanism, an activated conduction process previously suggested by Niffontoff [50] and Minn [36].

Van Steensel proposed that the activation energy arises due to the need for the electron to leave a metallic island and enter into the conduction band of the substrate. He assumed

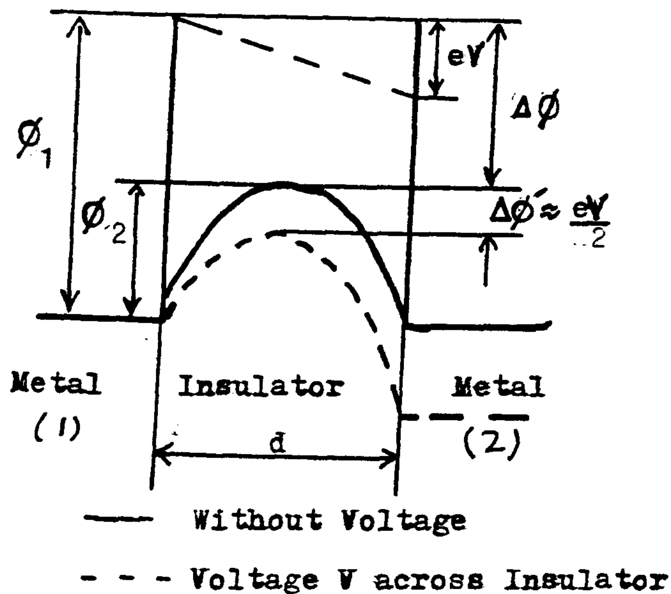

Fig. 3.4. Energy barrier between two metals(Van Steensel [45])

that only electrons with energies equivalent to at least the maximum barrier height ϕ_2 (Fig. 3.4) are transferred from one metallic island to a neighbouring island.

In the absence of an applied electric field, ϕ_2 is equal to the activation energy E_a given by:

$$E_a = \phi_2 = \phi_1 - \Delta\phi \quad \text{—— (3 - 18)}$$

where $\Delta\phi$ is $\frac{20}{\epsilon_h d}$, the Simmons correction term due to image forces in a capacitor structure. ϵ_h is the high frequency dielectric constant and d the barrier width.

If the maximum barrier height occurs half way between the two metallic islands, then when a small voltage V is applied, the barrier height is reduced by approximately $\frac{eV}{2}$. From the Richardson - Dushman equation [24] we can express the current flowing from island 1 to island 2 as:

$$J_{1-2} = A\,T^2 \exp - \left[\frac{(E_a - \frac{1}{2}eV)}{kT}\right] \quad \text{—— (3 - 19)}$$

and that from island 2 to 1 as:

$$J_{2-1} = A\,T^2 \exp - \left[\frac{(E_a + \frac{1}{2}eV)}{kT}\right] \quad \text{—— (3 - 20)}$$

where A is the Richardson constant for thermionic emission, being $\sim 120 A\ cm^{-2} K^{-2}$. Thus the net current density J is:

$$J = 2AT^2\ \mathrm{Sinh}\left(\frac{eV}{2kT}\right) \exp\left(-E_a/kT\right) \quad \text{—— (3 - 21)}$$

which for small values of V, reduces to the ohmic form:

$$J = AT^2\ \left(\frac{eV}{kT}\right) \exp\left(-E_a/kT\right) \quad \text{—— (3 - 22)}$$

In equation (3 - 22) it can be seen that J depends exponentially on the height of the potential barrier between two neighbouring islands. This height is decreased when two islands are close together because of the overlap of the image forces. It is this proximity effect which is believed to give measurable currents at temperatures much too low for ordinary thermionic emission to occur. On this basis Niffontoff calculated that for nichrome films (work function $\sim$5eV) at 300K, J is equal to or larger than the tunnelling current only if d $\geq$ 80A, whilst at 200K d must be $\geq$ 130A.

If thermionic emission is the dominant current mode in metallic films with large island separation, one would expect this current to be very small. On the contrary, the currents observed in films with large island separation at room temperature are many orders of magnitude larger than that predicted by equation(3 - 22). For this reason many workers [38, 41, 42] have rejected thermionic emission as a dominant conduction process in such films. Hill [48], however has presented a comprehensive analysis of electronic conduction in discontinuous films by taking into account thermionic emission as well as electron tunnelling.

3.3.3.3.2. HILL [48] THEORY B

Hill proposed that the substrate can either play an active or a passive role in the conduction process. For the active mode electrons tunnel through the substrate between metallic islands whereas for the passive mode, electron tunnelling occurs through the free space between islands. Hill [48] associated the activation

energy for tunnelling with the electrostatic energy of the the island. He used the same basic assumptions as Neugebauer and Webb [38] and extended the theory to include the effect of:

(i) varying the applied electric field;

(ii) the barrier height given by the metal-insulator work functions; and

(iii) active substrates.

His model based on three collinear metallic islands is shown in Figure 3.5. The injection of an electron into an island of diameter 2r, is considered to raise the potential of that island with respect to zero (defined at infinity) by an amount E_1 given by:

$$E_1 = \frac{e^2}{4\pi \epsilon_0 \epsilon \, r} \qquad (3 - 23)$$

(The symbols have been defined earlier in Section 3.3.1.)

This island will raise the potential of its nearest neighbour, a distance d away by an amount E_2 given by:

$$E_2 = \frac{e^2}{4\pi \epsilon_0 \epsilon \, (2r + d)} \qquad (3 - 24)$$

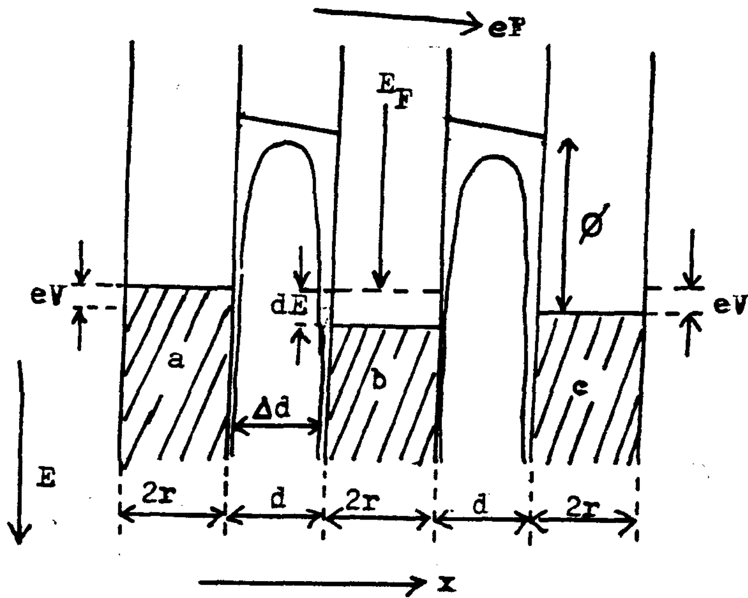

Fig 3.5. Energy diagram for 3 collinear islands in an applied electric field. Ø is the undistorted barrier height, V is the voltage drop between islands, and the Fermi level in island b is dE below that in islands a and c (Hill[48]).

The activation energy is the potential difference between these two islands. It is given by:

$$E_a = \frac{e^2}{4\pi\epsilon_0\epsilon}\left[\frac{r + d}{r\,(2r + d)}\right] \qquad (3 - 25)$$

When a small electric field ($F \sim 10^5$ Vcm^{-1}) is applied between the islands, E_a becomes:

$$E_a = \frac{e^2}{4\pi \epsilon_o \epsilon} \left[\frac{r + d}{r(2r + d)} \right] - Fe\,(2r + d) \quad \text{—— (3 - 26)}$$

For $E_a > kT$, Hill [48] obtained an expression for the electron current density J in the form:

$$J = \frac{8\pi me}{h^3 B^2} \operatorname{Sinh}\left(\frac{eV}{kT}\right) \frac{\pi BkT}{\operatorname{Sin}\pi BkT} \exp(+A\bar{\phi})^{\frac{1}{2}} \exp\left(\frac{-E_a}{kT}\right) \quad \text{—— 3-27}$$

and for $E_a \lesssim kT$, Coutts [51] obtained a corresponding expression:

$$J = \frac{8\pi me}{h^3 B^2} \operatorname{Sinh}\left(\frac{eV}{kT}\right) \frac{\pi BkT}{\operatorname{Sin}\pi BkT} \exp(-A\bar{\phi})^{\frac{1}{2}} \times$$

$$\exp\left(\frac{-E_a}{kT}\right) (1 - \exp - BE_a) \quad \text{—— (3 - 28)}$$

where

$$A = \frac{4\pi \Delta d\,(2m)^{\frac{1}{2}}}{h}; \quad B = \frac{A}{(2\bar{\phi})^{\frac{1}{2}}}; \quad \bar{\phi}$$

is the mean barrier height to tunnelling and Δd is the image-force reduced barrier width. The original expression for J given by Hill [48] for $E_a < kT$ has been found to be mathematically incorrect as it predicts infinite current as $E_a \longrightarrow 0$.

Like Van Steensel[45], Hill [48] has indicated that the conduction process in thin discontinuous metallic films is determined by the island size and the inter-island separation. Hill concluded that it was possible to classify films into four types depending on whether the island diameter is large or small (i.e. whether $\frac{e^2}{4\pi\epsilon_0\epsilon r} \gtrless kT$ and whether the inter-island spacing is greater or less than the tunnelling path length. The classification is summarised in Table 3.1.

Type of Film	Island size	Inter-Island spacing	Predominant type of conduction	Activation Energy
I	Small	Small	Tunnelling	Large
II	Small	Large	Thermionic Emission	Small
III	Large	Small	Tunnelling	Small
IV	Large	Large	Thermionic Emission	Small

Table 3.1. Classification of discontinuous metallic films (Hill [48]).

Hill [48] also proposed that there are two types of substrate-assisted tunnelling: Direct tunnelling in which a bias field has no effect, as in alkali-free substrates; and substrate-modulated tunnelling in which tunnelling depends on the presence of free alkali ions. In the latter case he assumed that a single ion is situated between each pair of metallic island with the result that the barrier height is reduced.

The conduction models discussed in Section 3.3. are applicable to discontinuous films of pure metals deposited on insulating substrates. Conduction in cermet films (metal-dielectric composite mixtures) will now be considered.

3.4. CONDUCTION IN CERMET FILMS

The structure of a cermet film differs from that of an island-structured pure metallic film in that the inter-island spacings are no longer separated by empty space but by solid dielectric material. Consequently the electronic conduction process will vary with the amount of dielectric in the film. In certain cermets (Cr/SiO [53, 54] and Mn/SiO [52, 55]) chemical reaction between the components may lead to varying phases (e.g. silicides) to be formed at certain metallic compositions. Glang et al [54] have made a detailed study of the structure of Cr/SiO cermet films. Up to the solubility limit of Si in Cr, the bcc Cr lattice is the stable crystalline phase, and the presence of Cr_3 Si is due to chemical reaction. Hence the films are not homogeneous but consist of small particles of Cr and silicides in a matrix of SiO_2.

In the absence of a chemical reaction, Morris [56] found that the conduction mechanism in Au island structures in SiO and that of Au/Si in SiO_2 could be interpreted by the N and W theory. On the other hand Coutts [57] suggested that when the metal in the cermet film is particulate, the N and W theory is valid but that this is no longer the case when the metal is filamentary.

3.4.1. COUTTS [51, 57] THEORY

Coutts studied the structural and electrical properties of gold-Corning 7059 borosilicate glass cermets, prepared by RF sputtering in argon. The substrates were also Corning 7059. He observed that the gold either formed capillaries or island structures. Hence he postulated that these structures gave rise to two independent conduction processes acting in parallel to one another.

He assumed that conduction in filamentary capillaries is analogous to conduction in thin wires having diameters less than the bulk electron mean free path given by Dingle [58]. The resistance R_1 due to normal metallic conduction in capillaries at a temperature T was given as:

$$R_1 = R_o (1 + \alpha \theta) \quad \text{—— (3 - 29)}$$

where R_o is a constant defined at a temperature T_o, $\theta = T - T_o$ and α is the TCR.

In the case of the island structure, he assumed an activated conduction expression based on the N and W theory, viz:

$$R_2 = R_{\infty} \exp\left(\frac{E_a}{kT}\right) \quad \text{—— (3 - 30)}$$

where E_a is given by equation (3 - 25) and R_∞ is a constant. R_o and R_∞ are constants only for one metal-insulator composition. If the metal ratio decreases, R_o increases and R_∞ decreases. The total film resistance R for the parallel system is given by:

$$R = \frac{R_1 R_2}{R_1 + R_2} \qquad \text{—} \qquad (3 - 31)$$

The capillaries in the films were 40 to 80A in diameter, but Coutts observed that some capillaries appeared to be broken up into large elongated islands (ellipsoids), as well as spherical islands, varying in sizes and separations. On average, the diameters were ~ 110A and their separations ~ 50A. Using Jeans' [59] electrostatic theory for ellipsoids having two equal short axes, Coutts modified the activation energy term in equation (3 - 30).

If the gold ellipsoids have axes labelled a, b, and c, where c represents the capillary length (major axis) then the geometric mean of a and b ($r = (ab)^{\frac{1}{2}}$) and not c was assumed to dominate the activation energy (E_a in equation 3 - 25). Taking a = 100A and b = 40A, we find that $r \approx 63$A giving an activation energy of about 40 meV which is within a factor of 2 to 3 of the value of E_a for the smaller islands (the value of r for smaller islands is not given but it is assumed to be between 50 and 100A).

As a result of this analysis, Coutts suggested that the ends of the ellipsoids where the field is greatest were interacting with the smaller islands. The model will be complicated further

if the metallic resistances of the larger islands are taken into account.

3.4.2. CHRISTEN AND HEWITT [60] THEORY

Christen and Hewitt studied the mechanism of electronic conduction in Au/SiO and Au/SiO_2 cermet films as the metallic content of the film was varied. Following Hill's structural classification (Table 3.1.), they categorised cermet films into three structural groups according to their metal-insulator content:

(i) films composed of isolated dielectric regions in a continuous metallic matrix, characterised by low resistivity;

(ii) films composed of isolated metallic regions in a continuous dielectric matrix, characterised by high resistivity; and

(iii) a transition region from high metallic content to a low metallic content characterised by a resistivity sensitive to both the metal-dielectric volume ratio and the structural changes during annealing

For group (i) films three dielectric scattering models of conduction were postulated. These are:

(a) the dielectric particle model ;

(b) the layered particle model ; and

(c) the filament model .

In the dielectric particle model, the dielectric islands are considered to act as scattering centres for the free electrons in

the continuous metal matrix. An expression was obtained in terms of the ratio of the cermet resistivity ρ to the intrinsic metal resistivity ρ_o, viz:

$$\frac{\rho}{\rho_o} = \frac{1 + \lambda_o n \pi r^2}{1 - \frac{4}{3} n \pi r^3} \qquad \text{—— (3 - 32)}$$

where $1 - \frac{4}{3} n \pi r^3$ is the volume fraction V_f

of the metal, r and n are the radius and density of the dielectric islands, and λ_o is the electron m.f.p. in the bulk metal . The variation of ρ/ρ_o with V_f indicated that film resistivity increases as V_f decreases and also that ρ/ρ_o increases as r decreases.

In the layered particle model, the films are considered to consist of alternate ultra-thin layers of metal and dielectric, there being no metal-metal or dielectric-dielectric layer contact. In this case the cermet resistivity ρ is given by:

$$\rho = \rho_L \frac{1}{V_f} \qquad \text{—— (3 - 33)}$$

where ρ_L is the resistivity of one metallic layer of uniform thickness t_m; and V_f is given by the ratio:

$\dfrac{t_m}{(t_m + t_d)}$ where t_d is the uniform

thickness of a dielectric layer. They used Fuchs[29] and Sondheimer [30] theories of electrical conduction in thin continuous metallic films to obtain an expression for the resistivity of the

metallic layer ρ_L in the form:

$$\frac{\rho_L}{\rho_o} = \frac{f(q)}{q} \quad \text{———} \quad (3 - 34)$$

where f(q) is given by equations (3 - 5) and (3 - 6) and q by t_m/λ_o. Combining equations (3 - 33) and (3 - 34), we have:

$$\frac{\rho}{\rho_o} = \frac{f(q)}{q\, V_f} \quad \text{———} \quad (3 - 35)$$

A graph of $\frac{\rho}{\rho_o}$ against $\frac{1}{V_f}$ indicates that $\frac{\rho}{\rho_o}$ is proportional to $\frac{1}{t_m}$ for a constant V_f. It was also shown that when t_m is small compared to t_d, the film resistivity increases as t_d increases.

The filament model assumes that there are numerous small metallic filaments aligned along the direction of the applied electric field. Adjacent filaments are separated by a layer of dielectric. The cermet resistivity is given by:

$$\rho = \rho_{f'} \frac{1}{V_{f'}} \quad \text{———} \quad (3 - 36)$$

where $\rho_{f'}$ is the resistivity of one filament and their volume fraction $V_{f'}$ is given by:

$$V_{f'} = \frac{\pi\sqrt{3}}{6} \left(\frac{2r_{f'}}{d}\right) \quad \text{———} \quad (3 - 37)$$

$r_{f'}$ and d are respectively the filament radius and the distance

between the centres of adjacent filaments. If $r_{f'} < \frac{1}{2}d$, there is no contact between filaments. For $r_{f'} > \frac{1}{2}d$, the conduction process is still assumed to be filamentary but no consideration was given to the possibility of interaction between the filaments.

The resistivity of filaments has been considered by Dingle [58] and Chambers [61] as:

$$\frac{\rho_0}{\rho_{f'}} = \theta(q) \quad \text{——} \quad (3 - 38)$$

where $q = \dfrac{2 r_{f'}}{\lambda_0}$

Using Dingle's analogy of conduction in thin wires and Chambers theory for conduction in thin wires in a magnetic field, Christen and Hewitt obtained an expression for the cermet-intrinsic metal resistivity ratio, viz:

$$\frac{\rho}{\rho_0} = \frac{1}{V_{f'} \, \theta(q)} \quad \text{——} \quad (3 - 39)$$

A graph of $\frac{\rho}{\rho_0}$ against $V_{f'}$ shows that $\frac{\rho}{\rho_0}$ decreases with increase in $r_{f'}$.

The resistivity of films in group (ii) usually lies between the high values of the dielectric and the low values of the metal. For this region they suggested that the conduction mechanism is similar to that occurring in ultra-thin discontinuous metallic films, where the film is made up of a planar array of islands as discussed in Section 3.3.

Group (iii) films fall into the transition region between groups (i) and (ii). They suggested that the film resistivity is very sensitive to change in phase of the dielectric, to small changes in the metal-dielectric volume ratio and to structural changes during annealing. In their experiment (ρ Vs volume composition of SiO_2 in an Au/SiO_2 cermet system) it was found that a resistivity jump occurred at about 50 vol % SiO_2. This resistivity jump is considered to be due to the transition from group (iii) to group (ii).

The main objection to Christen and Hewitt theory is that their models contained parameters which are difficult to determine. Although they successfully fitted their own Au/SiO experimental data to theory, as well as Ostrander and Lewis' [76] Cr/SiO data, when r is 5A, t_d is 2A and r_f is 2.86A, the success of the theory depends largely on the correct determination of these usually unknown parameters.

3.4.3. ABELES, SHENG, COUTTS AND ARIE [63] THEORY

Abeles et al proposed that conduction in cermet films (they referred to as granular metal films) is controlled by the amount of metal and dielectric in the film. Like Christen and Hewitt [60], they divided granular metal films into three structural groups - metallic, dielectric and transitional regime.

In the metallic regime, bulk metallic phenomena such as superconductivity and ferromagnetism [64, 65] which depend on the transfer of electrons, are retained but bulk properties such as

TCR and resistivity [66] which depend on electron m.f.p. are greatly modified due to strong electron scattering from the dielectric inclusions and the grain boundaries.

As the dielectric material is increased, the metallic continuum starts to break-up into isolated metallic particles. At some critical composition which depends on the metal-dielectric system, the dielectric islands become interconnected and a maze structure is formed. The resistivity then increases rapidly with further decrease in the metallic content and the TCR changes sign (from positive to negative), denoting a transition from the metallic to the dielectric regime. The authors observed that the transition regime occurred within the resistivity range 1 to 10 mΩ— cm.

In the transitional regime, conduction is said to be due to percolation along the metallic maze and electron tunnelling between isolated metallic islands. The two processes become comparable at the temperature and composition when the TCR changes sign.

The transition into the dielectric regime occurs at a percolation threshold metallic composition below which only tunnelling contributes to the conduction process. (Bulk superconductivity and ferromagnetism are observed to vanish abruptly at the percolation threshold although individual isolated metallic islands can retain their superconductivity and ferromagnetism if their size is larger than the critical size required for the existence of these phenomena).

Using a complex capacitor, Figure 3.6, consisting of a superconductor - insulator - granular metal - metal (Al - Al_2O_3 - $Ni\ SiO_2$ - Au) they proposed a tunnelling model based on the assumption that the tunnelling current consisted of two parts:

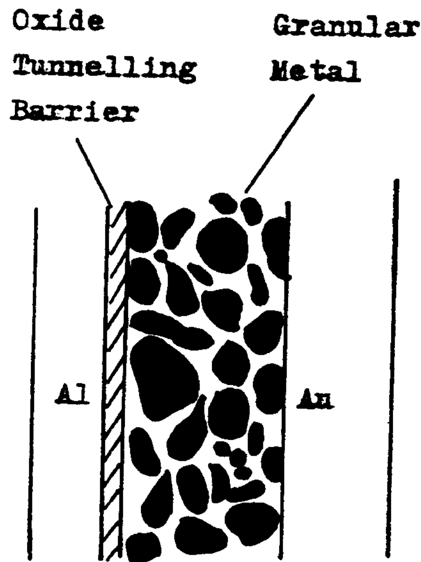

Fig. 3.6. Metal - Insulator - Granular metal Tunnel structure (Abeles [63])

(i) electron tunnelling into isolated metallic island from the insulator, (N and W theory [38]) and

(ii) electron tunnelling into the metallic continuum om the insulator.

In this case it was assumed that there is an effective junction capacitance C_e at the insulator granular metal interface, and the activation energy E is the charging energy for the capacitor and it is given by:

$$E = \frac{e^2}{2C_e} \qquad —— (3 - 40)$$

The total activation energy in the transition region is the sum of E_a (as given in equation (3-12) and E (equation (3 - 40)).

In the dielectric regime, they proposed that the conduction mechanism is by electron tunnelling and that it was both electric field and temperature dependent. At low fields $\frac{kT}{e}$ is taken to be much larger than the potential difference V between neighbouring metallic islands and an activated tunnelling process predominates leading to a low film resistivity ρ_L given by:

$$\rho_L = \rho_o \exp \; 2 \, (C/kT)^{\frac{1}{2}} \qquad —— (3 - 41)$$

where ρ_o is a constant independent of temperature and C is a constant independent of grain size and constituent metals and insulators. Equation (3 - 41) indicates that ρ_L is independent of applied electric fields and that:

$$\ln \rho_L \propto T^{-\frac{1}{2}} \qquad —— (3 - 42)$$

Experimental results [68] show equation (3 - 42) to be valid for granular metal films of Pt/SiO_2, Ni/SiO_2 and Au/Al_2O_3 in the dielectric regime.

At high fields, thermal-activated and field-enhanced tunnelling are the main conduction mechanism, with the latter becoming dominant when the resistors are non-ohmic. The transition from low to high field occurs when V becomes comparable or greater than $\frac{kT}{e}$. They assumed that the potential difference across neighbouring metallic islands is a constant value, so that the entire structure is divided into parallel equipotential surfaces perpendicular to the direction of the applied field as shown in Figure 3.7.

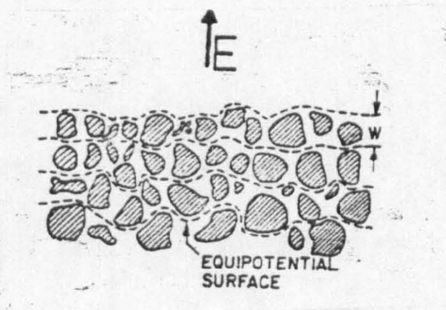

Fig. 3.7. Illustration of equipotential surfaces in a granular metal when an electric field E is applied (Abeles [63]).

The high field F, low temperature resistivity ρ_H is given by:

$$\rho_H = \rho_\infty \exp\left(\frac{E_o}{F}\right) \qquad \text{—— (3 - 43)}$$

where $E_o = \frac{C}{ew}$ and w is the separation between equipotential layers.

Equation (3 - 43) indicates that ρ_H is independent of temperature and that

$$\ln \rho_H \propto \frac{1}{F} \quad \text{—— (3 - 44)}$$

These authors obtained a good fit of experimental data to theory (equations 3 - 41 and 3 - 43) for both low and high electric fields applied parallel and perpendicular to the plane of film.

3.4.4. GASPERIC AND NAVINSEK [67] THEORY

Gasperic and Navinsek proposed a conduction model for cermet thin films (planar resistors) containing 5 - 30 vol % metal following a systematic investigation of electronic conduction in Cr/SiO system. They assumed that a cermet film is analogous to a three dimensional array of cubic bricks of equal sizes, with each layer consisting of metal and dielectric cubes arranged alternately. Such an arrangement constituted a combination of resistors in series and the resistivity ρ is given by:

$$\rho = \rho_m V_m + \rho_i V_i \quad \text{—— (3 - 45)}$$

where ρ and V are respectively, the resistivity and volume fraction with the subscripts m and i referring to metal and insulator respectively. As $\rho_m \ll \rho_i$ equation (3 - 45) reduces to:

$$\rho \approx \rho_i V_i \quad \text{—— (3 - 46)}$$

To enable ρ to be calculated, they used Stratton's [85] equation for the current density in an insulating film between two metallic islands to obtain ρ_i, viz:

$$\rho_i = \frac{22.8}{t_i} \exp\left[1.025 \ t_i (\bar{\phi} m_*)^{\frac{1}{2}}\right] \ x$$

$$\text{Sin}\left[0.5125\pi kT \left(\frac{m_*}{\bar{\phi}}\right)^{\frac{1}{2}}\right] \qquad \text{—— (3 - 47)}$$

where t_i is the thickness of the insulating layer $\bar{\phi}$ the mean barrier height and m_* is the ratio $\frac{m_i}{m_m}$ with m_i being the mass of an electron in the insulator and m_m the electron mass in the metal.

Gasperic and Navinsek stated that if ρ_i is known, it is possible to predict the resistivity of a cermet film (using this model) to within one or two orders of magnitude for films containing up to 60 vol % of the dielectric (5 to 30 vol % metal only). Hence the model is applicable only in the dielectric regime.

These authors were able to fit experimental data to theory for the Cr/SiO cermet system. They used m_* equal to 0.5, ρ_i values from computed $\bar{\phi}$ values in the range 0.1 to 1 eV and t_i values of 0 to 50A (using a metallic island thickness of 15A obtained from electron micrographs). Hence the success of the theory depends on the accurate determination of these parameters which usually suffer large deviations from their mean values.

CHAPTER FOUR

4. EXPERIMENTAL APPARATUS

The experimental apparatus may be conveniently divided into:

(i) deposition equipment; and

(ii) equipment associated with the measurement of electrical resistivity.

4.1. DEPOSITION EQUIPMENT

The deposition equipment consists basically of:

(i) a coating plant;

(ii) a film thickness monitor; and

(iii) a set of deposition masks.

4.1.1. THE COATING PLANT

The films were prepared by thermal evaporation in a 305 mm vacuum ceating plant (Edward model 12E3), illustrated schematically in Figure 4.1. The work chamber (Figure 4.2) is cylindrical, 305 mm diameter and 362 mm high. It is sealed at the bottom with a stainless steel top-plate 305 mm diameter and 13 mm thick. The base plate carried all the electrical feed-throughs, the shutter operating lever and a tripod stand, which supports a stainless-steel metal plate 240 mm in diameter and upon which is mounted a quartz crystal monitor (monitor cystal), a substrate heater and thermocouple wires. This plate also served as the

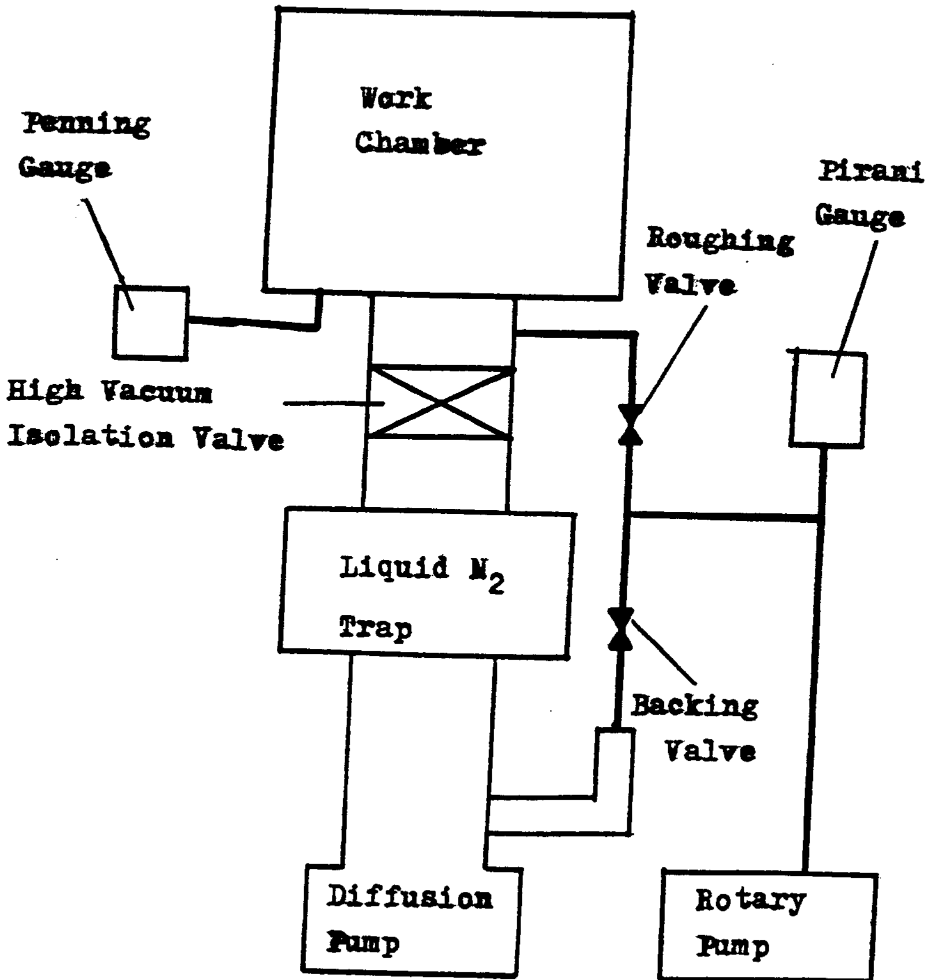

Fig 4.1. Schmatic diagram of a vacuum coating plant.

support for the specimen holder. All the electrical leads within the chamber were insulated electrically and thermally with alumina beads (see Fig. 4.2)

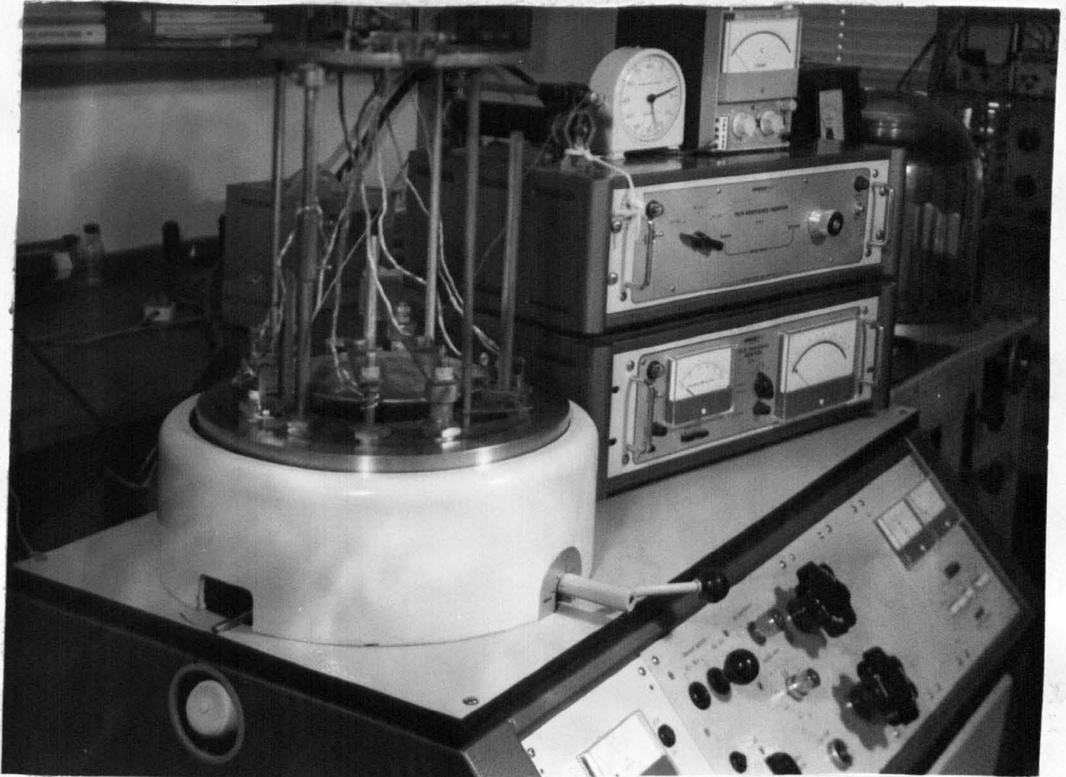

Fig. 4.2. The coating plant showing the work chamber

The chamber was evacuated with a diffusion - rotary pump assembly. The diffusion pump was an oil type (throat diameter 101.5 mm) capable of attaining an ultimate pressure of $5x10^{-7}$

torr if silicone pump fluid (Dow-Corning MS 704) is used. A single stage mechanical oil sealed rotary pump (having a displacement of 11.4 m^3 hr^{-1}) was used for evacuating the main chamber from atmosphere and for backing the diffusion pump. The pumping system was able to reduce the chamber pressure to 1×10^{-4} torr in 5 minutes and to 5×10^{-6} torr in 90 minutes, as monitored with a Penning cold-cathode ionization gauge. The backing pressure and the pressure in the main chamber during the rough vacuum stage were monitored with a Pirani gauge.

A liquid nitrogen trap (Dewar type) was used to reduce back-streaming and back-migration [74], thus reducing the risk of oil contamination. There is also a tube of Al_2O_3 balls to reduce back-migration from rotary to diffusion pump. All elastomer seals in the system were of Viton because they have low out-gassing properties at temperature up to $\sim$ 475K.

The coating plant is also provided with solid-state, fully variable high and low tension power supplies (3.5 kV/50 mA, 30V/30A and 10V/90A). The low tension power supply was adequate for all evaporations carried out in the system. These evaporations were performed using resistive heating.

4.1.1.1. RESISTIVE-HEATING FILAMENTS

Two forms of filaments were used; boat-shaped tantalum foils and tungsten wire spirals.

4.1.1.1.1 BOAT FILAMENTS

The boats used were approximately 15 mm long, 5 mm wide and 5 mm high with support flanges of about 10 mm long at each end. (Fig. 4.3). The evaporation area of the boat approximated a finite strip surface source [75].

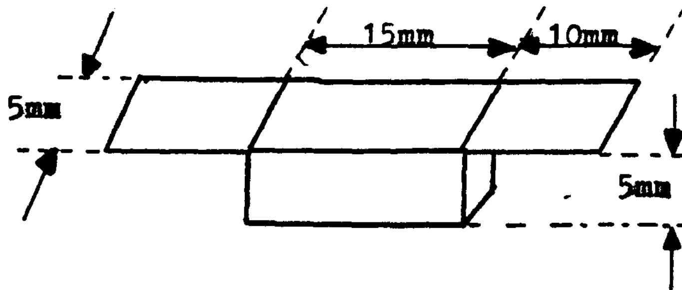

Fig. 4.3. Boat-shaped filament made of Tantalum.

The single boat offered a convenient way of evaporating an element (Mn) and a compound (MgF_2) with relatively close melting points (1525 and 1538K, respectively at a pressure of 1 standard atmosphere) Tantalum was found to be a suitable boat material as pure Mn and Mn/MgF_2 mixtures do not readily wet or react with it at the evaporation temperatures.

A great advantage of the single boat is that deposition can be carried out at constant rates whilst the percentage composition of the cermet is varied. Its main disadvantage is that the ratio of Mn to MgF_2 is by weight. Hence the proportion of Mn in the starting

composition is assumed to be the same as that of the deposited film as X-ray fluorescence was not available. This disadvantage was greatly reduced by putting a regulated amount of thoroughly-mixed Mn/MgF_2 cermet powder in the boat and carefully operating the heater filament controls to avoid spitting.

A double-boat system (Edward model E19A3 coating plant) consisting of two independently operated single boats was used to prepare some films for selected investigations; Mn was put in one boat and MgF_2 in the other (Fig. 4.4.). The disadvantages of the

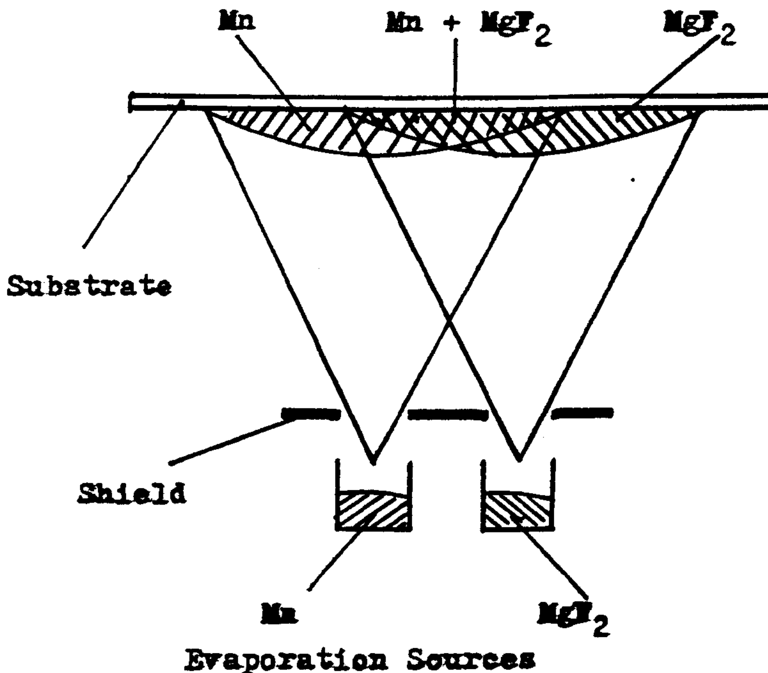

Fig. 4.4. Two boat arrangement yielding a variable film composition and thickness.

double boat system are that percentage compositions are expressed in volume % which are obtained by adjusting the evaporation rate of Mn with respect to MgF_2 or vice-versa. As we shall see later in Section 6.5, changes in the deposition rate causes changes in film structure and resistivity. Also to obtain films of uniform composition and thickness, the positions of the boats, the monitor crystals and the substrate become critical (Fig. 4.4.). A detailed account of thickness distribution as a function of substrate position has been given for the Cr/SiO cermet system by Ostrander and Lewis [76].

4.1.1.1.2. WIRE FILAMENTS

Multi-stranded tungsten filaments in spiral form were preferable to single stranded loop filaments for the evaporation of manganin and aluminium. It was found that the loop filament has a life span of only 3 to 4 evaporations before it developed acute necking as a result of evaporation of parts of the filament. In contrast, the multi-stranded filament provided up to 12 evaporations.

4.1.1.2 FILM THICKNESS MONITOR

The film thickness monitor (Edward model 1) was used for monitoring the thickness of the film during deposition. The equipment employs two AT cut crystals operating in a fundamental thickness shear mode [77]. A monitor crystal (oscillating at 6MHz) has a deposition area of 21.59 mm^3 and was housed in a crystal can which was placed 267 mm above the boat and 35 mm from the centre of the substrate. A reference crystal (oscillating at 6.5 MHz) was housed

in a steel box outside the deposition chamber.

The two frequencies are mixed and the difference amplified. After amplication, the resulting frequency is again mixed with the frequency from a variable local oscillator (in the amplifier circuit) to give a final difference of 0 to 150 kHz. During film deposition, the resonant frequency of the monitor crystal is reduced to give an increase (or a shift) in the final frequency difference. The frequency shift and its rate differential are displayed on meters. Before use, the thickness monitor was calibrated for Mn and Mn/MgF_2 cermets, as detailed in Section 5.1.3.

4.1.1.3 MASKS

Two out-of-contact mechanical masks were used for resistor fabrication, one for the resistor tracks and the other for the electrical contact pads (Fig. 4.5)

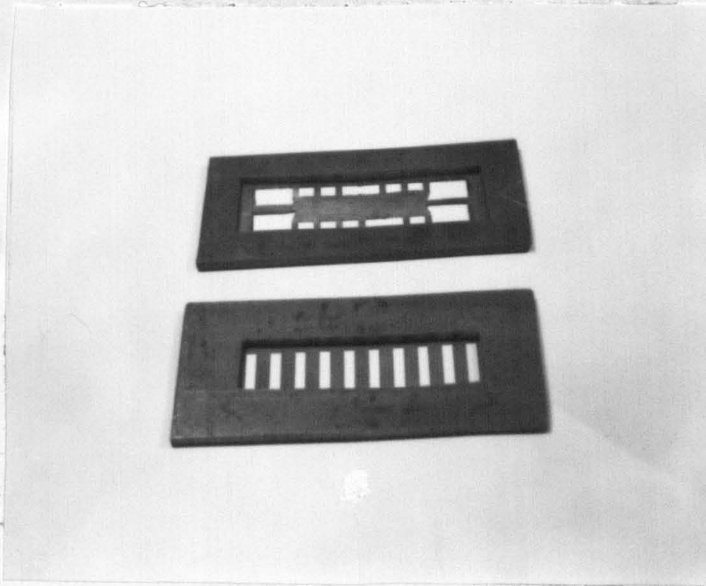

Fig. 4.5. Desposition Masks.

The masks were made from a thin sheet of molybdenum/copper alloy (15 mm x 15 mm x 0.5 mm thick), and the resistor tracks (15 mm x 3 mm) and the contact pads (5 mm x 5 mm) were produced by photo-lithographic techniques. The original pattern for the contact pads was later modified (Fig. 4.5) to allow for the two longer pads required in four terminal electrical measurement of resistance.

The masks were spot-welded onto a mild-steel frame 3 mm thick, 102 mm x 51 mm external dimensions and 78 mm x 27 mm internal dimensions. The frame also served as the substrate holder during film deposition.

4.2. EQUIPMENT ASSOCIATED WITH THE MEASUREMENT OF ELECTRICAL RESISTIVITY

Two distinct sets of apparatus were used for the electrical resistivity measurements:

(i) an auxiliary vacuum plant, for measurement *in vacuo* $\sim 5 \times 10^{-4}$ to 5×10^{-6} torr; and

(ii) a direct current potentiometer for measurements carried out in air.

4.2.1 AUXILIARY VACUUM PLANT

The auxiliary vacuum plant was a conventional type consisting of a work chamber, a liquid nitrogen trap and a diffusion-rotary pump assembly. (It was designed and assembled from locally available parts in the department.)

The work chamber was basically cylindrical (Fig. 4.6) but with four smaller cylindrical projections arranged vertically and horizontally in the direction of two cross diameters. It was made of stainless steel 300 mm in diameter and 300 mm long. There are two access points into the chamber: a front swing door (360 mm in diameter and 12 mm thick) which is fitted with a glass window (153 mm in diameter); and a brass top top plate (200 mm in diameter and 12 mm thick).

Fig. 4.6. The work chamber of the auxiliary vacuum plant.

The chamber walls and the door are water-cooled, thus reducing outgassing at elevated temperatures. The horizontal cylindrical projections from two side areas which carry all the electrical feed throughs into the chamber. All leads inside the chamber were insulated electrically and thermally with alumina beads.

The liquid nitrogen trap was of the Dewar type and the level of liquid nitrogen in it was automatically maintained by a Croyflow submersible Dewar pump (type CSMPB) in conjunction with an automatic level sensor (ALN L4) for liquid nitrogen (Edward High Vacuum Products) Thus maintaining a fairly constant rate of back-streaming and back-migration (oil contermination) at all times and at all temperatures.

The specimen holder and its heating and cooling assemblies were all incorporated in a single unit (Fig. 4.7). The cooling section is basically a liquid nitrogen condenser (95 mm x 70 mm x 82 mm) which is attached to the top plate by a steel pipe (Liquid N_2 refill pipe). Copper was used for the top and bottom of the condenser, but the walls were made of stainless steel to reduce loss of heat by conduction.

The hot stage consisted of a copper block (60 mm x 45 mm x 10 mm) welded onto the base of the condenser with maximum thermal contact. Nine equally spaced holdes (3.5 mm diameter) were drilled through the copper block, and into which thermally recrystalised alumina pipes (3.5 external diameter, 1.3 mm internal diameter and 60 mm long) were inserted. A nichrome wire(1.2 mm diameter) looped

through the pipes formed the insulated heater element.

The substrate recess (27 mm wide and 2 mm deep) runs along the middle of the copper block. This recess was planed and polished so that the substrate had intimate contact with it. Further the substrate was held in position by four spring-loaded contacts on an asbestos block which in turn was clamped firmly onto the condenser by a pair of brackets (Fig. 4.7). The ends of the spring-loaded contacts were highly polished as they also provided the electrical contacts between the thin film and the connecting leads. With this arrangement it was possible to cycle the temperature between 110 and 720K without admitting air into the system.

Temperatures above room temperature were obtained by passing a d.c. current through the heater element and the current was provided by a 30V/10A (Farnell model B 30/10) continuously variable power supply. The film temperature was monitored by two Comark electronic thermometers: type 1623 Cu/Con for low temperatures; and type 1602 Cr/Al for high temperatures.

The d.c current flowing through the test sample was provided by a stabilised power supply (Coutant model LA 100.2) which was fully variable in the range 0 to 30V and 0 to 2A) and capable of operating in either a constant current or a constant voltage mode. The current flowing through the test sample was monitored with an auto-ranging digital multimeter (Keithleys model 168) which has an accuracy of 0.1% on the current range. Another digital multimeter (Advance Instruments model DM M3) with an accuracy of 0.1% on the

voltage scale monitored the potential difference across the

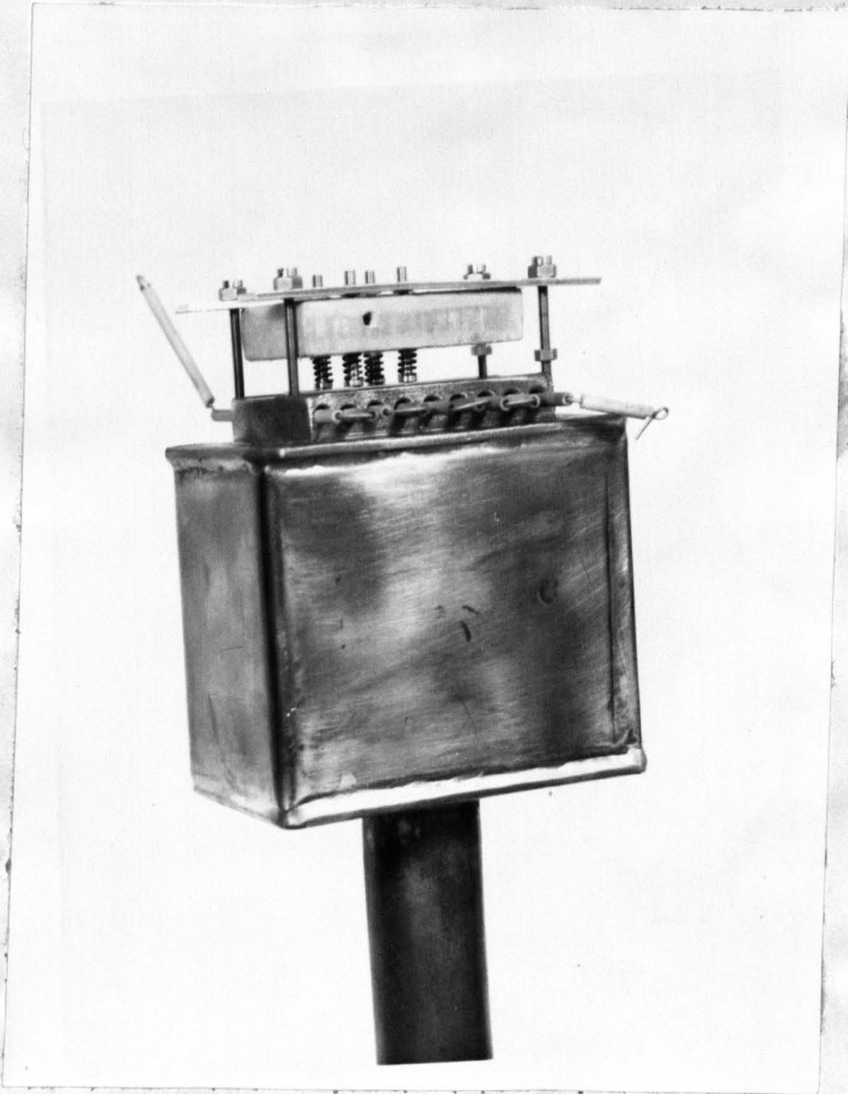

Fig. 4.7. The specimen holder showing its heating and cooling assemblies.

test sample. The diagram for this arrangement is shown in Figure 4.8.

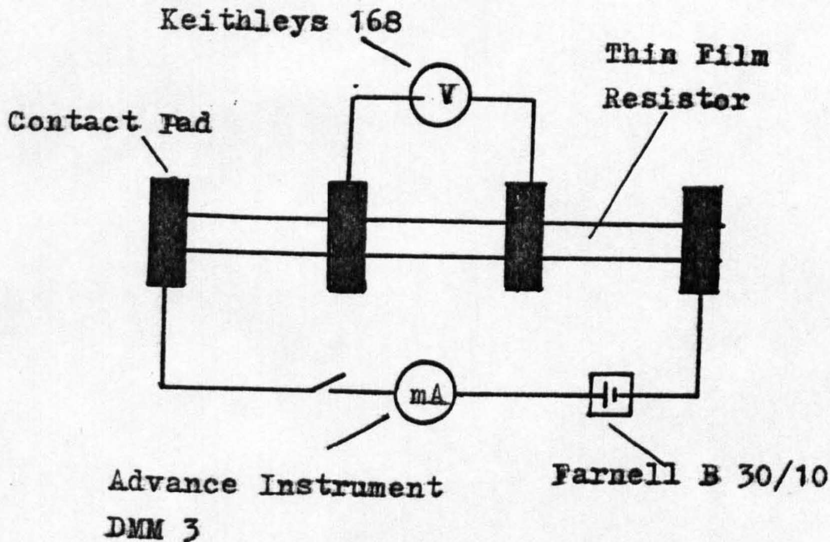

Fig. 4.8. Four Terminal resistance measurement.

4.2.2. D.C. POTENTIOMETER

A direct current potentiometer (Croydon Precision Instruments type 2) was used to measure the p.d. across the test sample when a current of 1 m A flows through it. The measuring circuit (Fig.4.9) consists of a dial having 17 steps of 0.1 volts and a calibrated slidewire (152.4 mm diameter) covering -5 mV to 105 mV with the smallest division being 0.5 mV. The instrument has 3 ranges: X 1; X 0.1; and X 0.01 with accuracies of 0.02, 0.03 and 0.04% respectively.

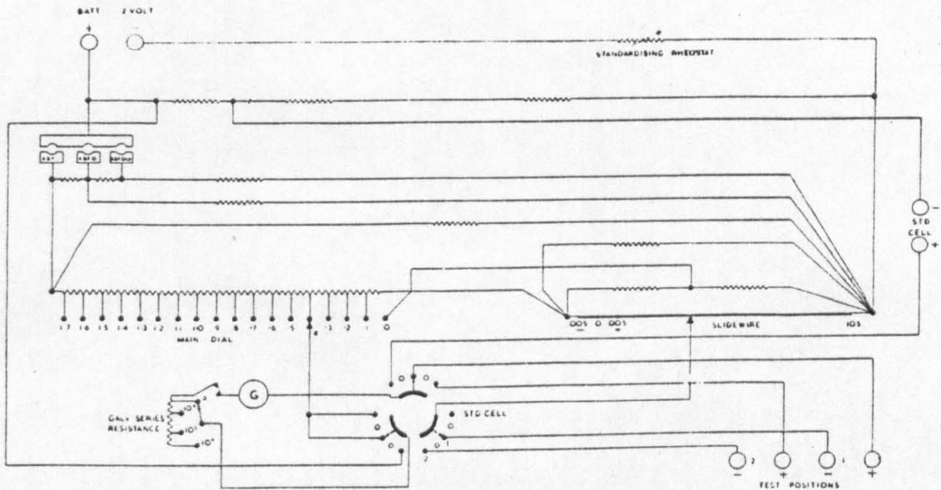

Fig. 4.9. Circuit diagram of d.c. potentiometer

The potentiometer has an independent standardising circuit, which is not affected by the operation of the main dial. The circuit incorporates a compensator which automatically corrects for the variation in the voltage of the standard cell, due to changes in environmental temperatures. The null position of the potentiometer was determined with a moving coil galvanometer (WPA type K107) having a sensitivity of 540 mm/μA.

CHAPTER FIVE

5. EXPERIMENTAL TECHNIQUES

This chapter contains two main sections:

(i) pre-deposition preparation; and

(ii) film deposition and resistivity measurement.

5.1. PRE-DEPOSITION PREPARATION

A description is given in this section of the various steps taken prior to film fabrication. It also includes films deposited for use in the calibration of the monitor crystal. However such films were not used in investigations involving resistivity measurements.

5.1.1. THE CERMET MATERIAL

The component materials used for the cermet mixtures were manganese of 99.9% purity, (Griffin and George Ltd.) and magnesium fluoride, 4 - 40 mesh, (British Drug Houses Ltd.). Prior to mixing, the magnesium fluoride was ground into a fine powder using a pestle and mortar. Then several grammes of the required mixture (10 to 100 Wt % Mn) were weighed in an Oerton balance, (with an accuracy of $\pm$ 0.1 mg). Further grinding ensured that complete homogeneous mixing was obtained. Only a small amount of the mixture ($\sim$ few milligrammes) was used at a time. This was ground again immediately before use to ensure that the mixture remained homogeneous.

5.1.2. SUBSTRATE AND SUBSTRATE CLEANING

Thin films were condensed on four types of substrates: Corning 7059, alkali free alumino-borosilicate glass for electrical resistivity measurements, and cellulose acetate paper, Kapton and freshly cleaved mica for structural investigations.

The glass substrates were washed in running tap water to remove dust adhering to them due to electrostatic charges. They were then loaded, five at a time, onto a silica glass rack and immersed in a degreasing solution containing one part of Decon detergent to 100 parts of de-ionised water held at bout 375K for ten minutes. The rack was then transferred to another beaker containing de-ionised water to remove the detergent from the substrate; to accelerate this process boiling water was used. Then the substrates were cooled in de-ionised water at room temperature for a few minutes before the rack was moved into a drying chamber containing isopropyl vapour.

This type of drying was preferred because it does not require a freshly distilled isopropyl alcohol for every cleaning run. Occasionally water marks were left on the substrates in areas where they were in contact with the rack. This problem was eliminated by placing the rack on a clean tissue for about 20 seconds between the final rinse and the drying. This cleaning method was unsuitable for the other substrates (mica, cellulose acetate paper and Kapton) which were degreased by immersion in freshly distilled Isopropyl alcohol at room temperature.

5.1.3 CALIBRATION OF THE MONITOR CRYSTAL

The general description and mode of operation of the monitor crystal is given in Section 4.1.1.2. However, before the crystal can give a standardised measurement of film thickness, it must first be calibrated using an absolute optical method, viz. by relating the frequency shift obtained during film deposition to the measured thickness of a material of known density (e.g. aluminium).

A number of frequency shifts, reasonably spaced, were selected and aluminium films of corresponding thickness were fabricated using the resistor masks described in Section 4.1.1.3. After the resistors were fabricated, a reflective coating of aluminium was deposited to cover them and the entire surface (film side only) of the substrate so that a step was produced at each resistor boundary.

The height of this step (film thickness) was measured using a multiple-beam interferometer [75]. A linear dependence of frequency shift on aluminium film thickness was obtained as shown in Figure 5.1. Using Figure 5.1 the frequency shift of various compositions of Mn and Mn/MgF_2 was obtained by relating their densities to that of aluminium and using suitable conversion factors.

5.1.4. CONVERSION FACTORS

If an aluminium film density d_1 and thickness t_1 is produced by a frequency shift of f_1 then [78]

$$f_1 \propto d_1 t_1 \qquad \text{—— (5 - 1)}$$

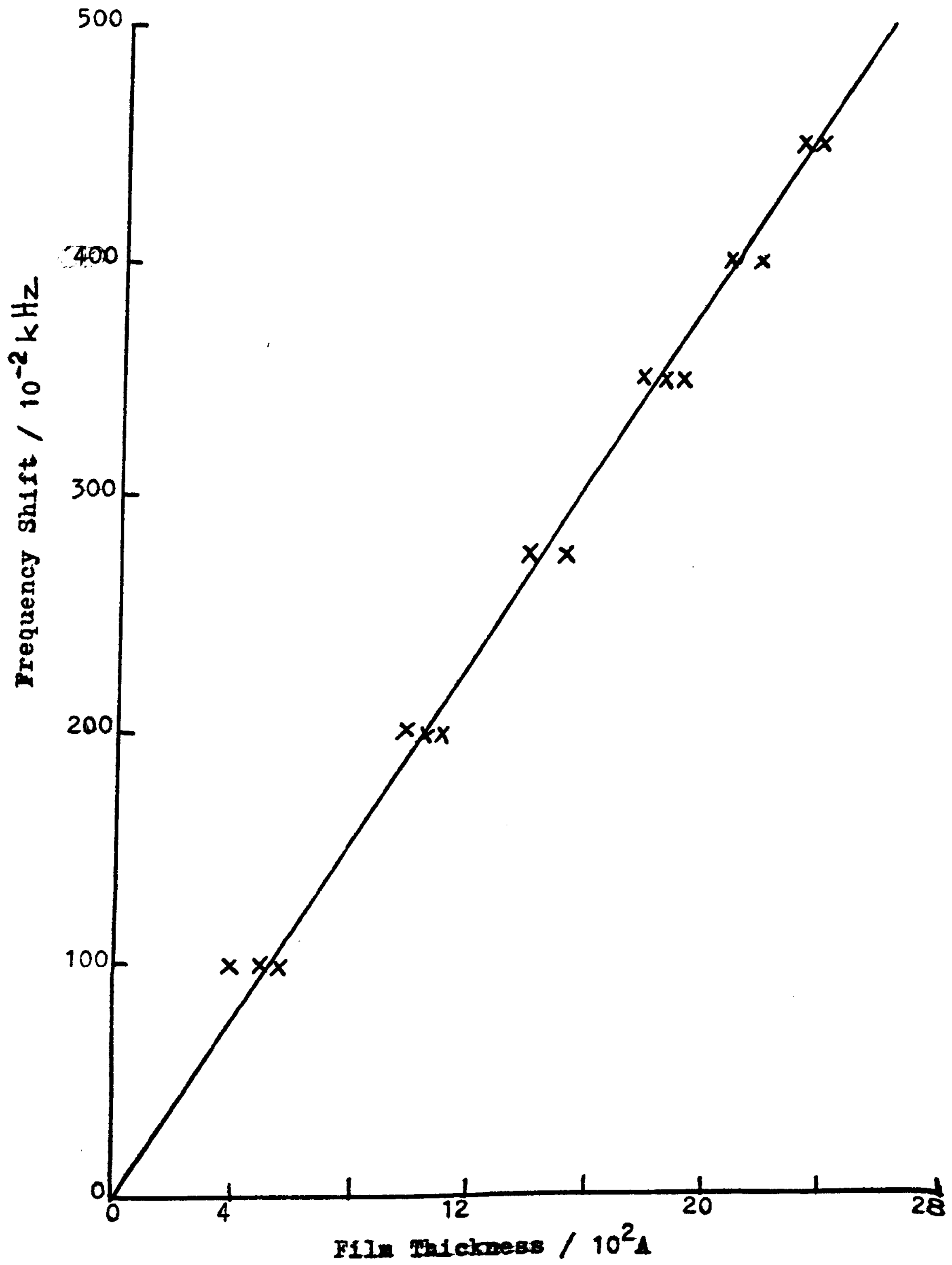

Fig.5.1 Frequency Shift Vs Aluminium Film Thickness

For a cermet having the corresponding parameters d_2 and t_2, the frequency shift is given by:

$$f_2 \propto d_2 t_2 \quad \text{—— } (5 - 2)$$

Combining equations (5 - 1) and (5 - 2) we find that:

$$f_2 = \frac{d_2}{d_1} \cdot \frac{f_1}{t_1} \cdot t_2 \quad \text{—— } (5 - 3)$$

where $\frac{f_1}{t_1}$ is the slope of the graph in Figure 5.1. If the conversion factor $\frac{d_2}{d_1}$ is known, f_2 can be calculated for any chosen value of t_2 (or vice-versa) within the sensitivity range of the thickness monitor. d_1 is known (for aluminium $d_1 = 2.7$g cm^{-3} at 273K) and d_2 was obtained as follows:

$$d_2 = \frac{m_2}{V_2} = \frac{\text{mass of cermet}}{\text{vol. of cermet}} \quad \text{—— } (5 - 4)$$

but

$$V_2 = V_3 + V_4 \quad \text{—— } (5 - 5)$$

where V_3 and V_4 are respectively, the volumes of Mn (density d_3) and MgF_2 (density d_4) in the cermet.

If x is the weight percentage composition of Mn then from equation (5 - 5)

$$V_2 = \frac{\left(\frac{x}{100}\right)m_2}{d_3} + \frac{\left(\frac{100 - x}{100}\right)m_2}{d_4} \qquad (5 - 6)$$

Substituting for V_2 in equation (5 - 4) and dividing by d_1 we find that:

$$\frac{d_2}{d_1} = \frac{1}{\frac{x}{100} \cdot \frac{d_1}{d_3} + \frac{100 - x}{100} \cdot \frac{d_1}{d_4}} \qquad (5 - 7)$$

The calculated conversion factors for the various Mn/MgF_2 compositions are shown in table 5.1. The relationship between the expected film thickness for Mn and Mn/MgF_2 based on the above mathematical calculation and the observed thickness from optical measurements was also investigated for a number of selected films. The expected film thickness were $\pm$ 15% of the measured value.

5.2. FILM DEPOSITION AND RESISTIVITY MEASUREMENT

Before commencing to describe the technique used for film deposition and resistivity measurement, here are some relevant definitions and derivations of some of the commonly measured resistance parameters and their importance.

A thin film resistor prepared by vacuum deposition is usually rectangular in shape. For a given mask, the resistor length l and width w are constant so that the film resistance R is directly proportional to the resistivity ρ and inversely proportional to the thickness t.

Wt.% Mn.	Density of cermet $g.cm^{-3}$	Density of Al. $g.cm^{-3}$	Conversion factor d_2/d_1	Cermet film thickness t_2 (A)	Frequency shift $x5x10^{-2}$ kHz
100	7.400	2.700	2.741	500	52.24
90	6.541		2.423		46.62
80	5.861		2.171		41.14
70	5.309		1.966		37.47
60	4.853		1.797		34.25
50	4.468		1.658		31.60
40	4.140		1.533		29.22
30	3.857		1.428		27.22
20	3.610		1.337		25.48
10	3.393		1.257		23.95
0	3.200		1.185		22.58

Table 5.1. Frequency shifts calculated for Mn/MgF_2 cermet films 500A thick using conversion factor d_2/d_1

R is given by:

$$R = \frac{\rho l}{tw} \qquad (5 - 8)$$

As $^{l}/w$ is a constant (Aspect ratio), equation (5 - 8) can be mormalised, i.e.

$$R = R_s \cdot \frac{l}{w} \qquad \text{—— } (5 - 9)$$

where R_s (= ρ/t) is the sheet resistance and it is usually expressed in units of ohms per unit square ($\Omega/\Box$).

R_s is a useful parameter for comparing thin films particularly those of the same materials deposited under similar conditions, as a knowledge of the film thickness is not required. A more accurate film comparison can be made using resistivity.

If t is known, the film resistivity ρ ($=\sigma^{-1}$, where σ is the conductivity) may be obtained from equation (5 - 8) to give:

$$\rho = \frac{R\,t}{(l/w)} \qquad \text{—— } (5 - 10)$$

ρ has units of ohm - cm (Ω - cm) and it is the most widely used parameter for describing a thin film resistor, because it enables us to compare films of different materials and thickness.

5.2.1. TEMPERATURE COEFFICIENT OF RESISTANCE (OR RESISTIVITY)

The Temperature coefficient of resistance (TCR) α_R is defined at a given temperature T as:

$$\alpha_R = \frac{R_1 - R_2}{R_T\,(T_1 - T_2)} \qquad \text{—— } (5 - 11)$$

for $T_1 > T > T_2$, where R_T is the resistance at a temperature T,

and R_1 and R_2 are resistances at temperatures T_1 and T_2 respectively.

When the TCR is small, as in some thin films α_R is obtained from the R Vs T curve. Here TCR is defined as:

$$\alpha_R = \frac{1}{R} \cdot \left(\frac{dR}{dT}\right) \qquad \text{——} \quad (5 - 12)$$

Similarly the temperature coefficient of resistivity α_ρ is defined as:

$$\alpha_\rho = \frac{1}{\rho} \left(\frac{d\rho}{dT}\right) \qquad \text{——} \quad (5 - 13)$$

For thermally activated conduction,

$$\alpha_\rho = \frac{-E_a}{kT^2} \qquad \text{——} \quad (5 - 14)$$

since $\rho = \rho_o \exp\left({}^{E}a/kT\right)$

It is usually assumed that α_R is equal to α_ρ. This is valid only if the linear coefficient of thermal expansion α_T is negligible. By differentiating equation (5 - 10) and dividing the result by ρ or its equivalent we have:

$$\frac{d\rho}{\rho} = \frac{dR}{R} + \left(\frac{dt}{t} + \frac{dw}{w} - \frac{dl}{l}\right) \qquad \text{——} \quad (5 - 15)$$

$$\therefore \frac{1}{\rho}\frac{d\rho}{dT} = \frac{1}{R}\frac{dR}{dT} - \frac{1}{l}\frac{dl}{dT}$$

since $\frac{dl}{l} >> \frac{dt}{t} + \frac{dw}{w}$

i.e.

$$\alpha_\rho = \alpha_R - \alpha_T \quad \text{— (5 - 16)}$$

For bulk metals $\alpha_T < 10^{-2} \alpha_\rho$ so that α_ρ is equal to α_R is valid. Due to expansion missmatch between the film and its substrate this is not the case for thin films. Hall [79] has shown that α_T can be as high as 65 ppm K^{-1} for fused glass. These values are significantly large as they are comparable to TCR values for cermet and thin metallic films. However α_T can be reduced considerably with the right choice of substrate as shown in Table 5.2. Corning 7059 lies in the fused silica group.

Substrate Material	α_T (%) at 775K
Fused Silica	0.03
Soda-Free Glass	0.22
Beryllia	0.32
Soda Lime Glass	0.45

Table 5.2. Percentage linear expansion of various substrate materials [80] at 775 K

Hence α_ρ can be equated with α_R for pure Mn films and Mn/MgF_2 cermet films.

Electrically discontinuous metallic and cermet films exhibit a non-linear negative TCR whilst thick films and bulk metals have a positive TCR. On this basis TCR gives an indication of the structure of a thin film (and hence its resistivity).

From Matthiessen's rule, the bulk resistivity ρ_o is given by equation (3 - 1), viz:

$$\rho_o = \rho_s + \rho_i$$

where ρ_s is temperature dependent and ρ_i temperature independent. If we differentiate ρ_o with respect to T we have:

$$\frac{d\rho_o}{dT} = \frac{d\rho_s}{dT} \quad \text{——} \quad (5 - 17)$$

combining equations (5 - 13) and (5 - 17) we find that:

$$\rho_o \alpha_o = \rho_s \alpha_s \quad \text{——} \quad (5 - 18)$$

It follows that for a thin film (as expressed in equation (3 - 3)

$$\rho \alpha = \rho_o \alpha_o \quad \text{——} \quad (5 - 19)$$

If the deposition parameters, and size effects are assumed to be constant Equation (5 - 19) predicts that the TCR for a thin film must be lower than that of the bulk metal since $\rho >> \rho_o$.

5.2.2. INITIAL INVESTIGATION

Initially, pure Mn films and Mn/MgF_2 cermet films were deposited onto clean Corning 7059 glass substrates in vacuo at a residual gas pressure of 1×10^{-5} torr (not rising above 2×10^{-5} torr) from a tantalum boat-shaped filament (see Section 4.1.1.1.). The films were deposited at low rates $\sim 4 \pm 1 Å s^{-1}$.

The substrates temperature was maintained at $295 \pm 4K$. The cermet composition was varied between 100 and 10 wt % Mn in 10 wt % steps. For each composition, a range of film thicknesses was used: 100, 250, 500, 750, 1000 and 1500Å. The resistor tracks were fabricated first followed by a subsequent deposition stage in which manganin conducting pads were prepared at room temperature. The thickness of the contact pads was not monitored, but they appeared to be very thick from visual observations and their sheet resistance was less than $0.01 \Omega/\square$. The contribution of the contact pads to the film resistivity was negligible, as the lowest sheet resistance measured was $29.6 \Omega/\square$.

Each film has to pass a visual test before any electrical measurements were made. The visual test consisted of holding the film against room light in order to detect the presence of pin-holes or non-uniform colouration in the specimen.

After fabrication, connecting leads were soldered onto the manganin contact pads. The four terminal resistance measuring technique was used for all the resistivity measurements. Although

a preliminary experiment to compare the two and four terminal methods gave an identical result, the four terminal method was chosen because it provided a more rigid mechanical connection at the soldered joint.

The test resistor (Fig. 5.2 was connected across terminal 1

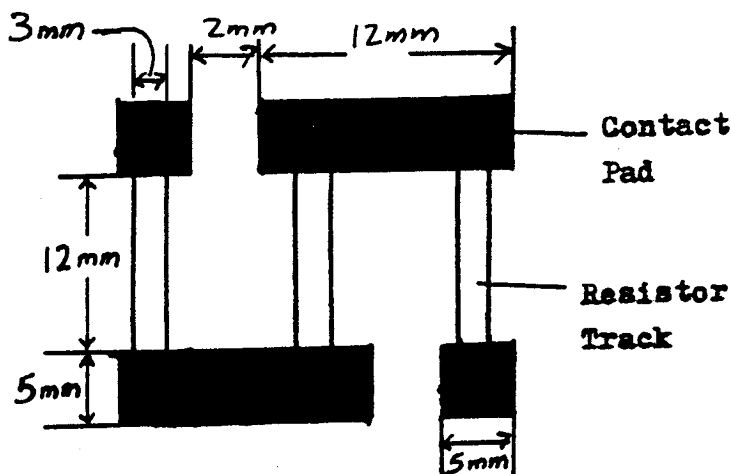

Fig. 5.2 Test Resistor

of the potentiometer (Fig. 4.9). After standardising the potentiometer, a current of 1mA was passed through the specimen and the potentiometer was balanced to give a null deflection. Then the direction of the current was reversed and the reading was repeated in order to obtain a mean value of resistance.

The current flowing through the sample was increased in stages during certain investigations to determine the break-down voltage of the resistor. After the resistance measurements were made, the test samples were stored in a dessicator under a rough vacuum, and

the film resistivity was calculated from the measured resistance using equation (5 - 10). The readings were repeated twice on every occasion a freshly prepared film was used: In cases where there were large variations in the resistivity value, further readings were taken until the reasons for the large spread were ascertained.

5.2.3 SUBSEQUENT INVESTIGATIONS

In the initial investigation, the films were fabricated at fixed deposition parameters. This section describes the procedure by which some of those parameters were varied and how the resulting film resistivity was measured and the film structure analysed.

5.2.3.1 SUBSTRATE TEMPERATURE

The investigations carried out in Section 5.2.2 were repeated with the substrate held at different temperatures (325, 375, 395, 425 and 455K). Films were not deposited at substrate temperatures lower than 290K, as the system was not provided with a cooling-stage for the substrate. The back of the substrate was heated by thermal contact with a mica insulated heating element. Prior to film deposition the temperature of the substrate was gradually raised to the required values and held there for 15 minutes in order to attain thermal equilibrium. The temperature was monitored on the film side of the substrate and at equilibrium it was not allowed to vary by more than $\pm$ 4K.

The highest deposition temperature (455K) was determined partly by the outgassing level of the chamber, as the pressure was not allowed to rise above 5×10^{-5} torr, and by the safest maximum

controllable temperature. After film fabrication the substrate was allowed to cool down for at least $1\frac{1}{2}$ hours. This being the the average time taken for the substrate temperature to fall from 455 to 295K after the heaters were switched off. In this investigation the deposition rate was maintained at 4 A s^{-1}.

5.2.3.2. DEPOSITION RATE

The variation of film resistivity with deposition rate, other parameters being kept constant, was investigated for three film compositions (100, 80 and 60 wt % Mn). Before this investigation was carried out, the deposition rate meter was calibrated as follows: films of given thicknesses and compositions were prepared. The reading of the rate meter (arbitrary units in divisions per second) was recorded for each thickness and the deposition time (s) noted. The rate meter reading was converted into a deposition rate (As^{-1}) by dividing the film thickness by the deposition time, i.e.:

$$\underset{(As^{-1})}{\text{deposition rate}} = \underset{(div\ s^{-1})}{\text{rate meter reading}} = \frac{\text{Film thickness}}{\text{deposition time}}$$

The required deposition rate was selected by regulating the boat filament current with the coarse and fine current controls of the low tension power supply and the selected deposition rate was kept steady (using only the fine current control) for about 20 seconds before the films were prepared. During film condensation the deposition rate was not allowed to rise above $\pm$ 0.1 As^{-1} for rates less than 5As^{-1}, 0.5 As^{-1} for rates less than 10As^{-1} and $\pm$ 2As^{-1} for rates less than 15As^{-1} and $\pm$ 4As^{-1} for those less than 25As^{-1}. These limits were averages obtained in trial runs at the specified deposition rates.

5.2.3.3. DEPOSITION PRESSURE

The effect on film resistivity of the residual gas pressure (other parameters being kept constant) was also investigated. The investigation consisted of two parts: in the first part, the pressure in the chamber was reduced to 5×10^{-6} torr, then dry air was bled into the chamber until the required air-pressure was obtained whilst in the second part the chamber was again evacuated to 5×10^{-6} torr, then it was flushed with 99.9 % pure argon (British Oxygen Company) for about 10 minutes at a residual gas pressure of 5×10^{-4} torr. In either case the required argon or air-pressure (5×10^{-6} to 5×10^{-4} torr) for each deposition run was carefully controlled by adjusting the needle value to the chamber and the pressure was held at that level for about 30 minutes prior to film deposition.

5.2.3.4 ANNEALING

The films (deposited by the method described in Section 5.2.2.) were transferred into the measurement chamber (Section 4.2.1). Aluminium was used for the contact pads instead of manganin because it was found that excessive mass diffusion occurred at the resistor/manganin contact pad boundaries (Fig. 5.3) when the substrate temperature was raised to a high value ($>$ 575K). This effect was not observed with resistors having aluminium contact pads.

The substrate temperature was raised at a rate not exceeding 4K $\min^{-1}$ until the required annealing temperature (375 to 720K) was reached. The temperature was then held at this level throughout the annealing time (1 to 3 hours). The resistance of the film was

(a)

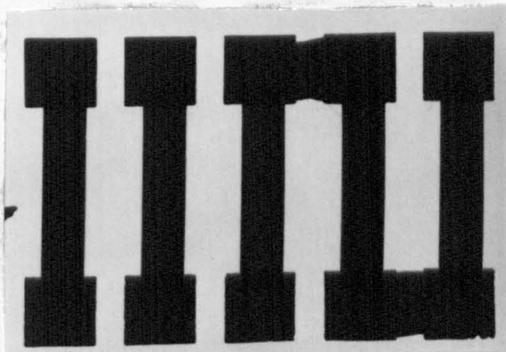

(b)

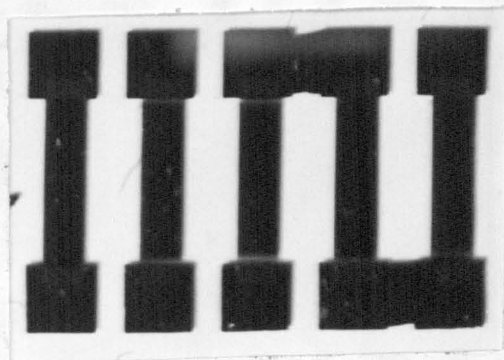

Fig. 5.3 100% Mn films with manganin contact pads (a) before annealing (b) after annealing at 620K for 1 hour.

continuously monitored throughout this study.

When the annealing process was completed, the substrate temperature was lowered (at the rate of 4K min $^{-1}$) to 110K and then raised again to the annealing temperature at the same rate. This cycle was repeated several times to determine whether the resistivity exhibited an hysteresis. The resistance was again monitored continually during the temperature cycling. In some investigations the temperature was allowed to stabilised for about 15 minutes at pre-set temperatures before any readings were taken but these

readings were similar to those obtained during the cycling periods.

An investigation was also carried out to determine the variation of resistivity with temperature for unannealed films. The procedure was basically the same as that given above for the annealed films except for the substrate temperature which was cycled between 110 and 295K.

5.2.4 STRUCTURAL ANALYSIS

5.2.4.1 X-RAY DIFFRACTION

The composition of the starting materials: Mn, MgF_2 and Mn/MgF_2 mixtures were investigated using the Debye-Scherrer X-ray diffraction technique [86]. α Cu radiation (35 KV, 30 mA) was used throughout the investigation. Both the specimen preparation and camera loading were carried out in the conventional way [86, 87].
The lattice spacings were measured and the structure identified using the ASTM X-ray powder data file.

Attempts were made to determine the structure of the thin films (Mn and Mn/MgF_2 cermets) using two different X-ray methods:

(i) the X-ray transmission technique. Here the diffraction pattern is produced by a beam of x-rays passing through both film and substrate; and

(ii) the X-ray glancing angle technique [88]. Now the incident beam is reflected at the film surface. The glancing angle was 0 to 15°.

In either case the test films were 500, 1000 and 2000A in thickness and were deposited on Corning 7059 glass, Kapton and Mica. Also the test specimen was rocked.

The transmission technique was unsuccessful because the X-rays were considerably absorbed by the substrates. In the case of the glancing angle technique, the specimen caused considerable scattering of the incident beam with varying efficiency because the X-rays were not monochromated. The diffraction patterns obtained were too weak and the information was insufficient to identify accurately any film structure.

5.2.4.2 ELECTRON MICROSCOPY

The structure of the deposited films were analysed using a transmission electron microscope (JEM 7). The films used for structural analysis were deposited simultaneously with those for the electrical measurements (Sections 5.2.2., to 5.2.3). Initially the films were deposited on cellulose acetate paper. These were removed by dissolving the substrate in a solution of methyl acetate. However, it was found that cellulose acetate paper was unsuitable for high temperature work as structural and chemical damage occurred above 395K. Several attempts were made to detach Mn and Mn/MgF_2 cermet films from Corning 7059 glass pre-coated with carbon by soaking in dilute hydrofluoric acid [57], but these attempts were unsuccessful because the acid attacked the films.

In investigations where it was found necessary to anneal the films at temperature greater than 395K, freshly cleaved mica pre-coated with carbon ($>$ 500A thick) were used. The test film was detached by floating the substrate in de-ionised water. In either case the film was collected on a copper grid and, after drying inserted into the microscope.

Various areas of the film were viewed and representative micrographs and diffraction patterns taken. The island and inter-island separations were measured from the electron micrographs whilst data for film structure were obtained from the diffraction patterns. The diameter of the rings enabled the lattice spacing to be calculated using Bragg's law. These calculations require a knowledge of the electron microscope camera length.

To obtain the camera length, a gold film, 250A thick was deposited on cellulose acetate paper. Representative diffraction patterns of the film were taken as described above. The diameter of the rings were measured and the ring number with their corresponding intensities noted. Using the lattice spacings for gold given in the ASTM X-ray powder data file, it is thus easy to estimate the camera length. The camera length L is given by [90]:

$$L = \frac{rd}{\lambda} \qquad (5 - 20)$$

where r is the radius of a diffraction ring, d the lattice spacing and λ is the wavelength of the radiation (= 0.042A at 80kV and 0.037A at 100kV)

Structural and electrical resistivity investigations were also carried out on the aging properties of films stored <u>in vacuo</u> and on the open shelf at atmospheric temperature and pressure. The experimental procedure was the same as that described above for films deposited on glass and mica simultaneously. In addition the resistance of the film deposited on glass was measured at set intervals of time and their structural investigation was made on a cut out portion of the film deposited on mica.

CHAPTER SIX

6. RESULTS AND DISCUSSIONS

6.1. INTRODUCTION

For the sake of clarity, the results of experiments described in Chapter 5 are presented in sections; each section relates to one type of experiment and also includes a discussion of the results. In the discussions, reference is frequently made to experimental results for other cermet systems. Some of the data are expressed in Volume % (Vol %), Atomic % (At %) and Weight % (Wt %) but mostly in Vol.%. To make the comparison of

Wt.% Mn.	Vol.% Mn.
100	100
90	79.55
80	63.36
70	50.22
60	39.34
50	30.18
40	22.38
30	15.63
20	9.75
10	4.58

Table 6.1. Conversion table for Mn/MgF_2 cermets from Wt % to Vol %.

these data with those of Mn/MgF_2 easier, an attempt was made to convert Vol % and At % into Wt %, but the information given by most of the authors was insufficient to make this possible (e.g. the resistor width and length are not usually quoted). Therefore Wt % and At % were converted into Vol %. The equivalent Vol % Mn/MgF_2 cermets are given in Table 6.1.

The experimental results of the effect of MgF_2 insulator phase on the resistivity of Mn under different deposition parameters and film thicknesses will now be presented.

6.2 VARIATION OF RESISTIVITY WITH COMPOSITION

The variation of resistivity with composition for the Mn/MgF_2 cermet system is shown in Figure 6.1. The graphs show that the film resistivity rises gently, and almost linearly in the case of films deposited at 375K, as the Mn content falls, until it reaches a certain critical composition. Beyond this composition, the resistivity rises fairly steeply as the Mn concentration falls further.

As can be seen the change in slope is not abrupt but occurs gradually over a range of compositions, the extent of which appears to vary with film thickness. For example for a film thickness of 250A this range is small, viz from 30 to 40 Vol % Mn, but becomes broader as the film thickness increases to 1500A, in which case the critical composition region is not apparent even at 22.5 Vol % Mn, the final composition studied.

This broadening of the critical composition in the thicker films may indicate that continuous paths of Mn are formed as the

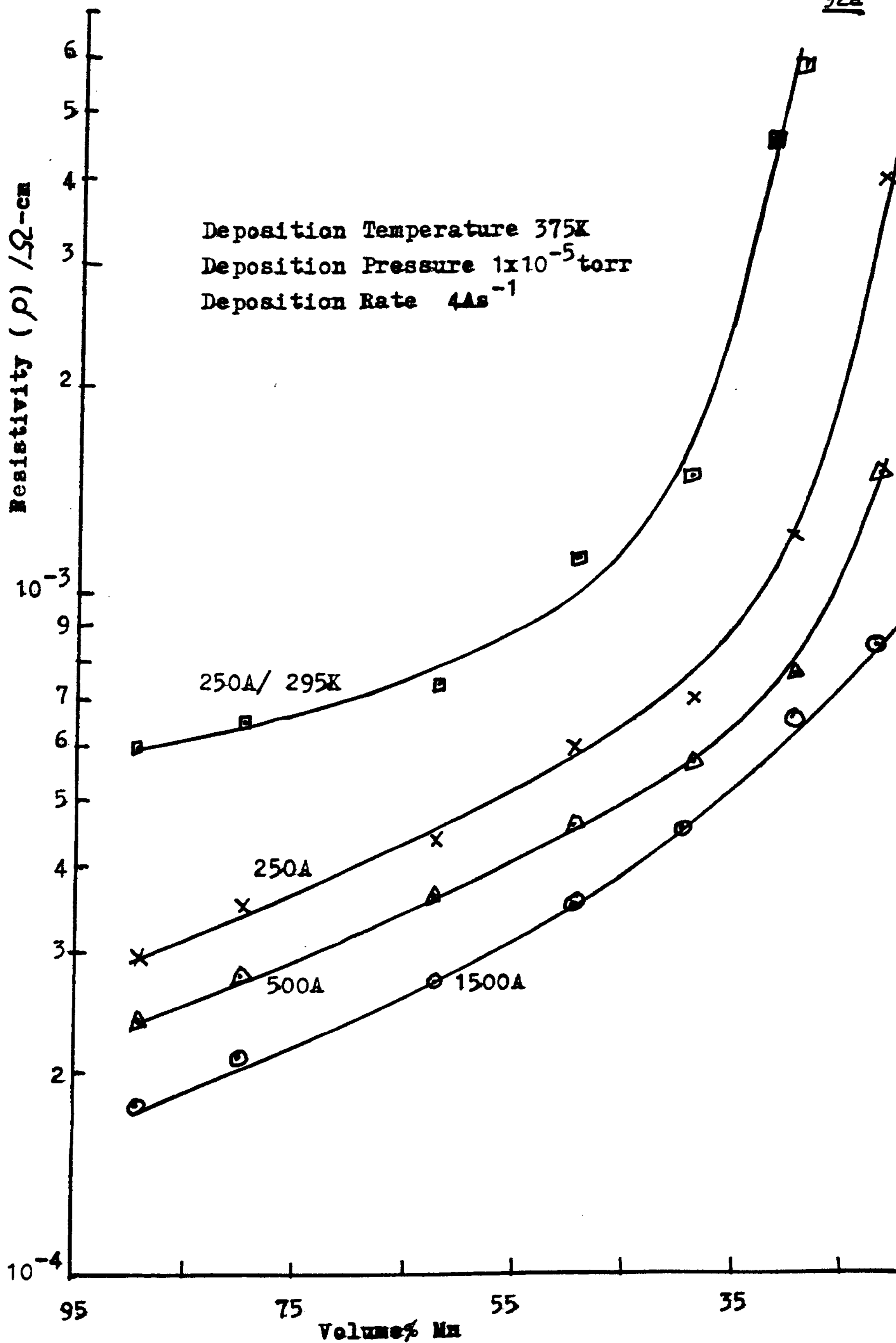

Fig.6.1 Resistivity Vs Composition of Mn/MgF_2

film thickness increases, thus maintaining the resistivity at a low level.

Figures 6.2a, 6.2b and 6.2c are transmission electron micrographs for 100, 63 and 39 Vol % Mn films, 250A thick. These show that the size of the metallic islands in the cermet films decreases and their separation increases as the proportion of Mn decreases.

Mn/MgF_2 cermet composition(vol%Mn)	Island radius (A)	Island separation (A)	Activation Energy (meV)
100	81.3 ± 21.1	333 ± 85	24.6 ± 6.0
63	37.3 ± 9.0	428 ± 139	59.0 ± 16.4
39	21.4 ± 4.0	714 ± 190	108.0 ± 21.5

Table 6.2. Variation of island radius, island separation and activation energy with composition for films 250A thick.

(a) 100% Mn

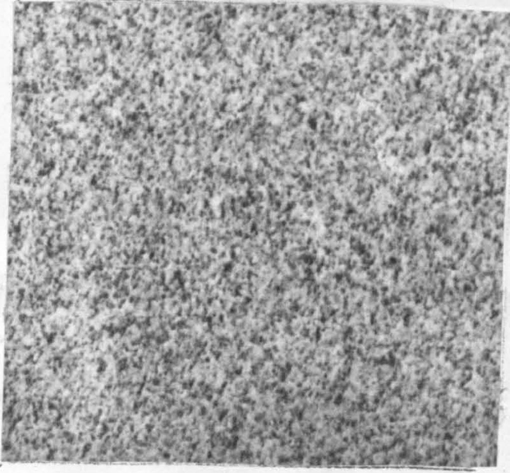

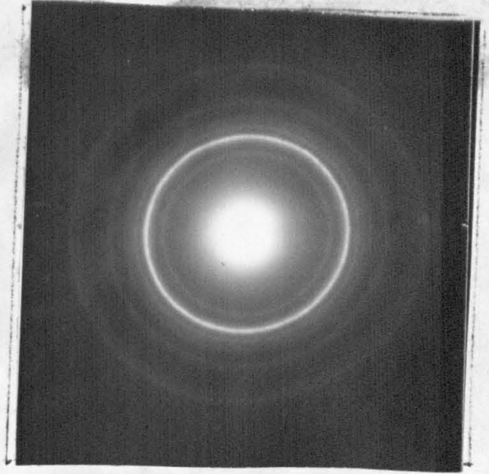

(b) 63Vol% Mn

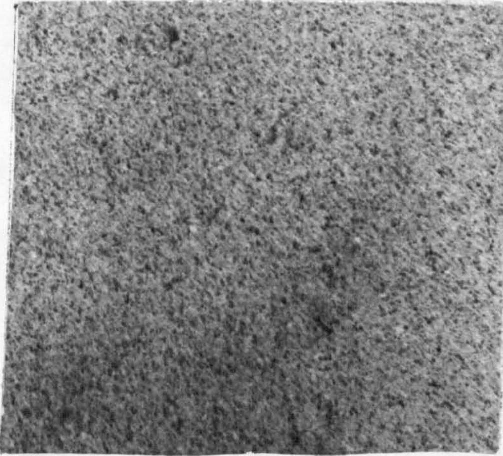

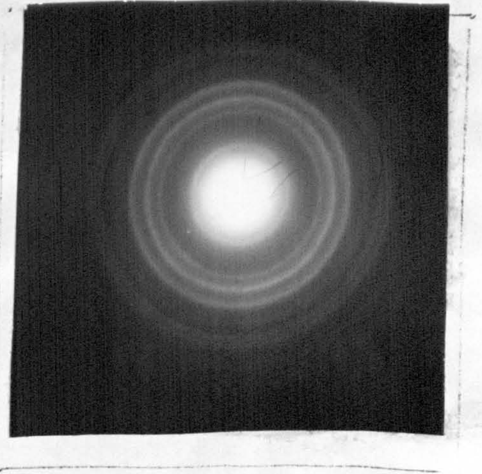

(c) 39Vol% Mn

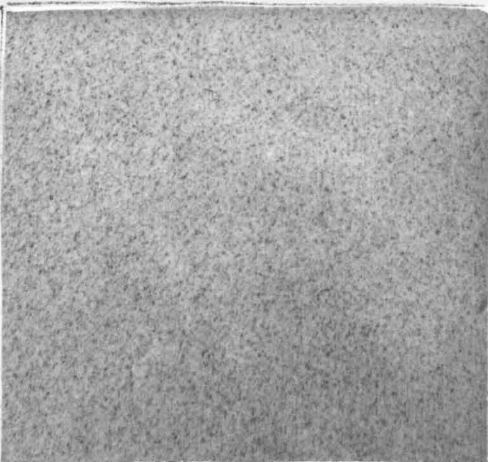

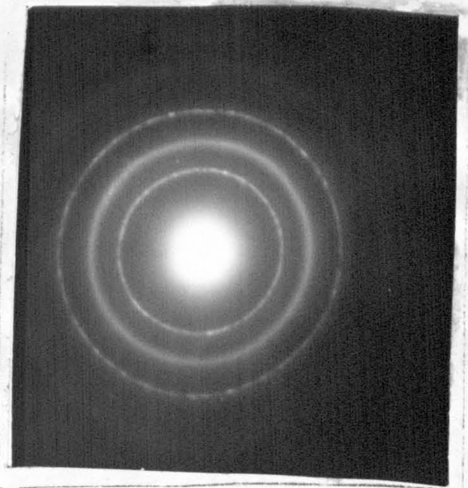

Fig.6.2 Electron Micrographs/Diffraction patterns of Mn and Mn/MgF_2 films 250A thick.

The activation energy for conduction was calculated from the electron micrographs using the Neugebauer and Webb theory [38] (see Section 3.3.1). The results are shown in Table 6.2. It can be seen that the activation energy increases as the Mn content in the film is reduced, which is in agreement with results obtained from resistivity measurement (see Section 6.7.2.1).

Structural investigation detected three distinct phases of Mn: gamma 2UMn at 100% Mn, β - Mn at 63 Vol % Mn and α - Mn at 39 Vol % Mn. These results (Table 6.3) confirm that no chemical reactions occurred between the starting materials and the tantalum

Mn/MgF_2 cermet composition(vol%Mn)	Identification
100	Manganese (I)oxide, gamma 2U Mn.
63	Manganese (II) oxide, β Mn, α MgF_2.
39	MnO_2 (pyrolusite), α Mn, α MgF_2, β Mn.

Table 6.3. Composition of Mn and Mn/MgF_2 cermet films 250A thick.

boat. However the results show that higher oxides of Mn are formed as the volume of Mn in the film is reduced.

Figure 6.3 compares the Mn/MgF_2 cermet system with the few available resistivity - composition data for other cermet systems containing MgF_2. These all show that ρ rises as the insulator content rises, but the rate of change of ρ with composition is different, as shown in Figure 6.3 possibly due to different deposition parameters. The graphs are interesting because they show that with Au/MgF_2 and Cr/MgF_2, the film resistivity tends to within one order of magnitude of the respective bulk metal values as the metallic content of the film approaches 100%; the bulk resistivities of a number of metals at room temperature are given in Table 6.4. Similarly the bulk and film resistivities for Mn and Mn/MgF_2

Metal	Bulk Resistivity at 295K ($\mu\Omega$-cm)	Reference
Ag	1.47	Maissel[26]
Cu	1.69	Maissel[26]
Au	2.44	Maissel[26]
Cr	12.9	Maissel[26]
α-Mn	185	Hampel[73]
β-Mn	44	Hampel[73]
γ-Mn	60	Hampel[73]

Table 6.4. Bulk resistivities of some Metals at 295K.

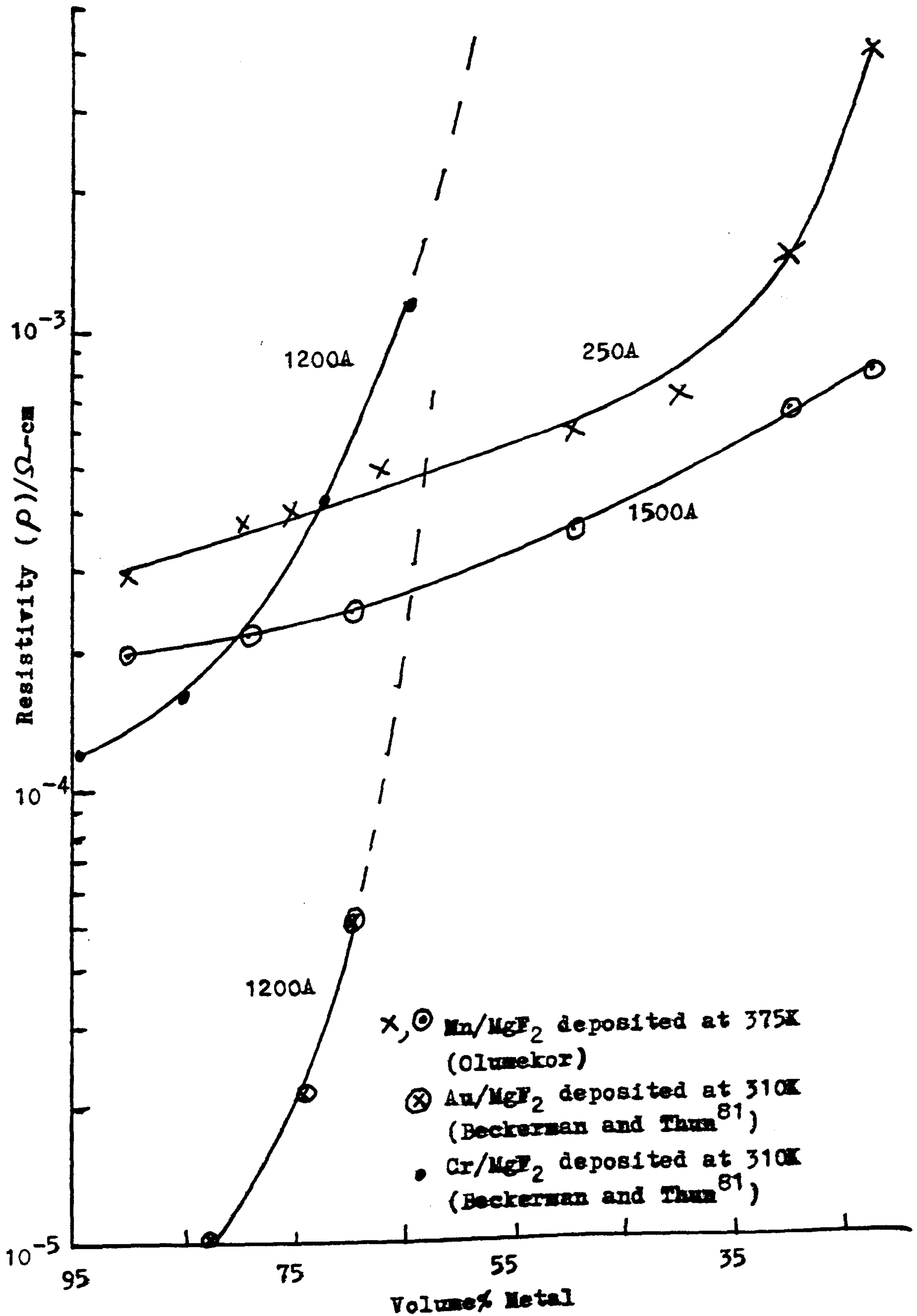

Fig.6.3 Resistivity Vs Composition of Metal/MgF_2

films agree within one order of magnitude, of the value for α-Mn if the latter is always used for bulk manganese. It can be seen that the bulk resistivity of gamma 2U Mn is about three times lower than that for α-Mn (Table 6.4). As α-Mn was identified in the 63 and 39 Vol % Mn films (Table 6.3), it is also possible that α-Mn is partly responsible for the observed increase in ρ with increase in MgF_2 content.

Figure 6.3 also helps to support the Fuchs- Sondheimer theories (equations 3 - 5 and 3 - 6) which state that the resistivity of a thin metallic film is dependent on its bulk metal resistivity. This figure shows that for 100% metal, Mn thin films have the highest resistivity followed by Cr and Au thus agreeing with the data in Table 6.4.

Comparing Cr/SiO with Au/SiO in Figure 6.4, we see that the former has the higher resistivity. However when these systems are compared with Mn/MgF_2 we find that at high metallic content 45 to 85 Vol % metal) the film resistivities of all but Cr/SiO [81] are within the same order of magnitude but differ markedly as the metallic content is decreased. Unlike Au/MgF_2 and Cr/MgF_2, the Au/SiO and the Cr/SiO graphs appear to be generally parallel to one another, although the Cr/SiO system [83] shows a "double-critical" composition region. Also it may be noted that the Mn/SiO system [55] shows a resistivity peak at about 85 Vol % Mn. Both the double critical composition region [83] and the resistivity peak [55] have been attributed to the formation of Cr and Mn silicides respectively.

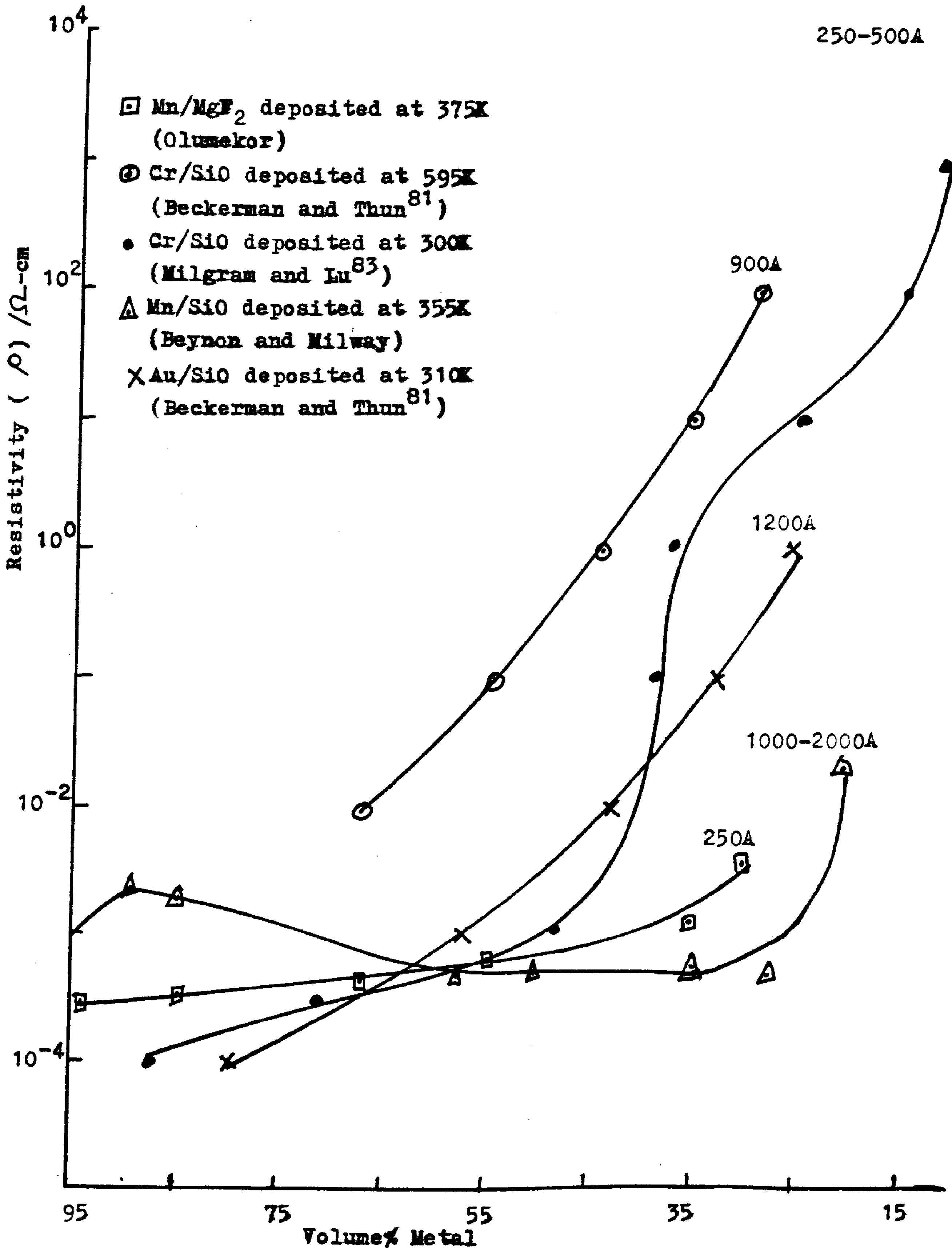

Fig.6.4 Resistivity Vs Composition of various Cermet Systems

The convergence of film resistivity towards the same order of magnitude has been observed by Neugebauer [66] for the Cr/SiO, Cr/SiO_2, $NiCr/SiO_2$, Cr/Si, Au/SiO and Au/SiO_2 cermet systems. He postulated that regardless of metal or deposition conditions, one curve alone gives a good fit for all metal/SiO cermet films, because their resistivities are determined only by the extent of volume dilution of the metal by the SiO or SiO_2. This conclusion seems doubtful because certain deposition parameters have been found to cause drastic changes in Mn/MgF_2 films [82, 91, 92] (see Sections 6.3 to 6.7). Figure 6.4 also shows that the postulate is only correct within a range of compositions (45 to 85 Vol % metal). Beckerman and Thun's results (Figure 6.3) also show that Neugebauer's postulate is not valid for Cr/MgF_2 and Au/MgF_2 cermet films with more than 65 Vol % of metal.

It can be thus seen that the resistivity of all cermet films containing MgF_2 increases only by about two orders of magnitude between 85 and 15 Vol%metal whilst the resistivity of those containing SiO increased by over four orders of magnitude.Also at 25Vol% metal,cermet films containing Mn are at least about two orders of magnitude lower than those containing Au and Cr.A combination of these two components (Mn and MgF_2) gave a resistivity increase of about one order of magnitude from 85 to 25 Vol% Mn.

6.3. VARIATION OF RESISTIVITY WITH THICKNESS

The variation of resistivity ρ with Mn and Mn/MgF_2 cermet film thickness is shown in Figure 6.5. It appears to consist of three distinct regions labelled A, B and C for convenience.

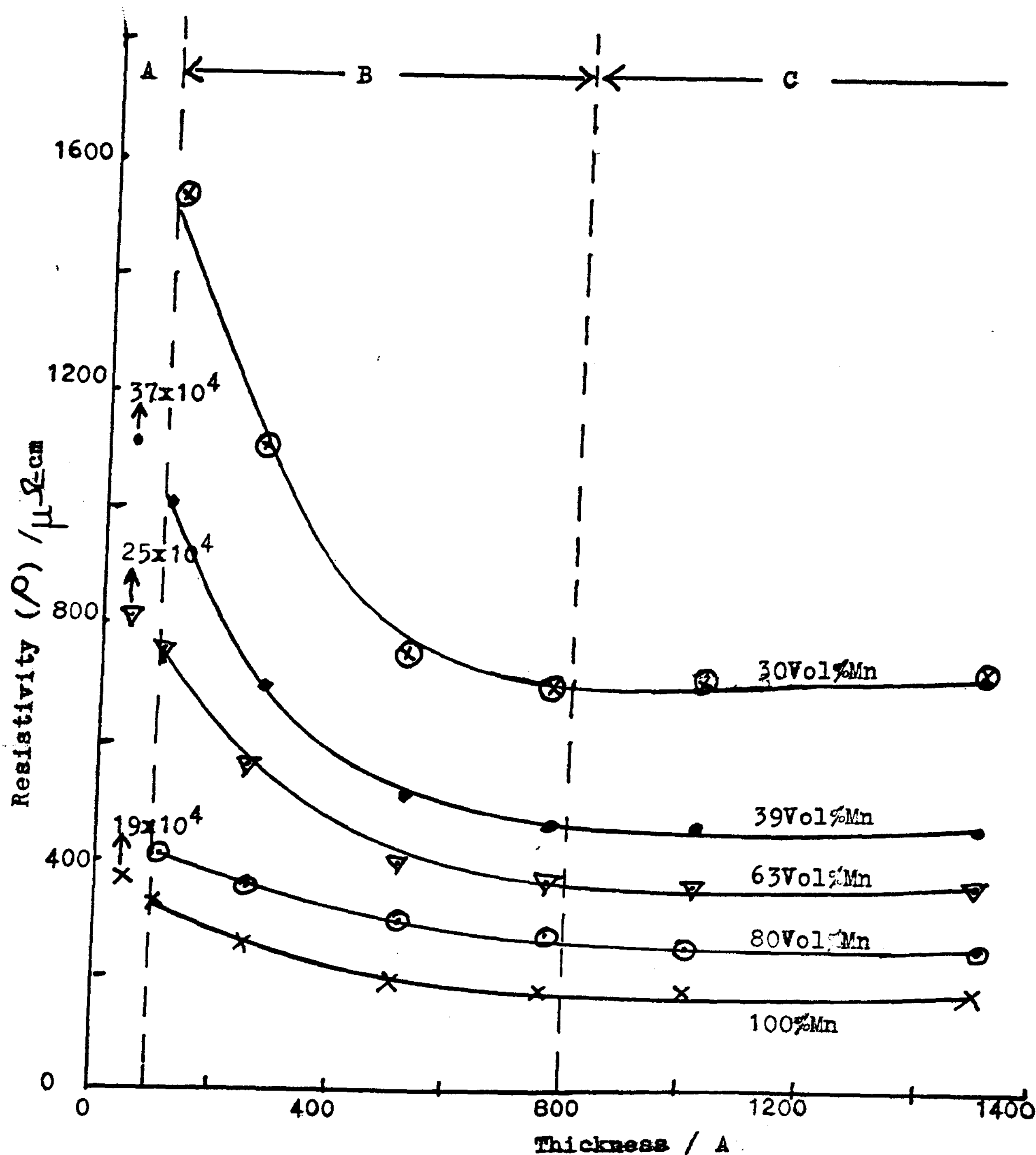

Fig. 6.5 Resistivity Vs Thickness for Mn/MgF_2 Cermets

Deposition Temperature 375K

Deposition Pressure $1x10^{-5}$ torr

Deposition Rate $4As^{-1}$

Region A ($< 100A$) is characterised by a sharp rise in ρ for a small fall in film thickness. For example ρ is $700\mu\Omega$ - cm for a 100A thick film of composition 63 Vol % Mn and rises to about 0.25 Ω - cm at 50A.

No electron micrographs were taken for films of 50A thickness but those for the 250A (Fig. 6.2) show a discontinuous film structure consisting of discrete metallic islands separated by dielectric. Hence region A must be characterised by such structural discontinuity. However, the dielectric spacing in this region will be larger and the metallic islands smaller. In the cermet films, such dielectric spacings are composed of MgF_2 and free space if the metal/insulator composition is to be preserved.

All films investigated showed an amorphous structure. The resistivity in this region is mainly due to the small size of the metallic islands and their large intermetallic islands separations. Films in this region were found to be highly sensitive to various deposition parameters, such as substrate temperature (Section 6.4), deposition rate[92] (Section 6.5) and deposition pressure [82] (Section 6.6), especially when the thickness falls to $\sim$ 50A. For these reasons films having reproducible values of resistivity were difficult to fabricate. A resistivity spread $\sim \pm 25\%$ was obtained for films 50A thick.

In region B, ($\sim$ 100 to 800A) large non-linear variations occur in ρ as the film thickness is increased from 100A. These variations are largest at 100A and become progressively smaller near 800A, as the film becomes structurally continuous. Films in this region are less sensitive to deposition rate and deposition

pressure than those in region A, but they are very sensitive to substrate temperature [60] (Section 6.4). Substrate temperature may decide whether the film becomes continuous or not. A resistivity spread ~ ± 10% was obtained for films in this region.

In region C (> 800A), the resistivity appears to be constant and independent of film thickness because the films have become electrically and physically continuous. It may also be noticed that the resistivity of the 100% Mn film in this region is about 170 $\mu\Omega$ - cm which is about three times higher than the value for gamma 2U Mn (see Section 6.2). Further a high degree of reproducibility was achieved as the cermets are not greatly affected by deposition parameters and further increase in film thickness. For a given substrate material and deposition mechanism, the factors controlling resistivity in this region are cermet composition and substrate temperature.

6.4. VARIATION OF RESISTIVITY WITH SUBSTRATE TEMPERATURE

As we have seen in Chapter 2, substrate temperature is the most important parameter affecting the nucleation and growth of a vacuum-deposited thin film. It appears to lower the degree of supersaturation, reduces the mean incident time of an adsorbed atom and increases the surface diffusion coefficient of the adsorbed atom.

Figure 6.6 shows how ρ varies with substrate temperature for 100% Mn films and 39 Vol % Mn cermets, 250, 500 and 1000A thick deposited at a constant rate (4 As^{-1}) and at a constant residual gas pressure (1×10^{-5} torr). The graphs are roughly similar in

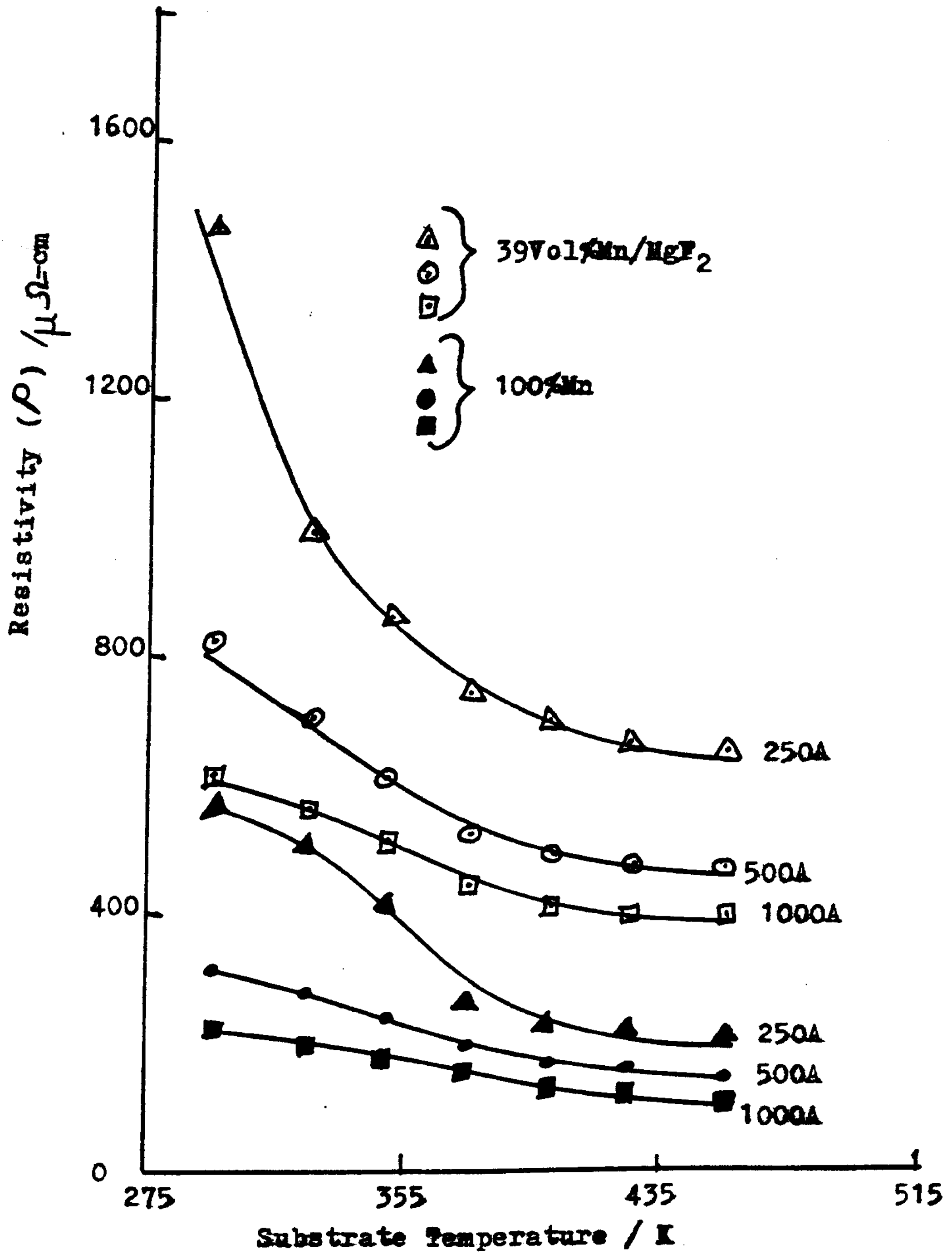

Fig.6.6 Resistivity Vs Substrate Temperature

shape and show a fall in ρ as the substrate temperature is increased from 295 to 455K. For each film this fall in ρ appears to be most rapid between 295 and 395K. However the magnitude of the fall in ρ is strongly dependent on the thickness of the film. For example the fall in ρ for the 39 Vol % Mn cermet in this temperature range are respectively 825 and 220 $\mu\Omega$ - cm for thicknesses of 250 and 1000A. The corresponding fall in ρ for the 100% Mn films are respectively 370 and 125 $\mu\Omega$ - cm.

We saw in Section 6.3 (Fig. 6.5 region C) that ρ for structurally continuous films varies only slightly with thickness. Similarly we find here that region C films are least affected by the increase in substrate temperature when compared with those in regions A and B.

The change in resistivity due to increasing substrate temperature arises from two main sources, assuming there is no contamination or the level of contamination is constant:

(i) a fall in the number of structural defects of which more are found in films deposited at low substrate temperatures; and/or

(ii) a fall in electron scattering at the grain boundaries.

Neugebauer [89] has indicated that dislocations are the most frequently encountered lattice defects in vacuum-deposited thin films. Their density is about $\sim 10^{10}$ to 10^{11} lines cm $^{-2}$. However, according to Maissel [93] (Table 6.5), they contribute very little to film resistivity. Also it would appear that the contribution to film resistivity from vacancies and interstitials is

Types of Defects	Contribution to film resistivity $\mu\Omega$-cm
Dislocations	0.1
Vacancies	0.5
Interstitials	1.0
Grain Boundaries	40.0
Impurities in equilibrium	180.0

Table 6.5. Approximate maximum contribution to the residual resistivity by various types of defects (Maissel [93]).

not significant and that the contribution from grain boundaries is the most important in contamination - free specimens.

Thin films have a larger grain boundary area than bulk material as the average grain size in the former is generally smaller although it is difficult to quantify. The grain size in vacuum-deposited thin films depends on the deposition parameters, as illustrated in Figure 6.7.

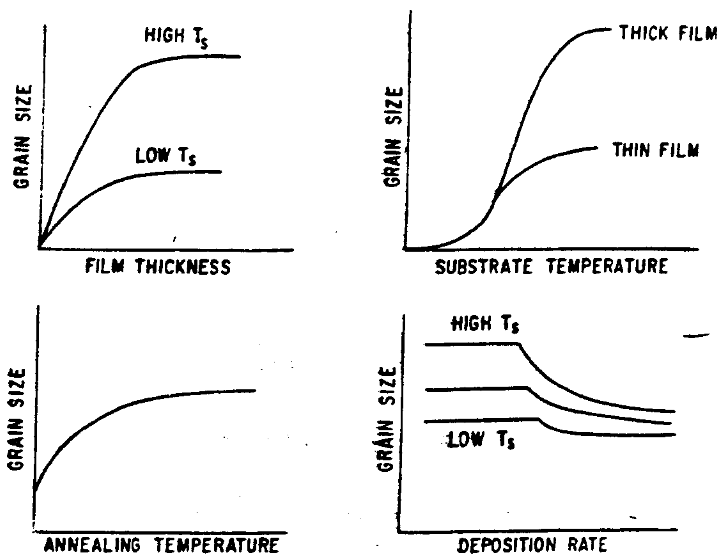

Fig. 6.7. Dependence of grain size on film thickness, substrate temperature, annealing temperature and deposition rate (Neugebauer [102]).

Large grain sizes are expected at high substrate temperatures or annealing temperatures because the surface mobility increases, thus allowing the total energy of the film to decrease by reducing its overall grain boundary area. Low temperature, on the other hand leads to small grain sizes.

If the grain size 2r is smaller than the mfp λ , internal diffuse scattering at the surface will increase the film resistivity. As the temperature is increased the grain size increases. The

activation energy required to transfer an electron from one grain to another is also reduced giving rise to a film of lower resistivity.

From these results and discussions, it would appear that films deposited at low substrate temperatures (295K) are desirable since they provide a higher resistivity than a corresponding film deposited at elevated temperatures (455K). However from experimental observations of pure Mn films and Mn/MgF_2 cermets, the indications appear contrary to these. Films deposited at elevated temperatures are more easily reproduced (for films of 500A thickness, ρ is $\pm$ 10% at 455K and $\pm$ 17% at 295K).

6.5 VARIATION OF RESISTIVITY WITH DEPOSITION RATE

It is generally agreed that the rate at which a film is condensed from the vapour phase _in vacuo_ (deposition rate) influences its electrical and structural properties [94 - 99]. The exact role played by deposition rate in film growth and in determining its electrical resistivity is not clearly understood as various workers [94 - 99] have different opinions about the various parameters which may affect it: viz deposition pressure, substrate material, deposition technique, substrate temperature, cermet material film thickness and source temperature. Ideally all these parameters should be kept constant during film deposition, but this is not always possible. However in this investigation, it was possible to keep all these parameters reasonably constant except source temperature.

Figures 6.8, 6.9 and 6.10 show the variation of resistivity with deposition rate for three compositions and three thicknesses. Figure 6.8 indicates that:

(i) ρ increases with film thickness;

(ii) the deposition rate appears fairly constant below 8 As^{-1}; and

(iii) ρ decreases with increase in deposition rate from 8 to 25 As^{-1}.

The variation of ρ with thickness has been discussed in Section 6.3. The variation of ρ with deposition rate for a fixed thickness (Fig. 6.8) shows that the resistivity of Mn films are higher at low deposition rate (2 to 8 As^{-1}) than at high deposition rates (8 to 25 As^{-1}). The electron micrographs of Figure 6.11 show that Mn films deposited at low rates have a coarse grain structure and those deposited at high rates a finer grain structure.

Figure 6.9 and 6.10 for the cermet films indicate that ρ increases with decrease in metal content. Unlike the pure metal, ρ increases with increase in deposition rate. The electron micrographs in Figure 6.12 also show that the grain size of Mn in the cermet films decrease with increase in deposition rate, but their size is considerably less than those of the pure metal at a corresponding deposition rate.

As discussed in Chapter 2, an evaporant atom impinging on a substrate is capable of executing random motion over the surface of the substrate. The mobility of adsorbed atoms leads to interatomic collision and increased agglomeration. At low deposition

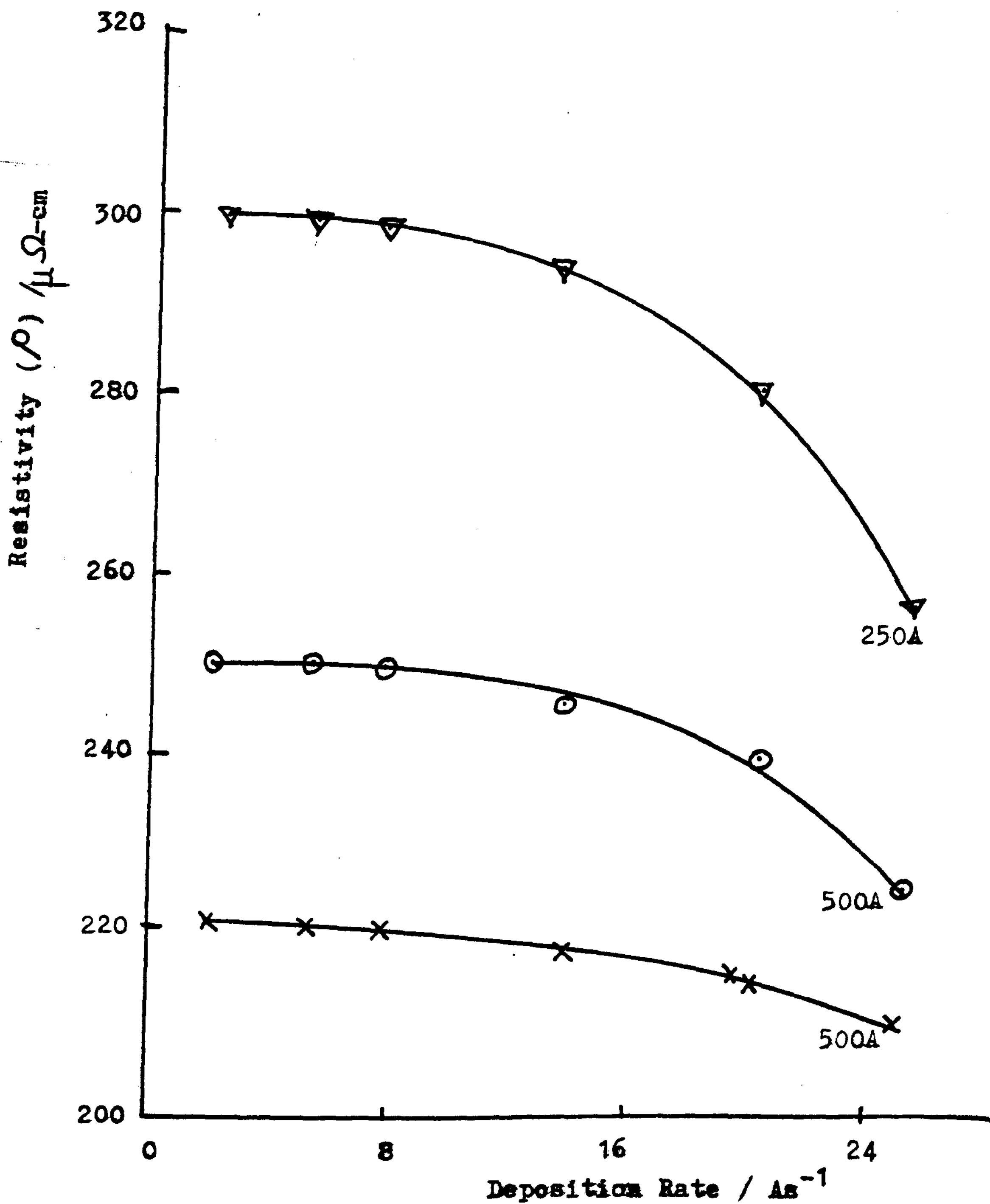

Fig.6.8 Resistivity Vs Deposition Rate
100%m

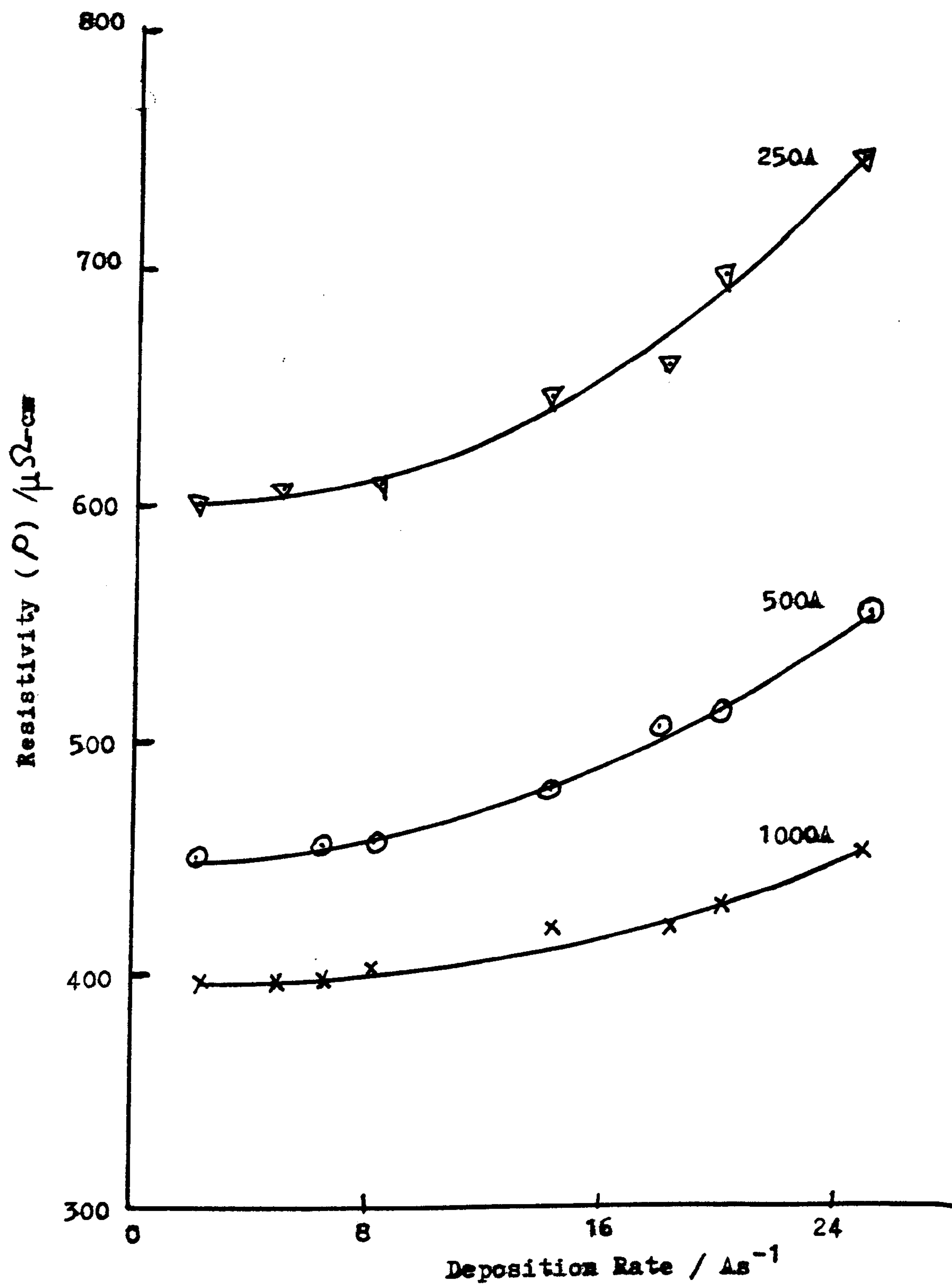

Fig.6.9 Resistivity Vs Deposition Rate
63Vol%Mn / MgF_2

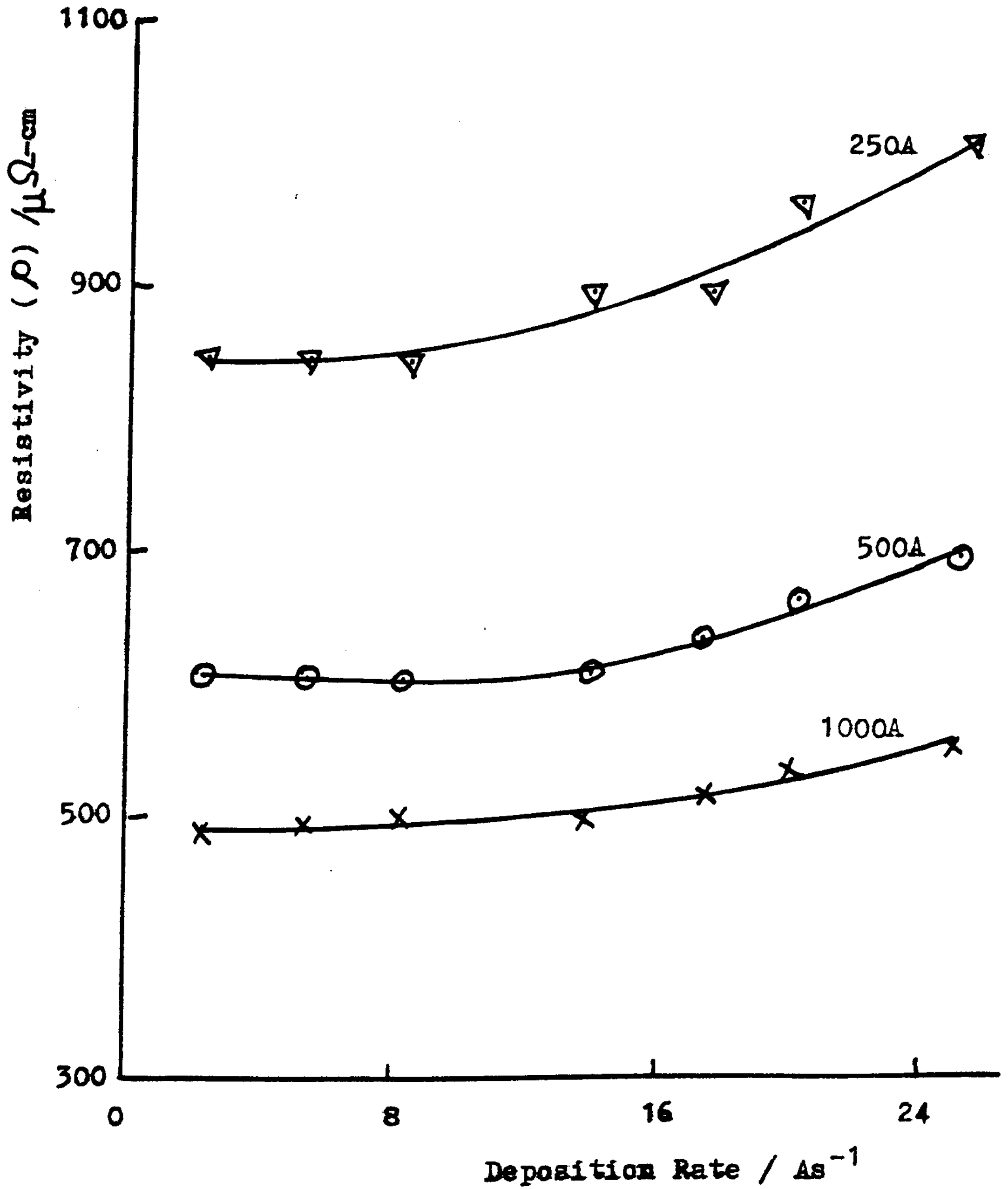

Fig. 6.10 Resistivity Vs Deposition Rate

39Vol%Mn/MgF_2

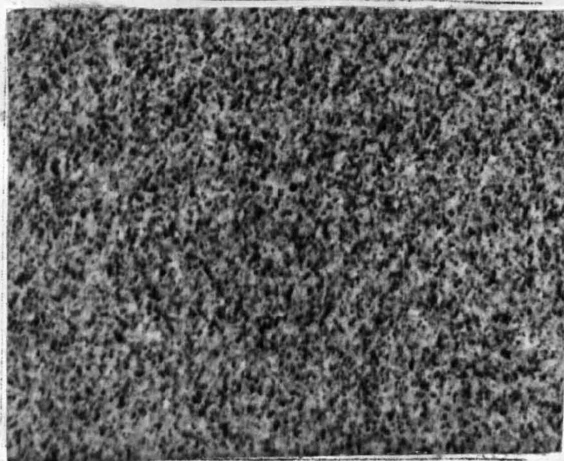

(a) deposited at $2As^{-1}$

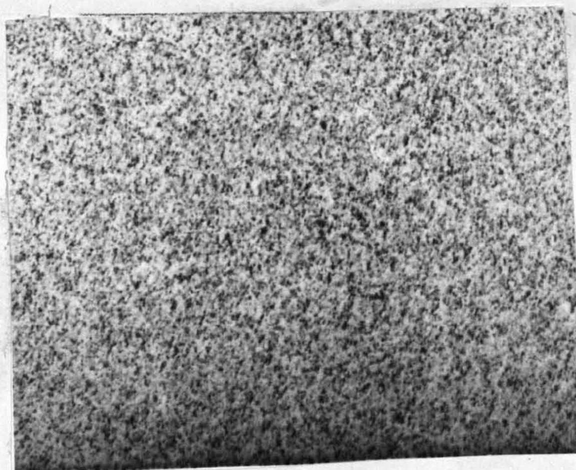

(b) deposited at $5As^{-1}$

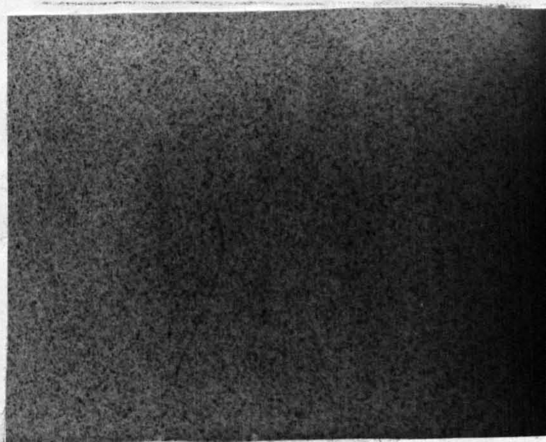

(c) deposited at $25As^{-1}$

0.5μm

Fig.6.11 Electron Micrographs of 100%Mn films 250A thick deposited at various deposition rates.

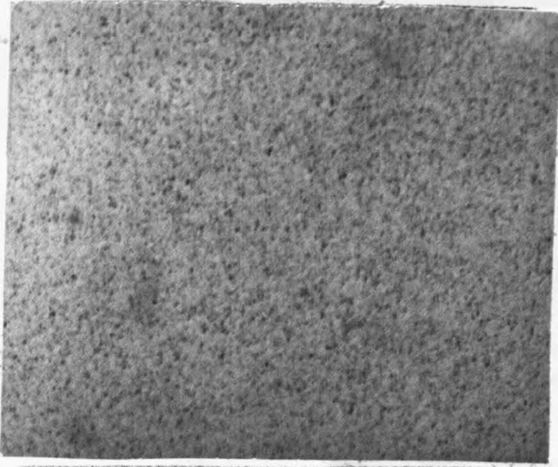

(a) 63Vol% Mn deposited at the rate of $2As^{-1}$

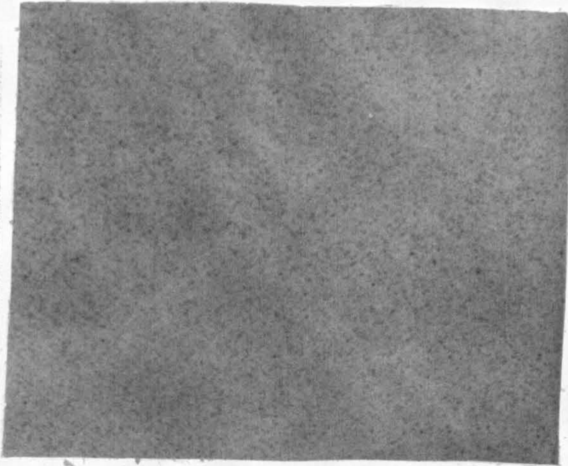

(b) 39Vol% Mn deposited at the rate of $2As^{-1}$

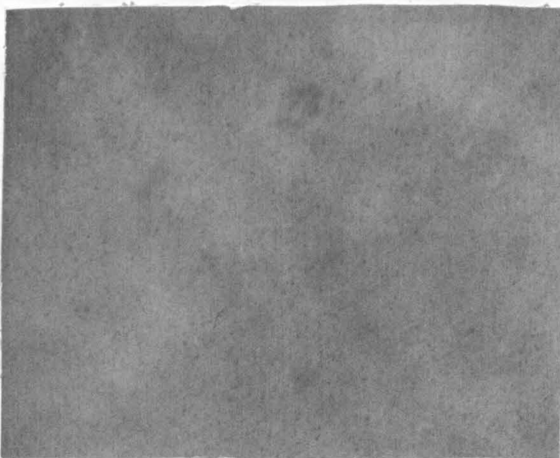

(c) 39Vol% Mn deposited at the rate of $10As^{-1}$

0.5μm

Fig.6.12 Electron Micrographs of Mn/MgF_2 cermet films 250A thick deposited at various deposition rates.

rates, the adsorbed atom are more mobile because the "time lag" between successive impinging atoms is relatively long compared with that for fast deposition. Hence the Mn islands in the pure metallic films are large and their inter-island separation (diffusion length) is also large resulting in high ρ .

As the deposition rate is increased, the "time lag" is reduced, thus reducing both surface mobility and the degree of agglomeration. Hence the Mn island size becomes finer with smaller inter-island spacings leading to a fall in ρ . Island growth in this case may be due to collisions from evaporant atoms impinging on already adsorbed atoms, as opposed to lateral growth in the case of films deposited at low rates.

In the case of the cermet films, both Mn atoms and MgF_2 molecules execute random motion on the substrate at low deposition rates. (Electron microscopic investigations indicate there is no chemical reaction between Mn and MgF_2 in the temperature range 290 to 455K). The rate of agglomeration of Mn - Mn particles should therefore be reduced. This would make the Mn island size in the cermet film smaller than that for a corresponding pure Mn film. These island should also be smaller because the amount of Mn in the cermet is smaller than that in pure manganese films of the same thickness.

Another possible explanation for the fall in island size with rise in deposition rate may be as follows:

(i) Neugebauer [89] postulated that for an inhomogeneous substrate, a relatively high density of small islands is formed at

tight binding sites (valleys). He obtained support for his hypothesis from Au films [96] deposited on rock salt. These films indicated that a high density of smaller island are formed in the region of the "staircase" of cleavage. The MgF_2 atoms may therefore be thought of as making the substrate less homogeneous to the impinging Mn atoms.

(ii) Campbell [100] observed that the tensile stress in LiF films deposited on mica increases with an increase in deposition rate. For example the tensile stress of a film 1000A thick is 6×10^{14} N m^{-2} at 6 As^{-1}, 9×10^{14} N m^{-2} at 50As^{-1} and 12×10^{14} N m^{-2} at 65A. Hence the increase in ρ with increase in deposition rate for Mn/MgF_2 cermet films may be due to the higher number of stresses present assuming that stress - deposition rate characteristic of MgF_2 and LiF are similar.

It was not possible to compare the present results (Mn/MgF_2) with those of other workers as there appears to be an absence of published data in this area. However in the case of pure metallic films where some data are available, no clear pattern has emerged for the relationship between deposition rate and film resistivity.

Learn and Spriggs [101] observed that the critical thickness (i.e. thickness at which the film becomes structurally continuous) of lead films deposited at 300K on crystalline quartz is constant at 400A when the deposition rate is low 0.25 to 0. 5As^{-1}, increases rapidly to a peak at 950A as the deposition rate is increased to 1As^{-1}, and then falls rapidly with further increase in deposition rate. If a structurally continuous film indicates a low film resistivity (see Fig. 6.5) it follows that ρ for the lead film was probably constant between 0.25 and 0.5 As^{-1}, then

rose to a peak at 1As $^{-1}$ before falling with further increase in deposition rate. They also obtained a similar result for tin films.

Fridrich and Kohout [97] have observed a decreasing agglomeration with increase in deposition rate for Aluminium films deposited on ceramic substrates. The critical thickness in these films occurred at 55A for a deposition rate of 6.6 As $^{-1}$, 122A for 1.3As $^{-1}$ and 260A for 0.64 As $^{-1}$. These results suggest a decrease in ρ with increase in deposition rate.

Adamov et al [98] found that the resistivity of sputtered and vacuum-deposited Au films on Borosilicate glass was higher at low deposition rates. For example, a thermally-evaporated film 600A thick has a resistance of 5 Ω when deposited at 0.5As $^{-1}$ and 3 Ω when deposited at 1As $^{-1}$. The corresponding values for sputtered films were respectively 2.5 Ω and 1.5 Ω.

The phenomena of decreasing agglomeration with increase in deposition rate is the most frequently observed in thin film studies. Thun [94] has postulated that a minimum deposition rate exists above which this phenomena will be observed and below which agglomeration remains constant with decrease in deposition rate. This is in agreement with results of Figure 6.8. His results for Cr films 1000A thick (Fig 6.13) also show that agglomeration decreases with increase in substrate temperature, and at a substrate temperature of about 300K the Cr island diameters were constant, and independent of deposition rate from about 10 to 450 As $^{-1}$.

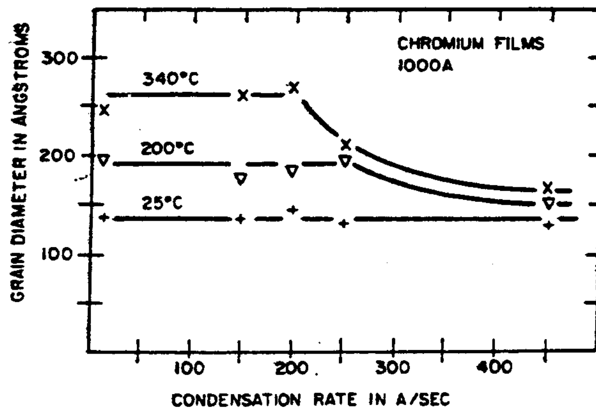

Fig. 6.13. Grain diameter from X-ray diffraction line broadening Vs condensation rate (Thun [94])

Using a Velocity selector to keep the incident kinetic energy of impinging atoms constant, Chopra and Randlett [103] observed that the island size in Au and Ag films deposited on glass and rock salt increased with increase in deposition rate to a maximum at about $20As^{-1}$. At higher rates $> 20As^{-1}$ the trend was reversed and agglomeration decreased with increase in deposition rate.

In a subsidiary study, it was observed that Mn/MgF_2 cermets prepared by a two boat arrangament (Section 4.1.1.1.1) have 20 to 30% higher resistivities compared with cermets prepared by the single boat method; in both cases the films have roughly the same thickness,

composition, substrate material, and were prepared at about the same residual gas pressure and substrate temperature. The only difference between the two techniques being that with the single boat system, the deposition rate was kept constant ($4As^{-1}$) at all cermet compositions whereas with the two boat system, the deposition rate of one boat was varied with respect to the other in order to obtain the required composition. However with pure Mn, both techniques produced films whose resistivities agreed to within $\pm 5\%$ for the same deposition rate $4As^{-1}$.

It was also observed that, the higher the deposition rate, the more difficult it is to obtain repeatable readings. ρ values for five separate runs at $50As^{-1}$ showed up to 50% deviation from the mean value whilst a deviation of 5% and 17% were obtained at $2As^{-1}$ and $25As^{-1}$ respectively. Scratch tests on these films also revealed that their hardness decreased with increase in deposition rate. Above $50As^{-1}$ it was possible to disrupt the film by wiping it with a clean lens tissue.

These results show that:

(i) a higher film resistivity may be achieved in pure Mn films by decreasing the deposition rate but the reverse is true for Mn/MgF_2 cermet films;

(ii) a high degree of reproducibility may be achieved by depositing Mn and Mn/MgF_2 cermet films at low rates (2 to $8As^{-1}$); and

(iii) poor adherence of the film to substrate occurs at high deposition rates ($> 50As^{-1}$).

6.6. VARIATION OF RESISTIVITY WITH RESIDUAL GAS PRESSURE

When thin films are fabricated by vacuum-evaporation, the chamber pressure is usually kept as low as possible in order to reduce the degree of contamination. Contamination usually arises from the interaction of the residual gases in the chamber with the evaporant vapour and/or with the adsorbed evaporant atoms/molecules at the substrate. Such contamination may alter the electrical and structural properties of the film. In the present study, the effect on the resistivity of Mn and Mn/MgF_2 cermets of varying the pressure of air and argon was investigated. Here the films were 250 and 500A thick and were prepared at a constant deposition rate ($4As^{-1}$) on mica pre-coated with carbon and Corning 7059 glass substrates held at 295K. The chamber pressure was varied from $5x10^{-6}$ to $5x10^{-4}$ torr for air and $1x10^{-5}$ to $5x10^{-4}$ torr for argon.

The results are presented in Figure 6.14 for the 250A films and Figure 6.15 for the 500A films. For a given film composition ρ increases with increase in pressure. This increase is gradual at first tending to saturate at around $5x10^{-4}$ torr. With each gas $\frac{\Delta\rho}{\Delta P}$ tends to increase as the insulator content increases. It can also be seen that for a given composition, thickness and pressure, the resistivity of films deposited in air is higher than those deposited in argon. For example, with the 100% Mn films 250A thick, ρ is 900 $\mu\Omega$ - cm when the film is deposited in air at a residual gas pressure of $5x10^{-5}$ torr and 702 $\mu\Omega$ - cm when deposited in argon, a fall of $\sim$ 22%. With the 100% Mn films 500A thick, deposited at $5x10^{-5}$ torr, the corresponding fall in the resistivity

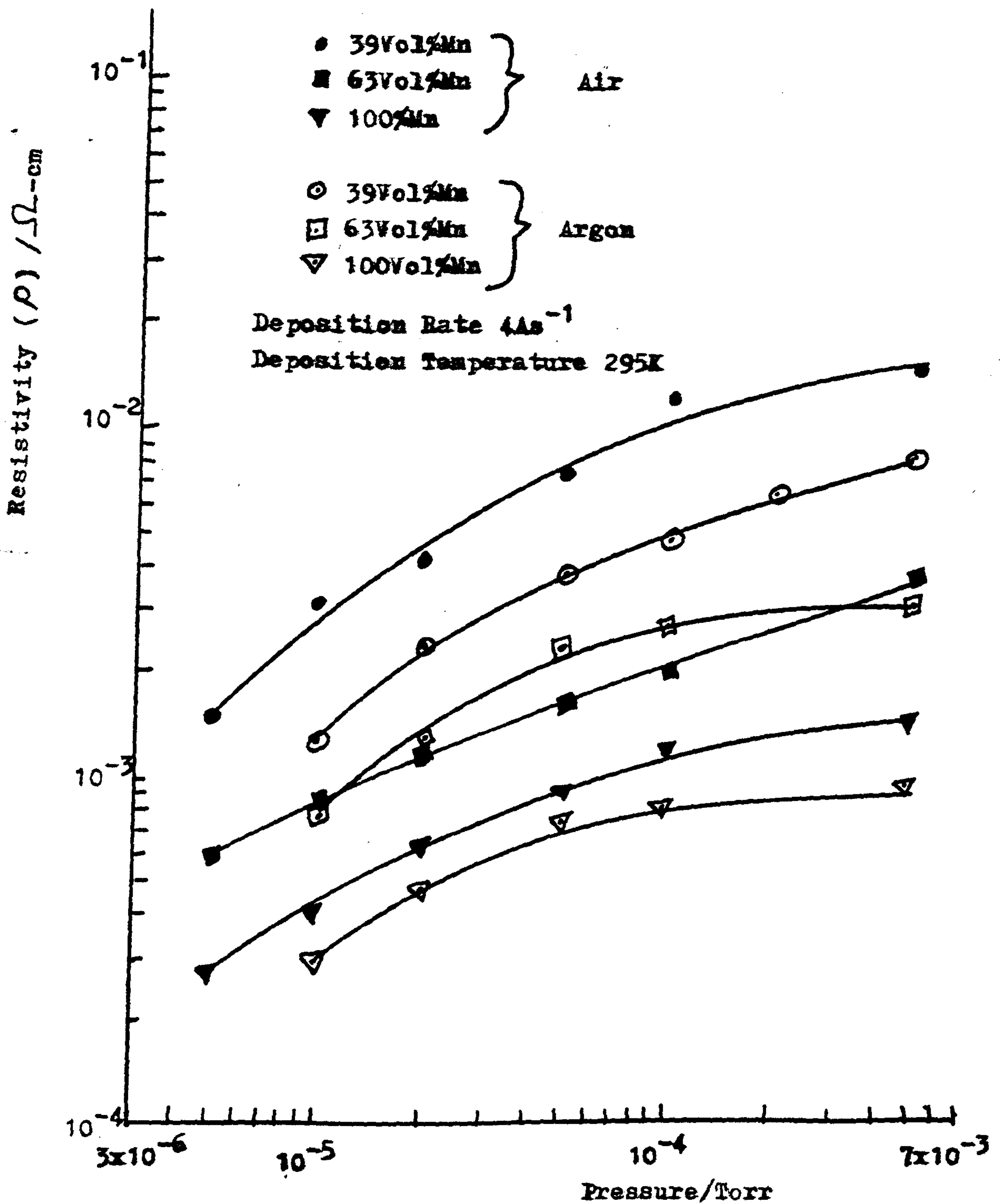

Fig. 6.14 Resistivity Vs Pressure for Mn and Mn/MgF_2 films 250A thick.

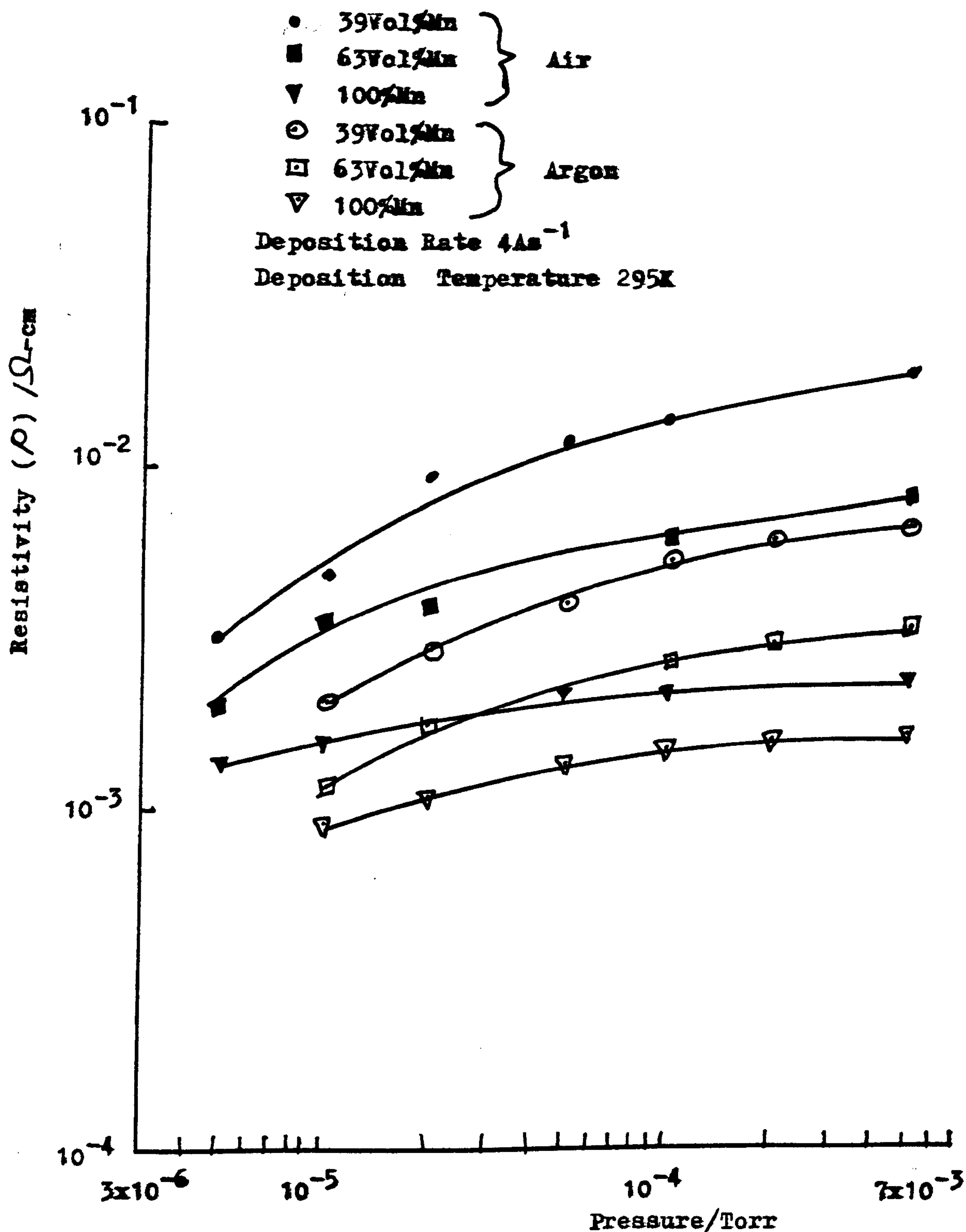

Fig. 6.15 Resistivity Vs Pressure for Mn and Mn/MgF_2 films 500A thick.

of air deposited films was $\sim$ 30%.

With cermet films, the fall in ρ appears to be larger. For example, the 63 Vol % Mn cermet, 500A thick, and deposited at 5×10^{-5} torr, has a resistivity in air of 580 $\mu\Omega$ - cm and 240 $\mu\Omega$ - cm in argon, a fall in ρ of about 60%.

The electron micrographs for the 100% Mn air-deposited films (Fig. 6.16) clearly shows that the size of Mn islands decreases as the deposition pressure is increased.

As the chamber pressure is reduced, the number of residual air molecules trapped in the vapour stream per unit time decreases. Hence substrate contamination should decrease which implies that the surface mobility of adsorbed Mn atoms increases. If we assume that most of the vapour-gas collisions occur on the surface of the substrate, this results in increased agglomeration and hence a lower film resistivity. This assumption is not unreasonable if one considers that the m.f.p of air at 1×10^{-4} torr is $\sim$ 50 cm at 295K, so that the probability of forming oxide molecules through collisions in the vapour phase will be very small. Instead collisions are more likely to take place at the substrate surface which is exposed to the evaporant and air molecules.

It is known [104, 105] however, that the oxidation of a metal surface proceeds at particular nucleation sites and results in the formation of a non-homogeneous oxide layer. The latter prevent surface diffusion and so reduces agglomeration. The higher resistivity of air-deposited films over the argon-deposited ones can probably be

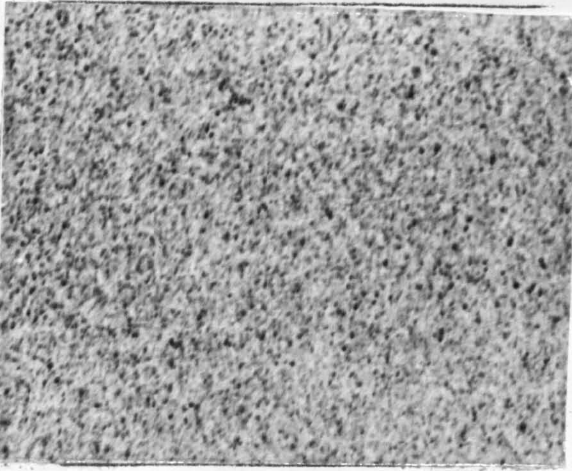

(a) 100%Mn deposited at $1x10^{-5}$torr.

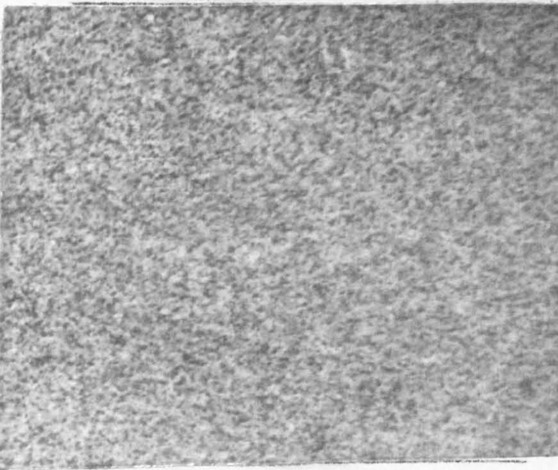

(b) 100%Mn deposited at $1x10^{-4}$torr.

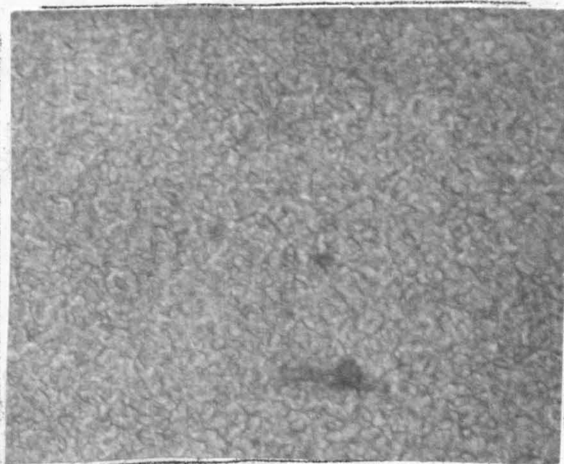

(c) 100%Mn deposited at $5x10^{-4}$torr.

0.4μm

Fig. 6.16 Electron Micrographs of pure Mn films 250A thick deposited at different air pressures.

accounted for in most part by oxidation although no definite structure could be obtained using a transmission electron diffraction technique.

6.7. HEAT - TREATMENT OF PURE Mn AND Mn/MgF_2 CERMET FILMS

The films used in this investigation were prepared by the method described in Chapter 5. After fabrication the films were transferred into the auxiliary vacuum plant (see Section 4.2.1) and their temperature raised gradually at a rate of 4K min^{-1} from about 295 to 620K. The film were held at the annealing temperature for a period varying from 1 to 3 hours. Then the temperature of the film was cycled between 620 and 110K. The film resistivity was monitored throughout the heat treatment (annealing) and the temperature cycling operation (post-annealing).

Figure 6.17a is a schematic representation of the resistivity-temperature graphs for both pure Mn and Mn/MgF_2 cermets with thicknesses $\geq$ 1000A whereas Figure 6.17b represents those for Mn/MgF_2 cermets $\leq$ 500A. The graphs have been divided into two regions A and B for convenience, depending on whether they show a reversible or an irreversible change in resistivity with change in temperature.

6.7.1. ANNEALING

Figure 6.18 shows the actual resistivity variation with annealing temperature for the 100% Mn, 63 Vol % Mn and 39 Vol % Mn cermets of 500A thickness. These curves correspond to region A in Figure 6.17.

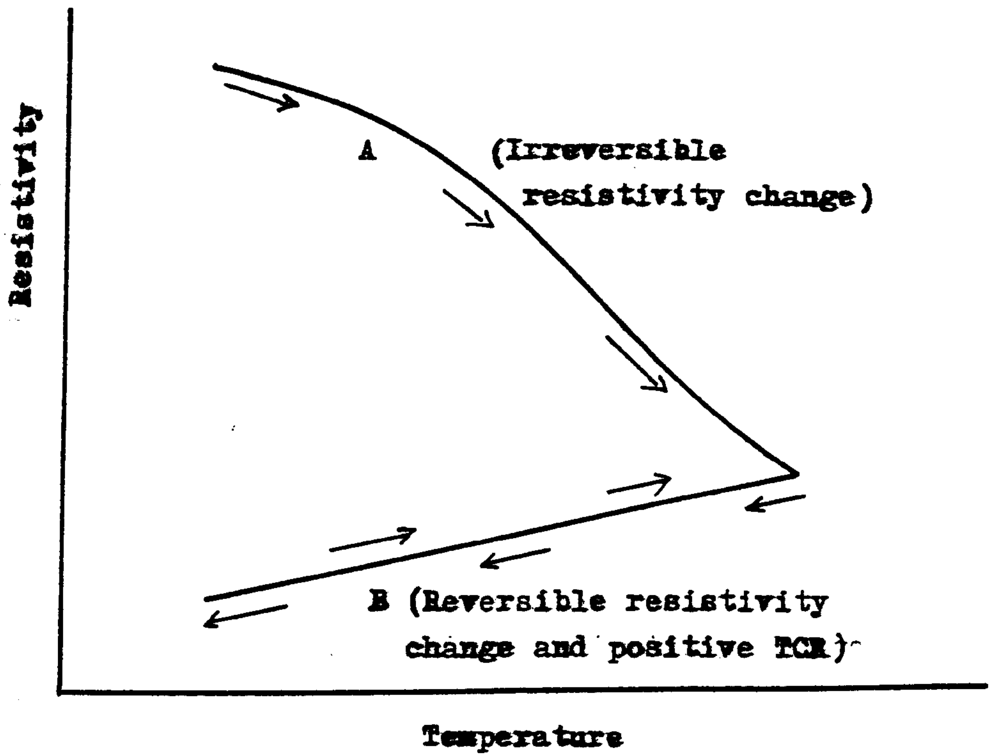

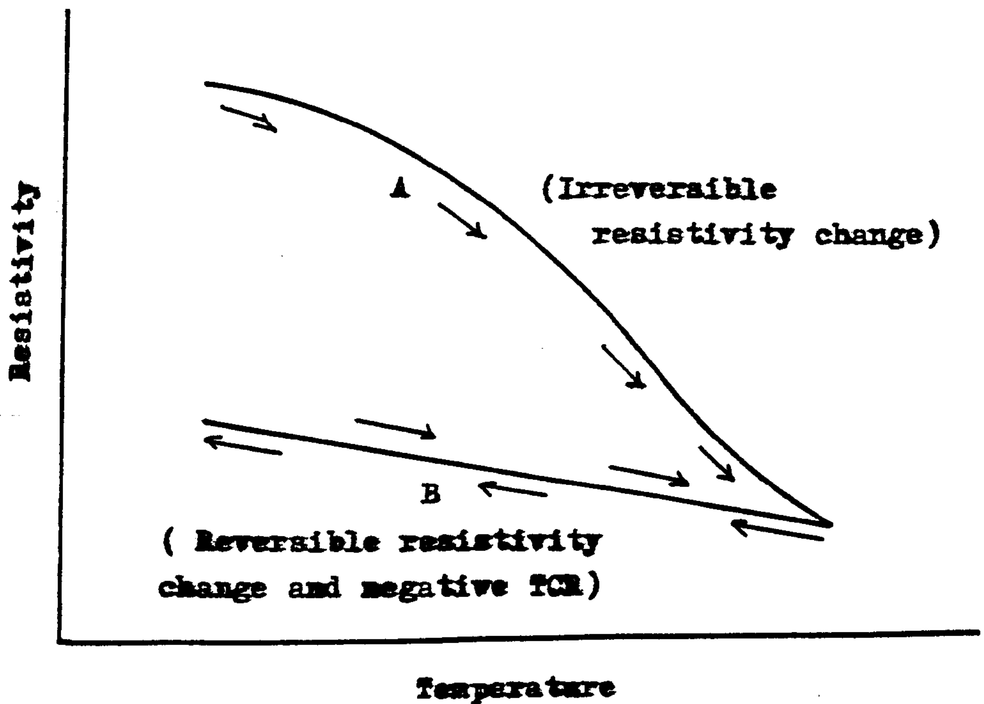

Fig.6.17 schematic representation of Heat treatment of Mn and Mn/MgF_2 thin films

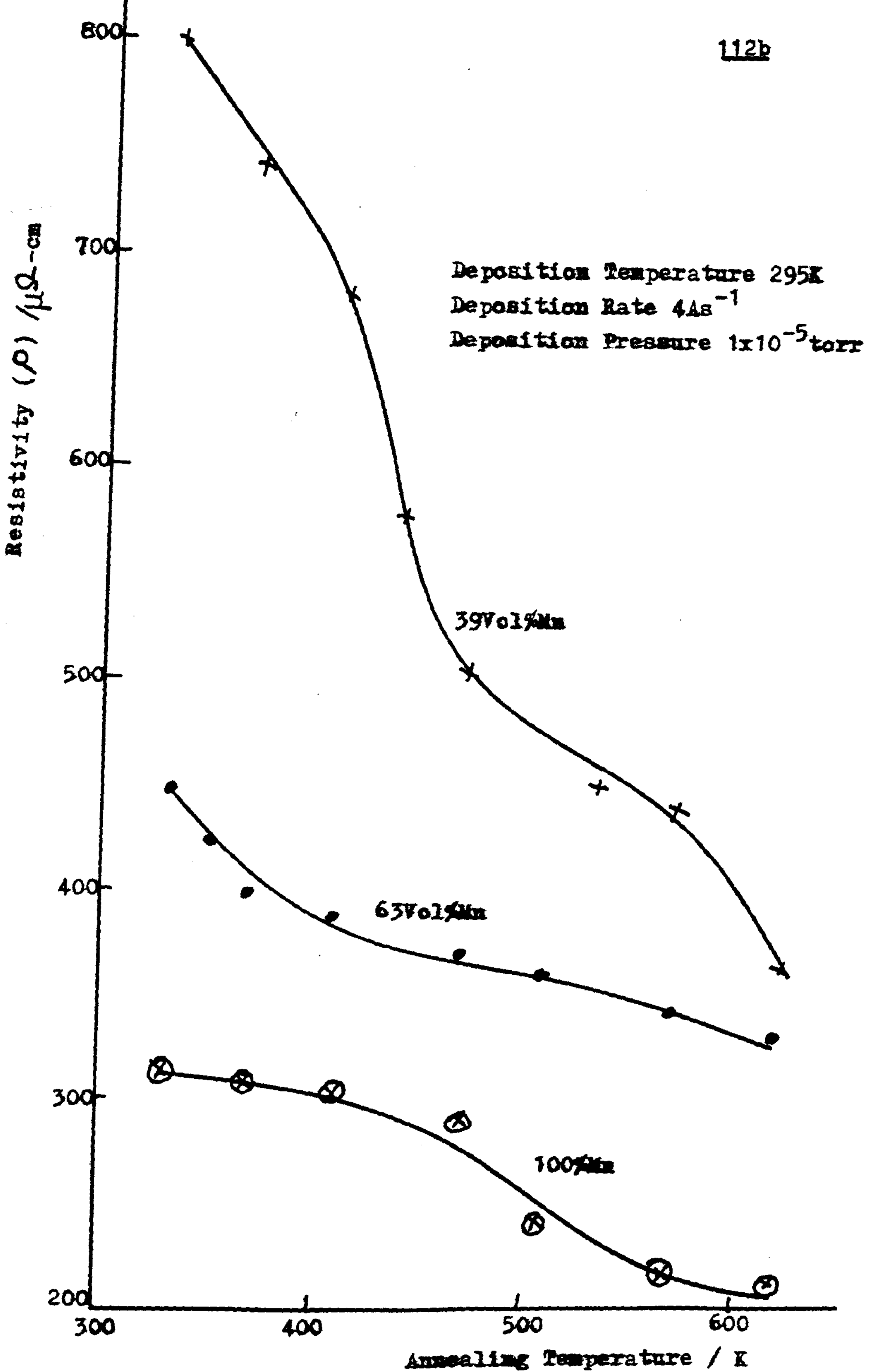

Fig. 6.18 Resistivity Vs Annealing Temperature for Mn/MgF_2 films 500A thick.

Pure Mn films experience a fall in ρ with rise in annealing temperature. Initially ρ decreases very slowly from 312 $\mu\Omega$ - cm at 295K to 305 $\mu\Omega$ - cm at 410K, then more rapidly from 305 to 235 $\mu\Omega$ - cm between 410 and 575K and finally drops off again beyond 575K.

The resisitivity of the cermet films can be seen to decrease rapidly as the annealing temperature is increased, the decrease being most rapid between about 400 and 500K. However the fall is steeper in the 39 Vol % Mn films than in the 63 Vol % Mn. Similarly the fall in the 63 Vol % Mn films is steeper than that for the 100% Mn.

A similar decrease in ρ was obtained with films deposited at elevated substrate temperatures (295 to 455K) (see Section 6.4). The important difference between the two experiments being that films deposited at elevated substrate temperatures (Fig. 6.6) have a lower resistivity than those annealed at a higher temperature (see Table 6.6).

The fall in ρ with increase in the annealing temperatures is usually attributed to the removal of structural defects incorporated into the film during growth, as this process is irreversible. The result in Figure 6.18 suggests that the number of structural defects in the films increases as the MgF_2 content increases. Like films deposited at elevated temperatures (Fig. 6.6), these films (Fig. 6.18) exhibit a less steeper fall in ρ with increase in film thickness.

Mn/MgF_2 Composition (vol.% Mn)	Annealling or deposition temperature (K)	RESISTIVITY at 295K ($\mu\Omega$ - cm) Films deposited at 295K and then annealed	Films deposited at elevated temperature
100	295	315	312
	350	250	312
	400	176	306
	455	150	288
63	295	490	450
	350	425	425
	400	365	388
	455	315	370
39	295	825	800
	350	620	775
	400	500	700
	455	475	550

Table 6.6. Resistivity of Mn and Mn/MgF_2 films, 500A thick, deposited at 295K and then annealed compared with that for films deposited at elevated temperatures.

As we have seen in Section 6.4, an increase in substrate temperature may lead to an increase in agglomeration. This may account for part of the observed fall in ρ . The electron micrographs in Figure 6.19 show that there was a considerable mass transfer in both pure Mn and Mn/MgF_2 cermets of 250A thickness, annealed at 620K for 1 hour.

Vand [106] has also given an explanation for the fall in resistivity of metallic films with annealing temperatures. In the next section, an attempt is made to interprete the fall in ρ of pure Mn films in terms of his theory.

6.7.1.1. VAND'S THEORY [106] OF THE EFFECT OF ANNEALING ON RESISTIVITY

According to Vand, the defects incorporated in Vacuum-evaporated metallic films lattice distortions, are a "combined type"consisting of vacancies and interstitials in close proximity to one another. He assumed that a characteristic energy E is required to allow the defects to combine and cancel out but that the energy required to bring about the migration of these defects towards each other is negligible.

If r (E) is the contribution to the residual resistivity made by one distortion per unit volume, N_o (E) the initial number of distortion per unit volume (i.e. at time s = o) and N_o (E) Δ E is the number of distortions per unit volume that have decay energy between E and E + Δ E, then the total contribution to the film resistivity ρ_i due to imperfections is given by:

$$\rho_i = \int_{-\infty}^{\infty} r(E)\, N_o(E)\, dE \qquad (6-1)$$

(a)

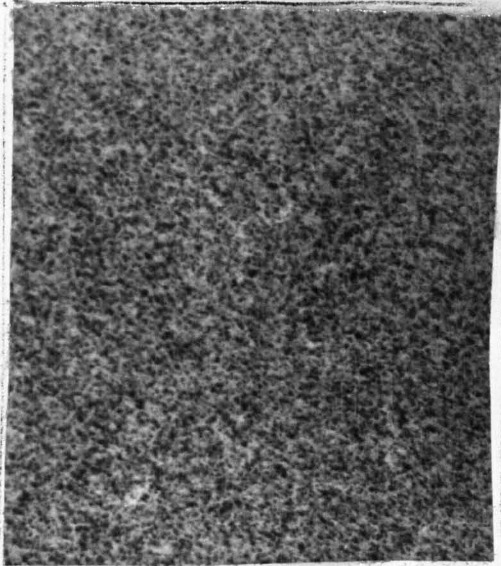

100%Mn
before annealing

(b)

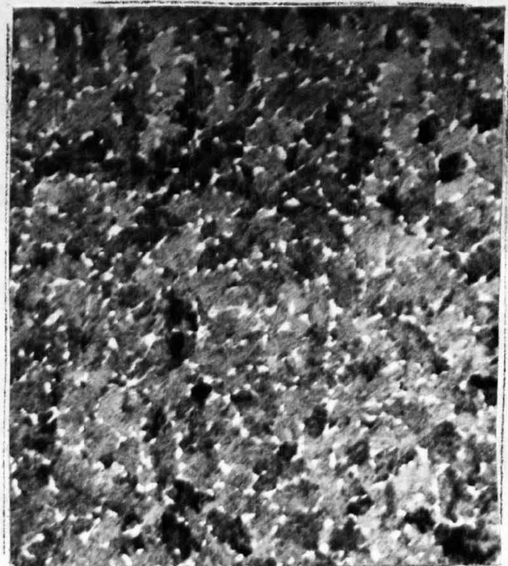

100%Mn
after annealing

(c)

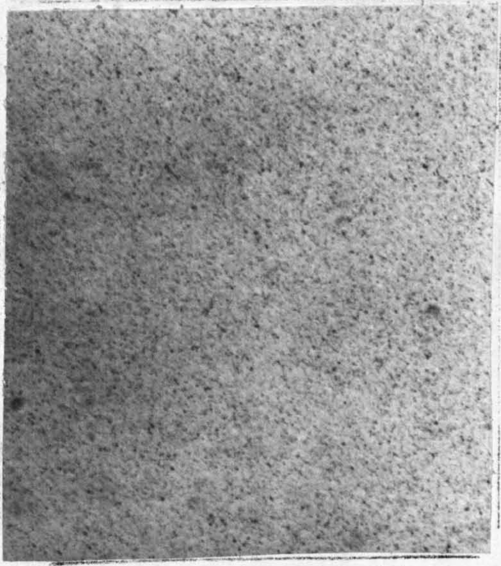

0.45μm

39Vol%Mn
before annealing

(d)

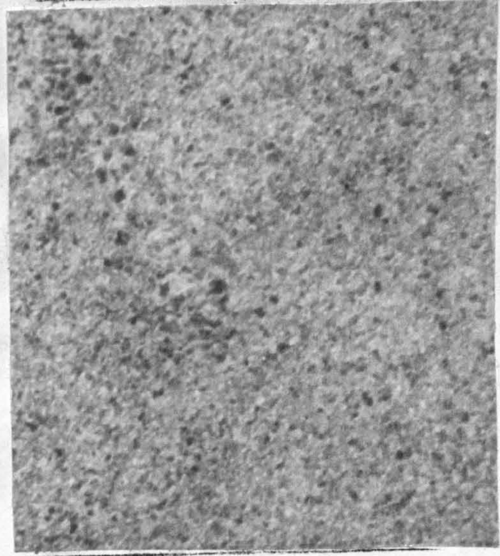

39Vol%Mn
after annealing

Fig.6.19 Electron Micrograph of Mn and Mn/MgF_2 films 250A thick before annealing and after annealing at 620K for one hour.

The distribution function F_o (E) describing the energy spectrum of the distortions in the film is given as:

$$F_o (E) = r (E) N_o (E) \quad \text{——} \quad (6 - 2)$$

A complete analysis of equations (6 - 1) and (6 - 2) gives:

$$F_o (E) = \frac{1}{kU} \left(\frac{d\rho_i}{dT} \right) \quad \text{——} \quad (6 - 3)$$

where $\frac{d\rho_i}{dT}$ is the slope of the resistivity Vs temperature graph when the temperature of the film is raised at a uniform rate and the resistivity is measured as a function of temperature, and therefore of time, k is Boltzmann's constant and U is defined by:

$$U = u \frac{(u + 2)}{u + 1} \quad \text{——} \quad (6 - 4)$$

where:

$$u + \log u = \log 4 n s \nu_{max} \quad \text{——} \quad (6 - 5)$$

and n is the number of atoms that can initiate a defect (this number is unknown but it is estimated [106] to be ≈ 10), ν_{max} is the characteristic maximum vibrational frequency for the lattice assumed to be the same for the distorted lattice of a metallic film and s is the time for the film to reach the particular temperature at which $\frac{d\rho_i}{dT}$ is measured. u is obtained by successive approximation of equation (6 - 5) so that F_o (E) may be plotted against E (= uk T) to give the lattice distortion spectrum.

6.7.1.1.1. ESTIMATION OF THE LATTICE DISTORTION ENERGY IN PURE Mn FILMS

The lattice distortion energy F_o (E) and the decay energy E for pure Mn Films have been calculated using experimental ρ - T data. The graphs of F_o (E) Vs E are given in Figure 6.20. They show that E lies between about 330 and 600 meV with the maximum energy for distortion E_{max} occurring at about 425 meV for the 1000A film and 485 meV for the 500A films. The corresponding curves for the cermet films have not been plotted as it was not possible to obtain a value for ν_{max} for the Mn/MgF_2 system.

Considerable difficulties were encountered in obtaining a suitable value for ν_{max} in pure Mn films. Finally ν_{max} for α - Mn was calculated from the Debye temperature θ_D (= 385 at OK) given by Meaden [25], using equation (3 - 2).

The shape of the graphs in Figure 6 - 20 is similar to those obtained by Shah and Naik [107] for Cu and Au films, Damodara-Das and Jagadeesh [108] for Sn/Sb alloy films, and Wilkinson and Birks [110] for Au films in that they clearly show the presence of a peak value for F_o $(E)_{max}$. However in certain cases [108] where two or more elements are present, multiple F_o $(E)_{max}$ peaks may be obtained.

When F_o (E) and E were related to Mn film thickness it was observed that both quantities decrease with increase in film thickness as shown in Table 6.7. These results are in agreement with Vand's suggestion that both F_o $(E)_{max}$ and E_{max} should decrease with increase in film thickness. Toyoda and Negashima [109] using Vand's

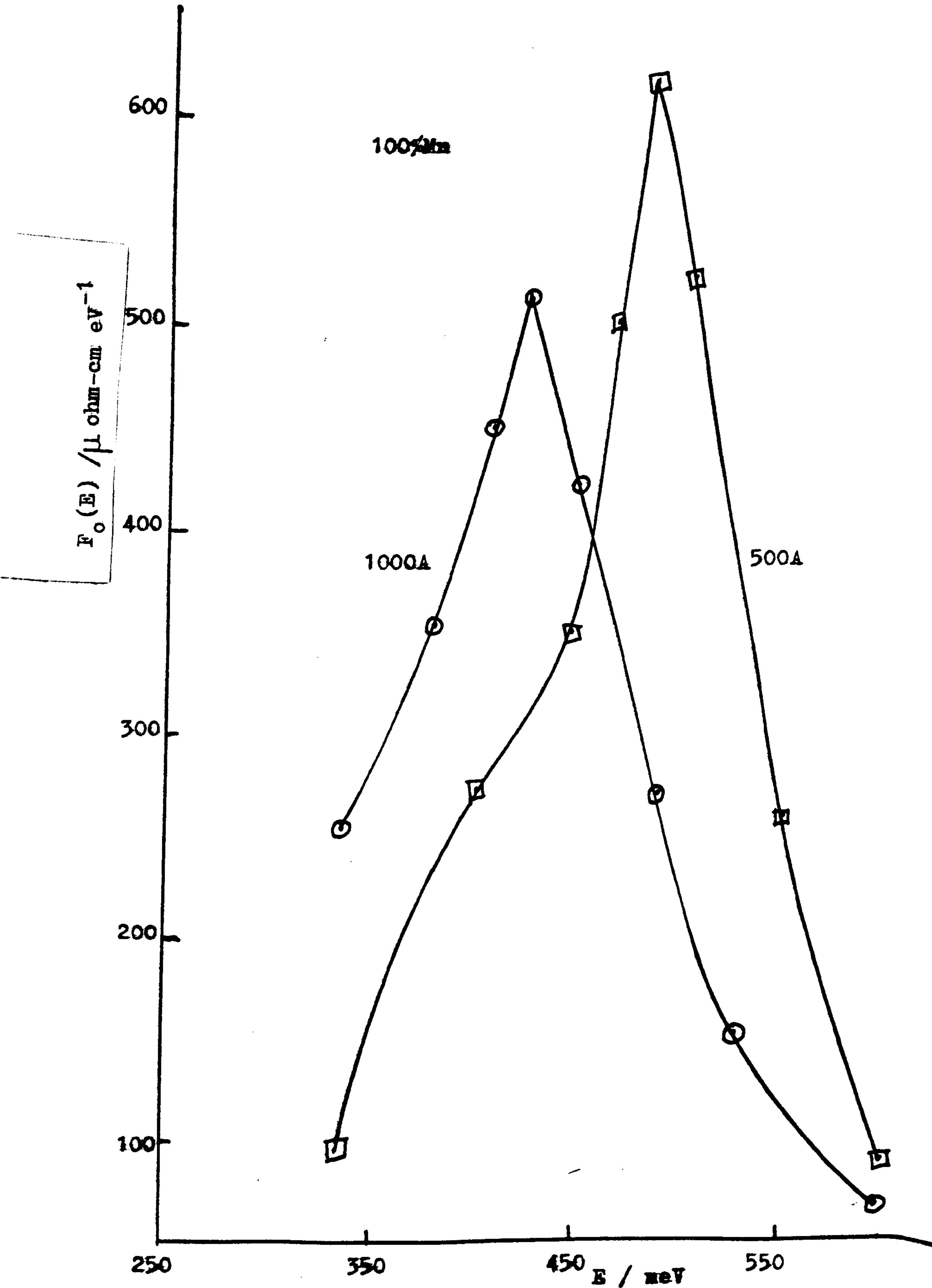

Fig.6.20 Lattice distortion $F_o(E)$ Vs Decay Energy (E)

Film thickness (A)	$F_o(E)_{max}$ ($\mu\Omega$cm eV^{-1})	E_{max} (meV)
250	715	665
500	632	485
1000	512	425

Table 6.7. Variation of F_o $(E)_{max}$ and E_{max} with Mn film thickness.

theory on carbon films also found a similar thickness dependence. In their case F_o $(E)_{max}$ for 110A films occurred at 2.3 eV and at 1.6 eV for the 380A films. On the contrary, Wilkinson and Birks [110] with Au films found that F_o $(E)_{max}$ was independent of thickness over the range 100 to 900A for a constant deposition rate. (The deposition rate was not given but it is assumed to lie between 0 and 5.5 μg cm^{-2} min^{-1}). However they observed that F_o $(E)_{max}$ does increase with increase in deposition rate, thus indicating that Au films prepared at lower deposition rates have fewer structural defects.

Toyoda and Nagashima [109] explained that the fall in resistivity during annealing may be due to imperfections being displaced into regular lattice sites. An alternative explanation by Haffman et al [111] assumes that:

(i) the number of vacancies in the film far exceeds the equilibrium value;and

(ii) that during annealing the vacancies coalesce to form progressively larger groups until they finally arrange themselves into sheets and collapse to form dislocation rings. They supported this hypothesis with results from strain measurements on nichrome films in the process of being annealed. The volume change corresponded fairly closely with observed resistivity change.

6.7.2. POST-ANNEALING HEAT-TREATMENT

The results for the post-annealing heat-treatment of Mn and Mn/MgF_2 cermet films (250, 500, and 1000A thick) are presented in Figures 6.21, 6.22, 6.23 and 6.24. The resistivities of all the films investigated were found to be completely reversible at all temperatures below the maximum annealing temperature (i.e. no hysterisis was observed), and irreversible above this temperature. These correspond to the reversible region B in Figure 6.17.

Figure 6.21 for the 100% Mn films shows that after annealing at 620K for 1 hour, the resistivity of all films $\geqslant$ 250A increases with increase in temperature and vice versa during the following temperature cycling (110 to 620K) (i.e. the films have a positive TCR). This is an indication that the films have become structurally continuous. The electron micrographs Figure 6.19 for the thinnest of these

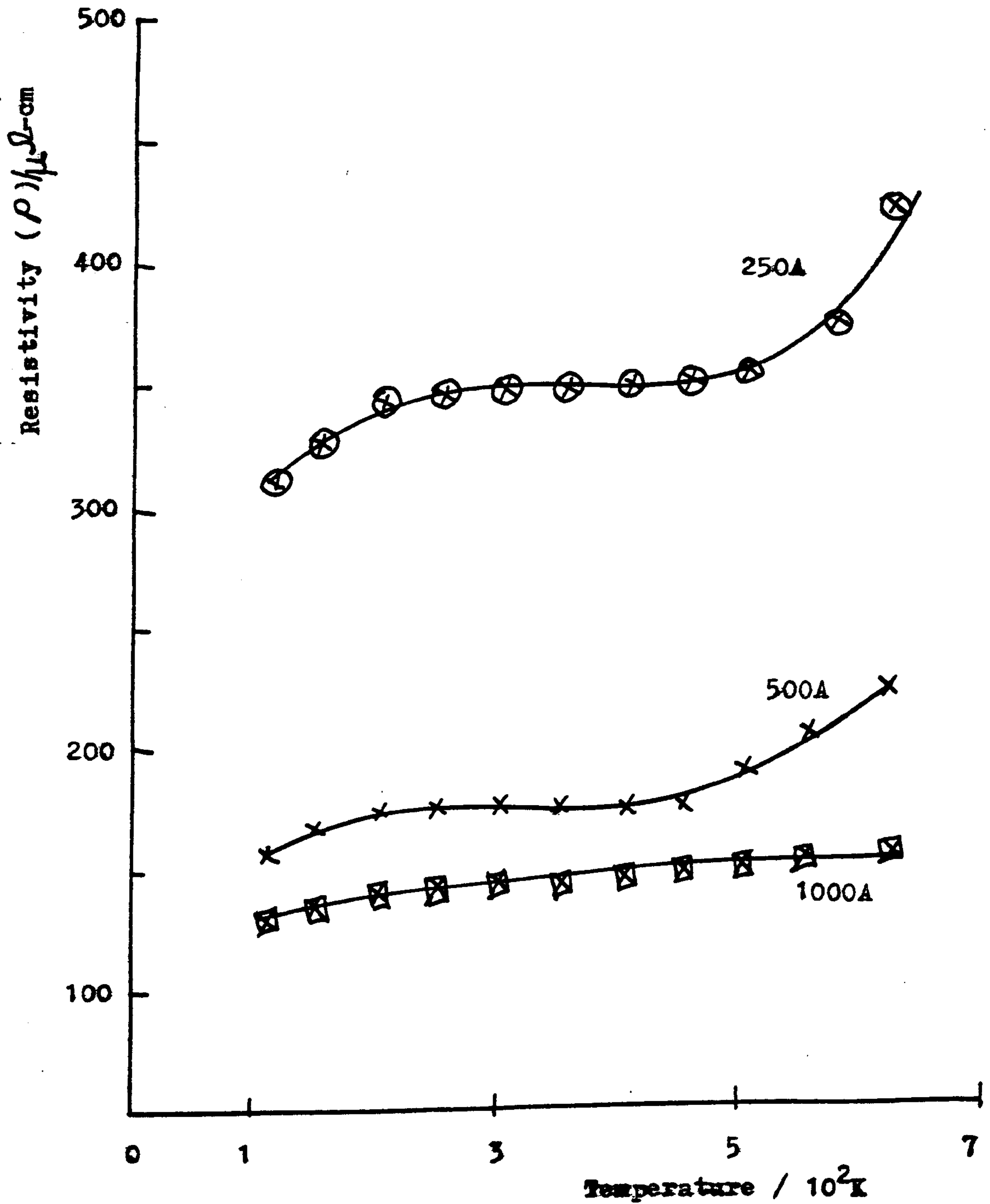

Fig.6.21 Resistivity Vs Temperature for 100%Mn films annealed at 620K for 1 hour.

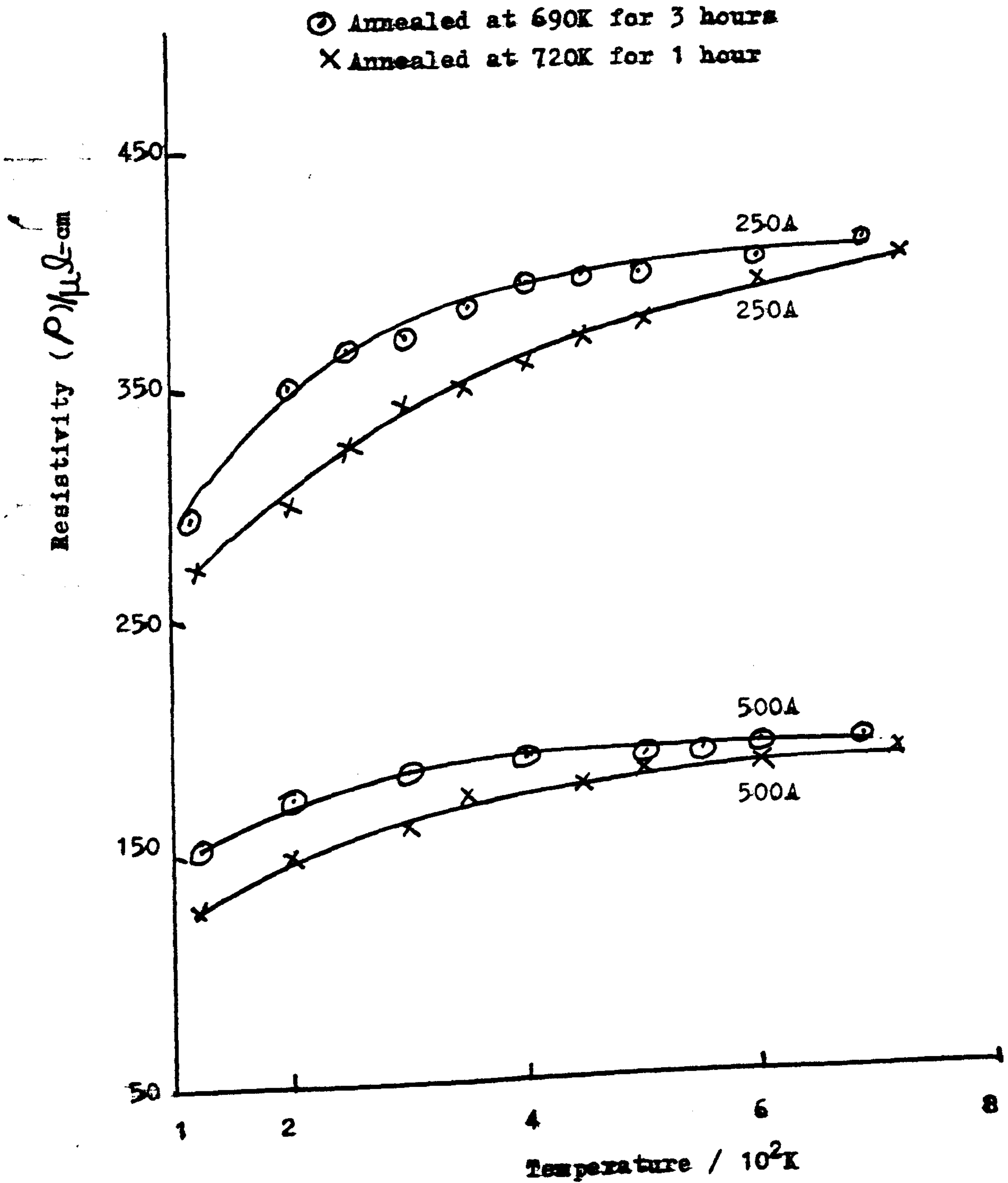

Fig. 6.22 Resistivity Vs Temperature for 100%Mn Films.

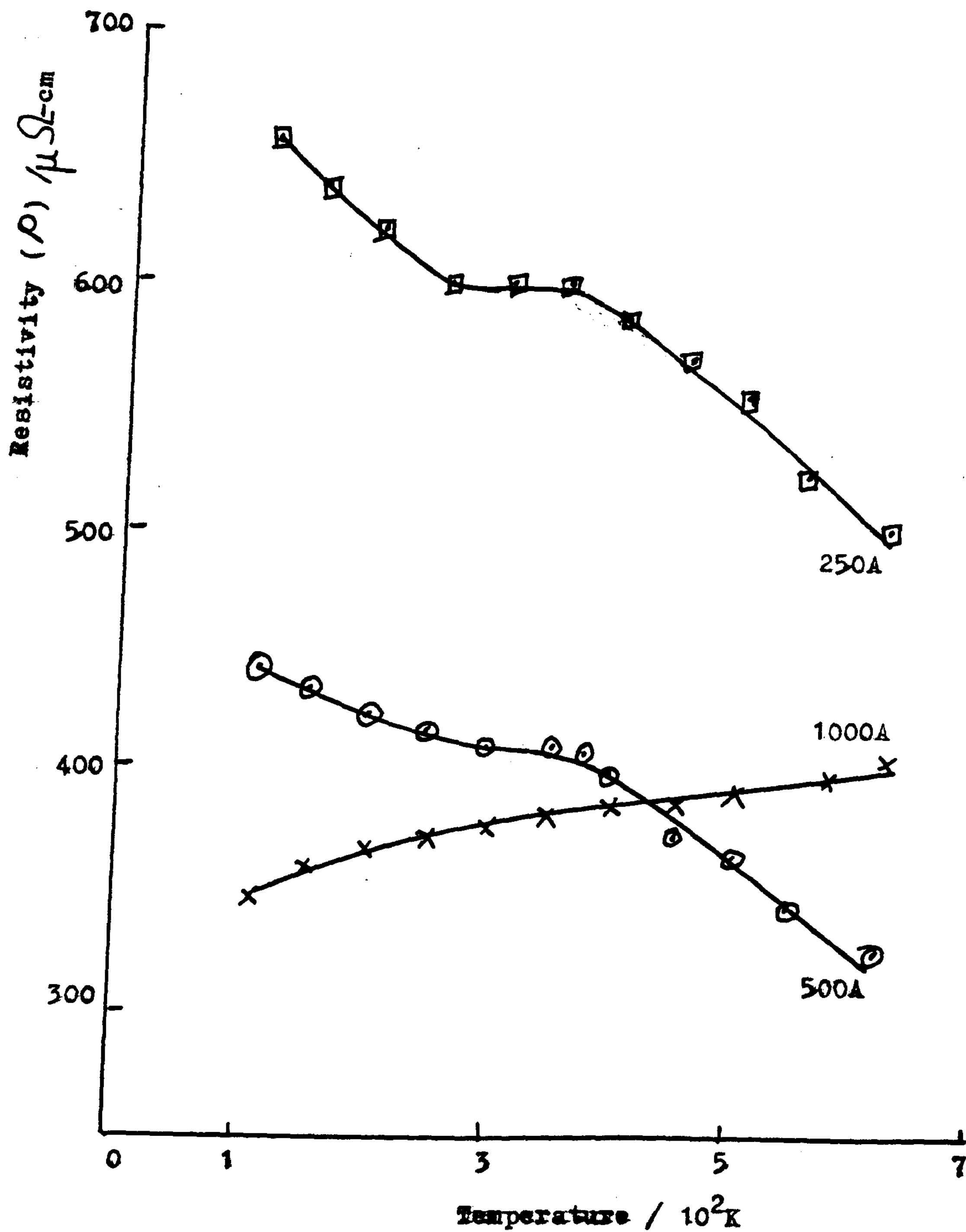

Fig.6.23 Resistivity Vs Temperature for 39Vol%Mn/MgF_2 Cermet Films annealed at 620K for 1 hour.

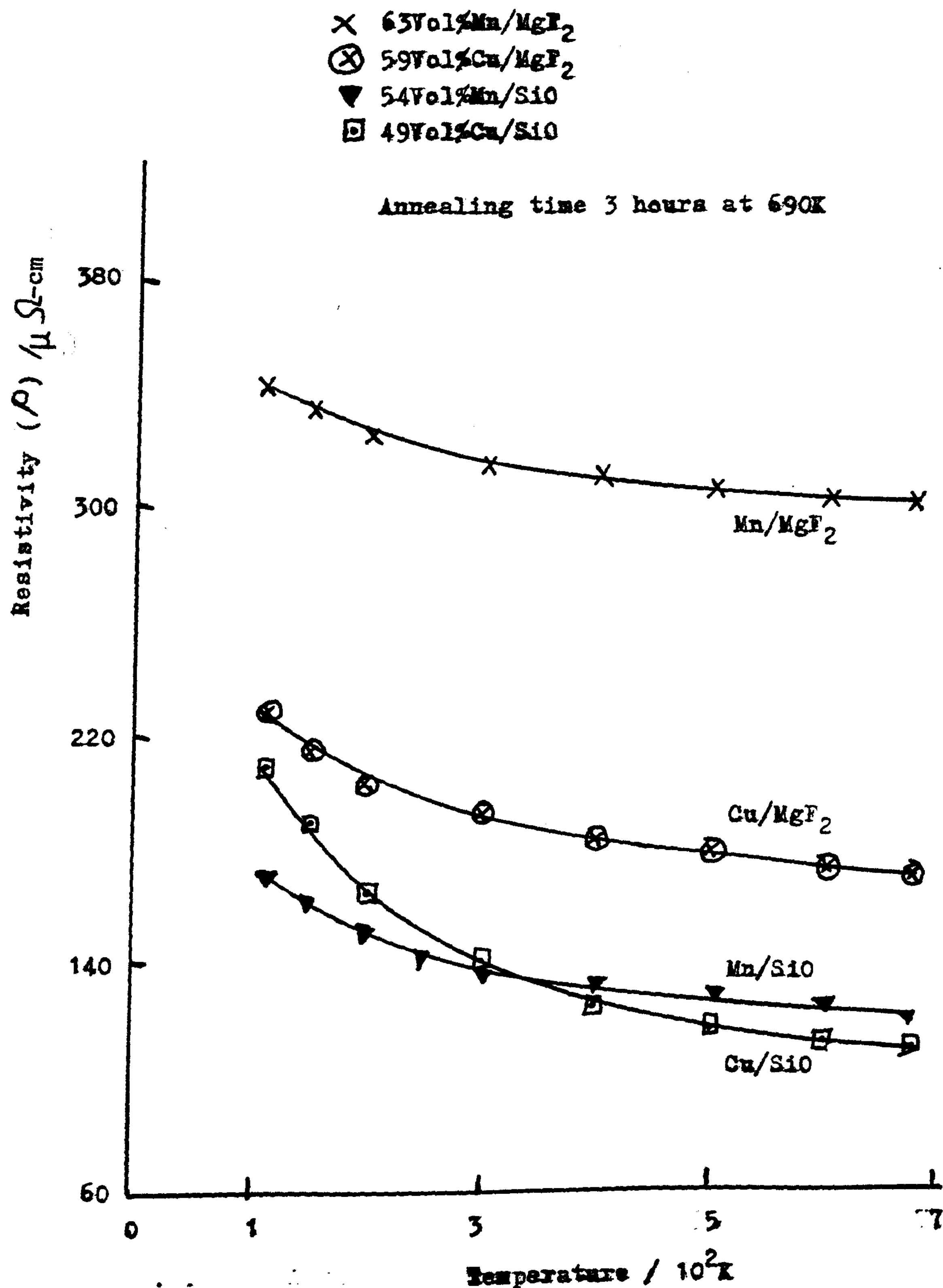

Fig. 6.24 Resistivity Vs Temperature for 500A Cermet Films.

films (250A) confirms that they have indeed become structurally continuous. Figure 6.19a shows the presence of Mn islands prior to annealing, typical of a discontinuous film. Figure 6.19b shows that the islands have grown laterally with the larger islands touching to create continuous Mn paths throughout the film. Although no electron micrographs were taken for the thicker Mn films (500 and 1000A), the presence of a positive TCR suggests that they must also be structurally continuous.

The Mn films of 1000A thickness exhibit a practically linear relation between ρ and T. The resistivity increases only by 20 $\mu\Omega$- cm between 110 and 620K, a percentage increase of about 15%. From data presented by Meaden [25] (Fig. 6.25), the change in resistivity for high - purity annealed bulk Mn is + 13%, being 123 $\mu\Omega$ - cm at 50K and 139 $\mu\Omega$ - cm at 295K. Figure 6.25 clearly shows that the temperature variation of the resistivity in bulk Mn is considerably smaller than that for Cr, Cu and Au whose resistivities increased by between one and two orders of magnitude.

The thinner Mn films of 250 and 500A thickness have a non-linear ρ - T characteristics (Fig. 6.21) when the films are annealed at 620K for 1 hour. It can be seen that between 300 and 450K, the resistivity appears to be constant. This may be a consequence of incomplete annealing, as a similar result was not observed in films annealed for 3 hours at 690K or at 720K for 1 hour (Fig. 6.22). This plateau region has been interpreted by a number of workers [112 - 115] in terms of incomplete ordering.

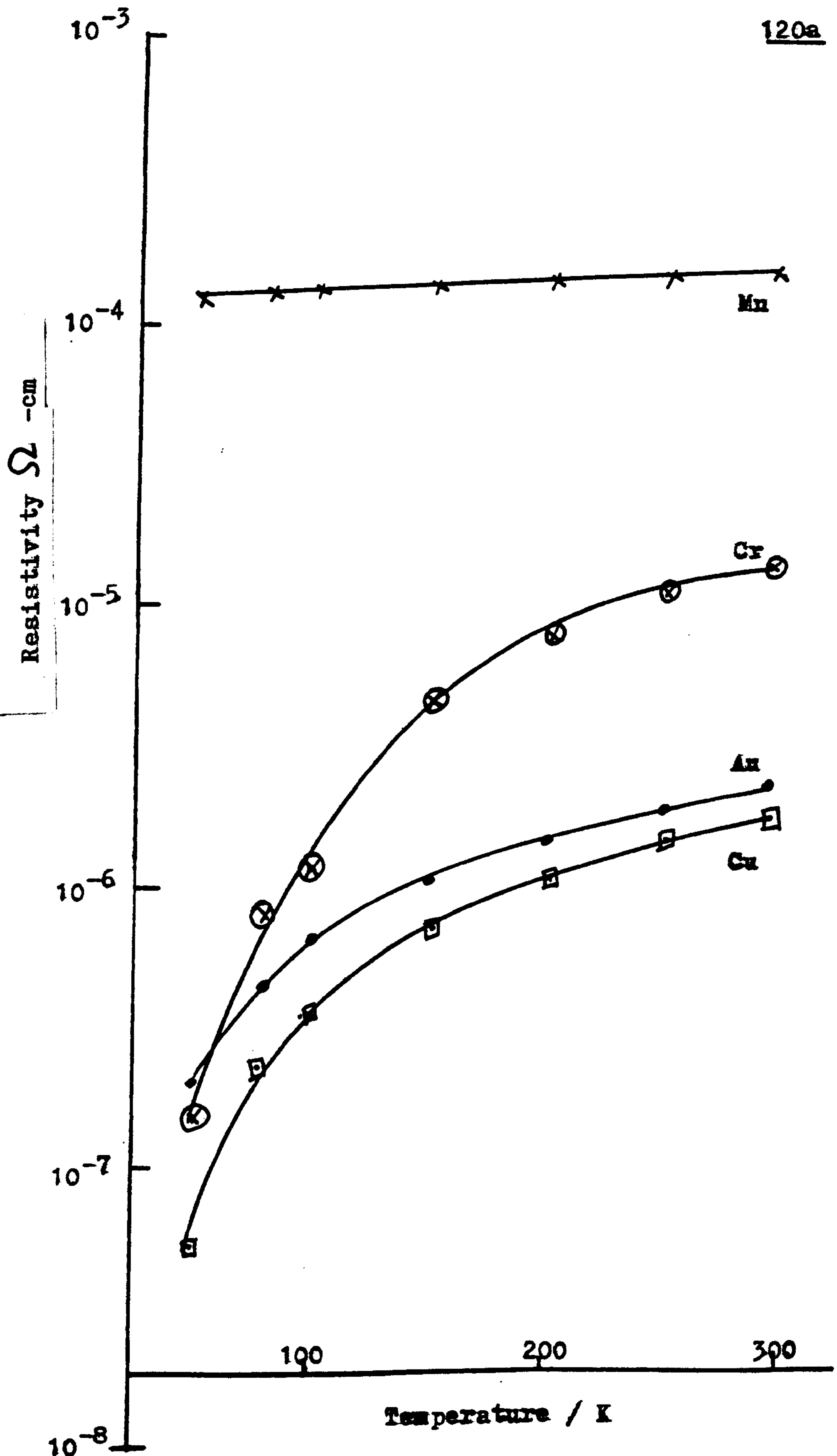

Fig.6.25 Bulk Metal Resistivity Vs Temperature

The ρ - T characteristics for the 39 Vol % Mn cermet films annealed at 620K for one hour are presented in Figure 6.23. Here the 250 and 500A films have smaller plateau regions ($\sim 100^{\circ}$) and a negative TCR whilst the 1000A film has a positive TCR. As with pure Mn films, the plateau was not observed in cermet films annealed at 690K for 3 hours and at 720K for 1 hour. This variation of TCR with thickness is an interesting result because it indicates that when Mn/MgF_2 cermets are annealed at 620K for 1 hour, the sign of the TCR is dependent on the film thickness, and on the amount of Mn in the film. A similar result was obtained for the 63 Vol % Mn cermet films.

It is evident from Figure 6.19b that a considerable amount of mass movement of Mn particles occurs during the annealing process. A similar migration of Mn particles also occurred in the cermet films $\sim$ 250A thick (Fig 6.19d) but to a lesser degree so that the film remained discontinuous after annealing. No electron micrographs were obtained for the 1000A cermets but it is assumed that on annealing, the quantity of Mn atoms and their dispersal within the fabricated films were sufficient to produce a network of conducting paths.

Small variations in resistivity with temperature were observed in all annealed Mn/MgF_2 cermet films. Auxiliary investigations were carried out to compare Mn and Cu cermets, using MgF_2 and SiO as insulators in order to attempt to establish the reason for the small resistivity variations with temperature in Mn/MgF_2 cermet films. The results are presented in Figure 6.24. The films contained

between 37 and 51 Vol % insulator (corresponding to 80 Wt % metal/20 Wt % insulator), 500A thick and were annealed at 690K for 3 hours.

The Mn/MgF_2 system has the largest resistivity after annealing but the subsequent variation in resistivity with temperature (110 to 690K) was the smallest being $\sim$ 40 $\mu\Omega$- cm. That is, the value of ρ at 690K increased by about 14% at 110K. Between these temperature limits, the corresponding increase in ρ for Cu/MgF_2, Mn/SiO and Cu/SiO are respectively 35%, 46% and 91%.

From these results (Fig 6.24) it appears that:

(i) MgF_2 cermets have a higher ρ than SiO cermets although the variation of ρ with T in the former is smaller (14 and 35%) compared with the latter (46 and 91%);

(ii) Mn/SiO cermets have a smaller variation of ρ with T (46 %) compared with Cu/SiO (91%);

(iii) a combination of Mn and MgF_2 produced films of high ρ which is only slightly affected by variations in temperature. Hence the small resistivity variation with temperature in the Mn/MgF_2 system appears to be both Mn and MgF_2 dependent with neither component showing a distinct dominance. However further work is necessary using more Mn and Cu cermet compositions and other metals to test these conclusions.

It also appears that the use of SiO as an insulator reduces the resistivity of Mn/SiO and Cu/SiO to within the same order of magnitude. This is interesting because in a limited way it gives support to Neugebauer's hypothesis [66] that one curve can be used to describe the resistivity of all metal/SiO system as the SiO content

in the film is reduced, regardless of the type of metal used or other deposition parameters. However cermet films containing MgF_2 do not appear to have this property. This is consistent with the resistivity - composition results for Mn/MgF_2 cermets presented in Section 6.2.

Let us now examine more closely the activation energy of both annealed and unannealed Mn/MgF_2 cermets.

6.7.2.1. ACTIVATION ENERGY OF UNANNEALED Mn/MgF_2 CERMETS

Three film compositions of 100% Mn, 63 Vol % Mn and 39 Vol % Mn were investigated. Their thicknesses were between 250 and 1500A. The substrate temperature was 295K during deposition and no high temperature annealing was carried out. The activation energy was estimated between 110 and 295K from the variation of $\ln \rho$ with T^{-1} (see Fig. 6.26). Figure 6.27 shows the variation of activation energy with thickness.

Figure 6.26 shows that the $\ln \rho$ Vs T^{-1} graphs are linear for all the film thicknesses indicated. However the 1000A thick films for 100% Mn and the 63 Vol % Mn were non-thermally activated; the are not shown in the diagram. Figure 6.26 also indicates that the activation energy increases with decrease in Mn concentration but decreases with film thickness. The latter is more clearly seen in Figure 6.27. The activation energy decreased rapidly from 74.5 meV at 250A thickness to 10.4 at 1000A, and then more slowly to 7.1meV at 1500A.

A comparison of the activation energies of films of 250A thickness obtained from resistivity measurements (Fig.6.26) with those calculated using data collected from electron microcopy (Table 6.2) shows that the former are about 30 to 35 % lower . However when the xxxxxxxxxxxxxxxxxxxxxxxxx

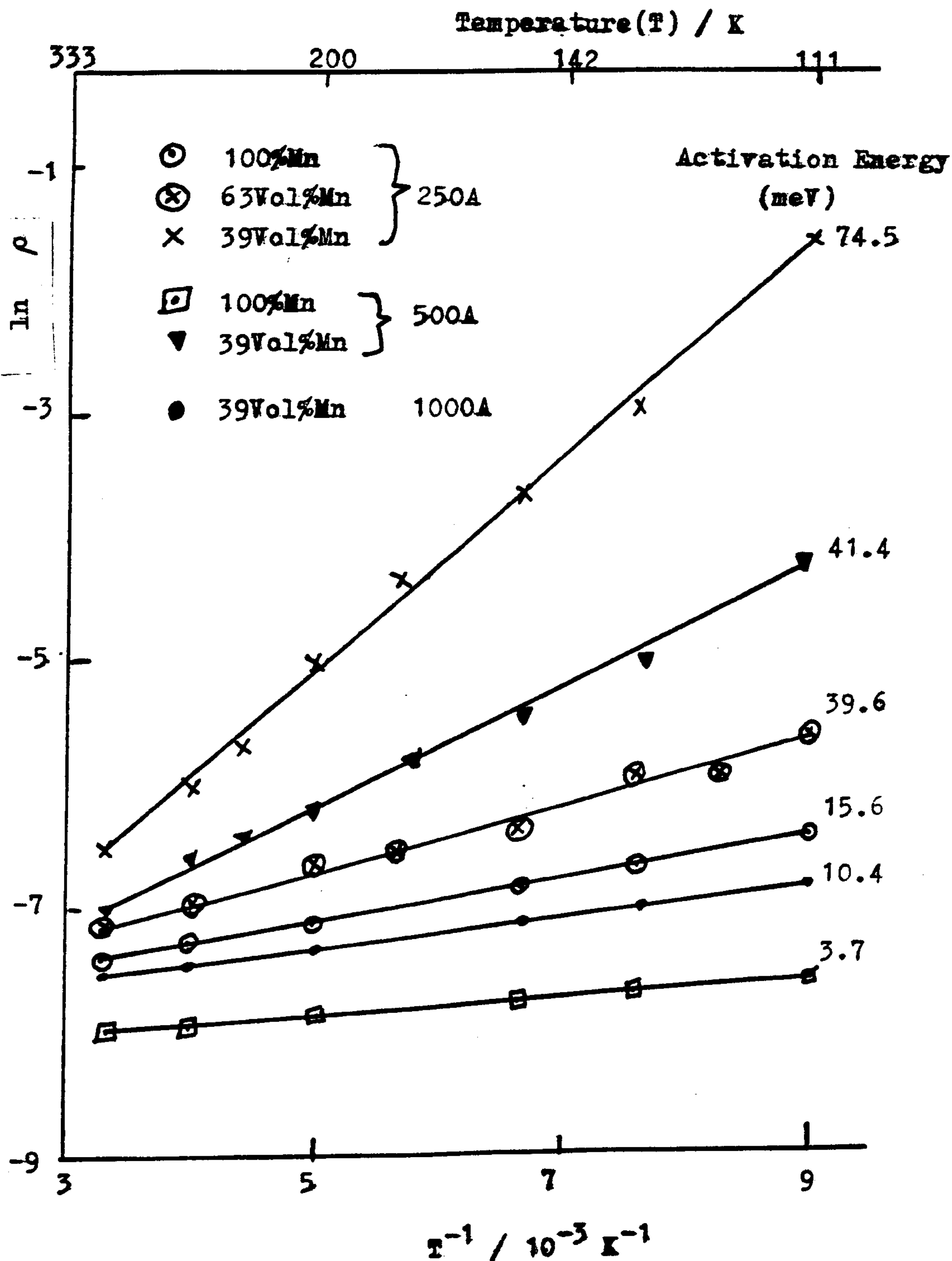

Fig.6.26 ln ρ Vs T^{-1} for Mn and Mn/MgF_2 films deposited at 295K (unannealed)

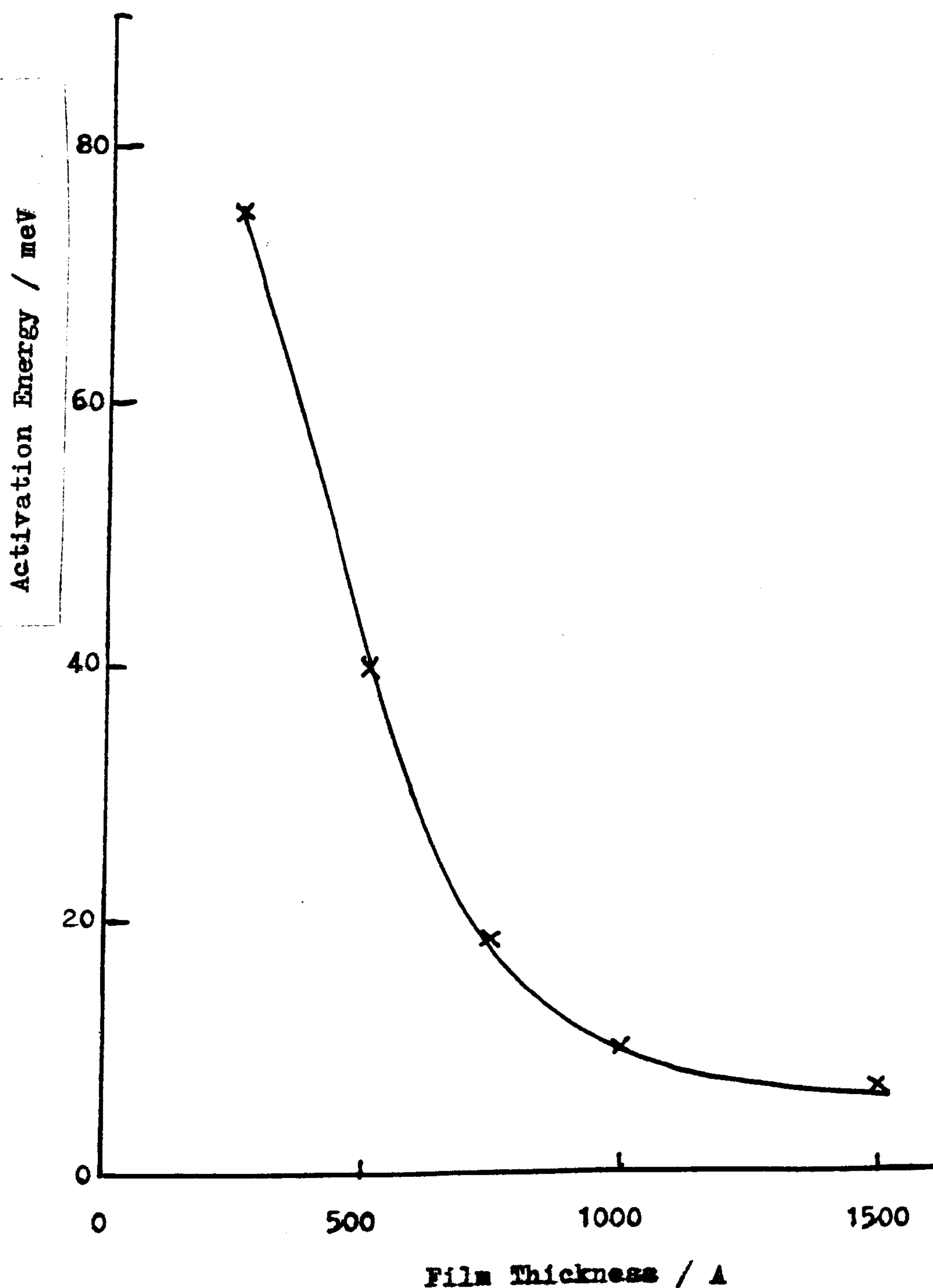

Fig.6.27 Activation Energy Vs Film Thickness for the 39Vol%Mn / MgF_2 cermets deposited at 295K. Activation Energy is measured between 110 and 295K.

error limits in the microscopic measurements are taken into account the difference between the two values is less than 14%. Hence the two sets of activation energies are in reasonable agreement with each other.

This shows conclusively that between 110 and 295K, Neugebauer and Webb's theory [38] (Section 3.3.1) appears to be applicable to all unannealed Mn films and MgF_2 cermets of 250A thickness when deposited at 295K. Hence electronic conduction is probably by a thermally - activated tunnelling of electrons between the metallic islands. Although there are no electron micrographs to give a direct comparison, it is assumed that the conduction mechanism in all the 500A and the 1000A film with 39 Vol % Mn is also by thermally activated tunnelling because of the linear relationship between $\ln\rho$ and T^{-1} in the same temperature range.

6.7.2.2. ACTIVATION ENERGY OF FILMS ANNEALED AT 620, 690 and 720K

Figures 6.28 and 6.29 show the variation of $\ln\rho$ with T^{-1} for annealed cermet films of 250 and 500A thickness. The 1000A cermet films and all pure Mn films have not been included as both are non-activated and metallic conduction prevails (see Figs. 6.21 and 6.23).

Figures 6.28 and 6.29 show that there appears to be a spectrum of activation energies. Hence the activation energy values shown in the figures merely demonstrate an order of magnitude. However Figure 6.28 indicates the presence of three distinct regions for the 250 and 500A films annealed at 620K for one hour: a high temperature region, a low temperature region and a transition region, the

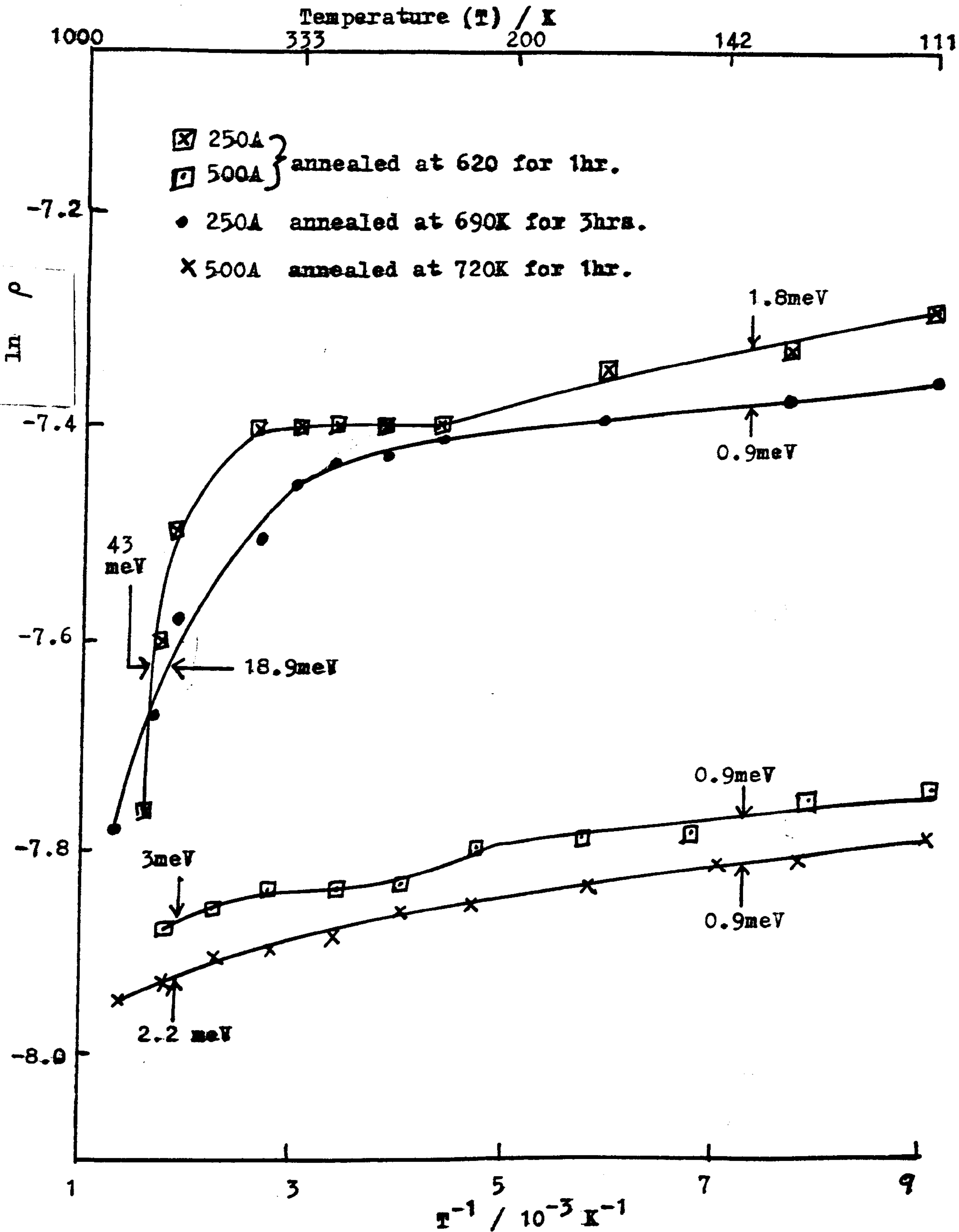

Fig.6.28 ln ρ Vs T^{-1} for 39Vol%Mn / MgF_2 Cermets

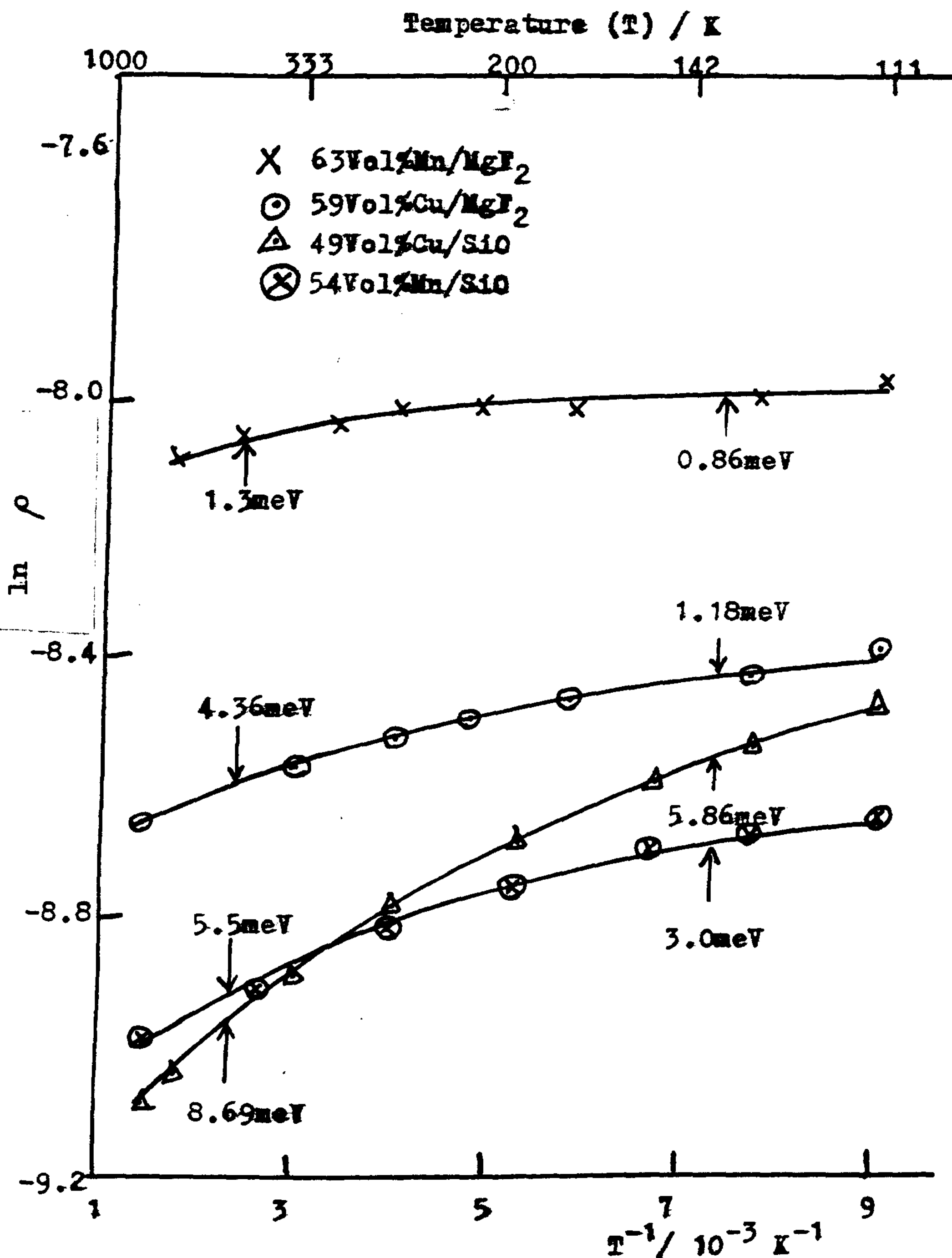

Fig.6.29 ln ρ Vs T^{-1} for Cermet Films of 500A thickness annealed at 690K for 3 hours.

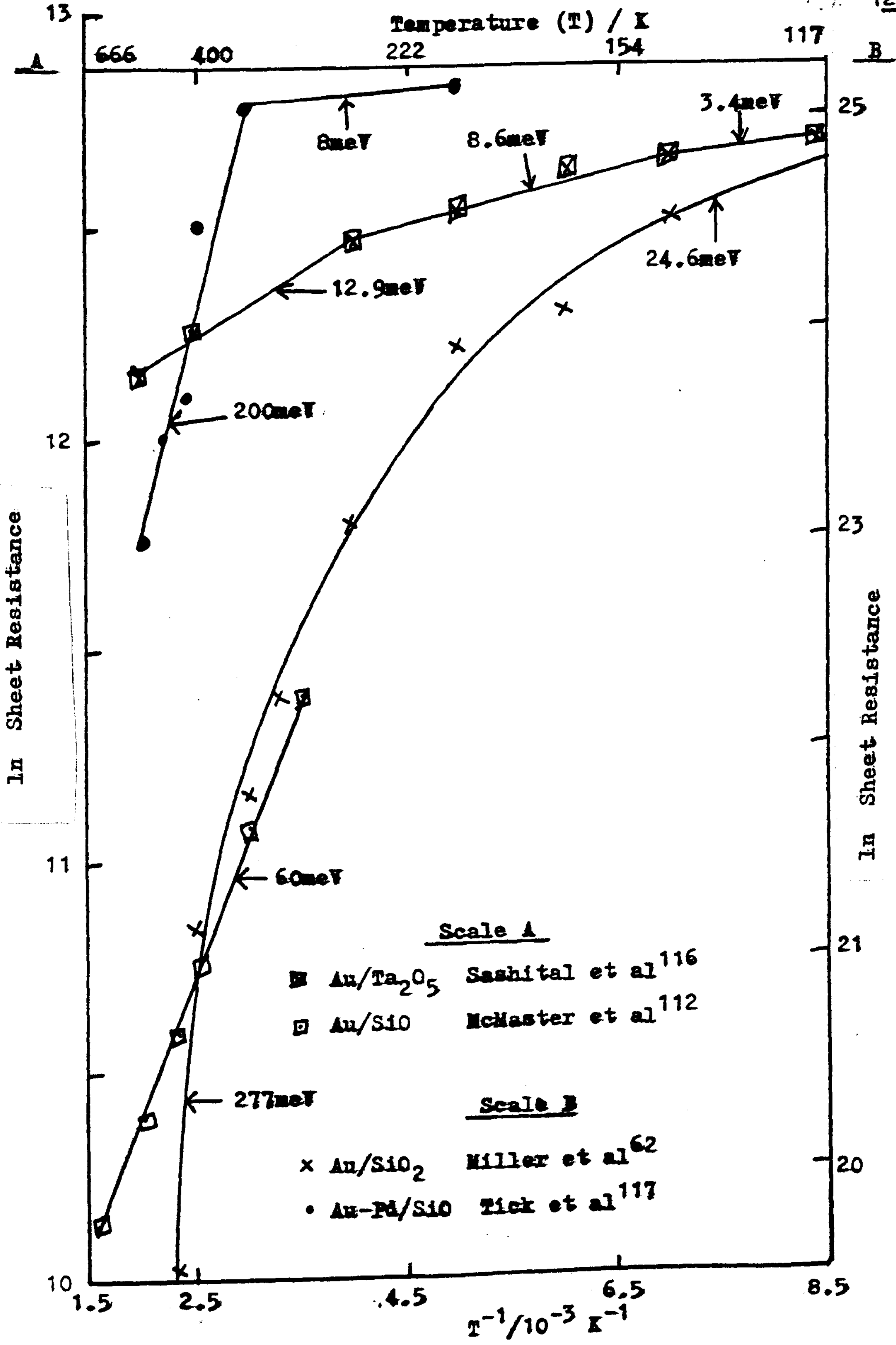

Fig.6.30 ln Sheet Resistance Vs T^{-1} for different cermets

latter corresponding to the plateaux in Figure 6.23. The low and high temperature activation energy regions are also evident in similar films annealed at 690 and 720K.

For a given film thickness the activation energy for the low temperature region is lower than that for the high temperature region as indicated in Figure 6.28. It can also be seen from this figure that the activation energies in both temperature regions decreased as the cermet thickness increases. This is in agreement with the unannealed results.

Figure 6.29 shows that there also exists a spectrum of activation energies for the 63 Vol % Mn cermets (of 500A thickness annealed at 690K for 3 hour) and other cermets investigated; viz: 59 Vol % Cu/MgF_2, 49 Vol % Cu/SiO and 54 Vol % Mn/SiO.

It is interesting to note that similar spectra of activation energies have been observed by many authors [45, 62, 116, 117] for different cermet systems as shown in Figure 6.30. For example Sashital and Pakswer [116] obtained 3 different activation energy regions of 12.9, 8.6 and 3.4 meV for Au/Ta_2O_5 in the temperature range 93 to 433K. It is more likely however that their ln ρ Vs T^{-1} graph is a continuous curve rather than three distinctly separate regions.

On the contrary McMaster and Fuschillo [112] obtained a single activation energy of 60 meV for co-evaporated 15 Vol % Au/SiO cermets deposited on SiO_2 substrates in the temperature range 300 to 873K. Extensive precipitation of Au in the cermet was also

reported by these authors after annealing at 873K. No low temperature results were reported.

Tick and Fehlner [117] (Fig. 6.30) observed two activation energy regions of 8 meV (low temperature) and 200 meV (high temperature) for Au - Pd - SiO composite films with the transition occurring at 233K. Miller and Shirn [62] with Au/SiO_2 observed a gradual increase in activation energy from 24.6 meV at 111K to 277 meV at 423K with the knee of the curve occurring at about 290K. It is interesting to note that the transition from low to high temperature activation energy occurs below 400K.

The origin of the high and low temperature dependent conduction processes is not known. Tick and Fehlner [117] suggested that the conduction process is dominated at low temperature by closely-spaced gold-rich islands and at high temperatures by activated tunnelling between the palladium - rich islands. On the other hand Sashital and Pakswer [116] proposed that the conduction mechanism may be due to electron tunnelling between metallic islands; thermionic emission of charge carriers; and electronic conduction through trapping levels in the different temperature regions. They assumed that these processes may operate either individually or jointly but they were unable to describe the exact relationship between the various processes and the three activation energy regions in Figure 6.30.

In their paper Miller and Shirn presented the low temperature ($<$ 300K) activation energy only, but by using their quoted resistivity values, a spectrum of activation energies may be obtained as indicated by the curve in Figure 6.30. According to these authors,

resistivities in the low temperature region should vary linearly with temperature. They explained that conduction in this region was due to thermally - activated charge carriers from the Au region tunnelling through the intervening SiO_2 matrix; the process being analogous to conduction in discontinuous metallic films [38].

Van Steensel [45] obtained a non-linear relation between ρ and T^{-1} for Au films. In one example he obtained a low temperature activation energy of 44 meV and a high temperature value of 140 meV. He found that his results were best interpreted by thermionic emission of charge carriers. He explained that at high temperatures the larger inter-island spacings (corresponding to higher energy barriers) start to contribute significantly to the conduction process. Hence the difference between the high and low activation energies observed in cermet films may be due to the dielectric making a significant contribution to the activation process at high temperatures.

6.7.23 ELECTRONIC CONDUCTION MECHANISM IN ANNEALED Mn/MgF_2 CERMETS

From the literature review of Chapter 3, it appears that there are two main ways in which the resistivity of annealed Mn/MgF_2 cermets may depend on temperature, viz $\rho \propto \exp(T^{-1})$ and $\rho \propto \exp(T^{-\frac{1}{2}})$. In either case the film is considered to be composed of isolated metallic islands separated by dielectric.

Both Figures 6.28 and 6.29 as well as the $\ln \rho$ Vs $T^{-\frac{1}{2}}$ graph of Figure 6.31 indicate that conduction in Mn/MgF_2 cermets

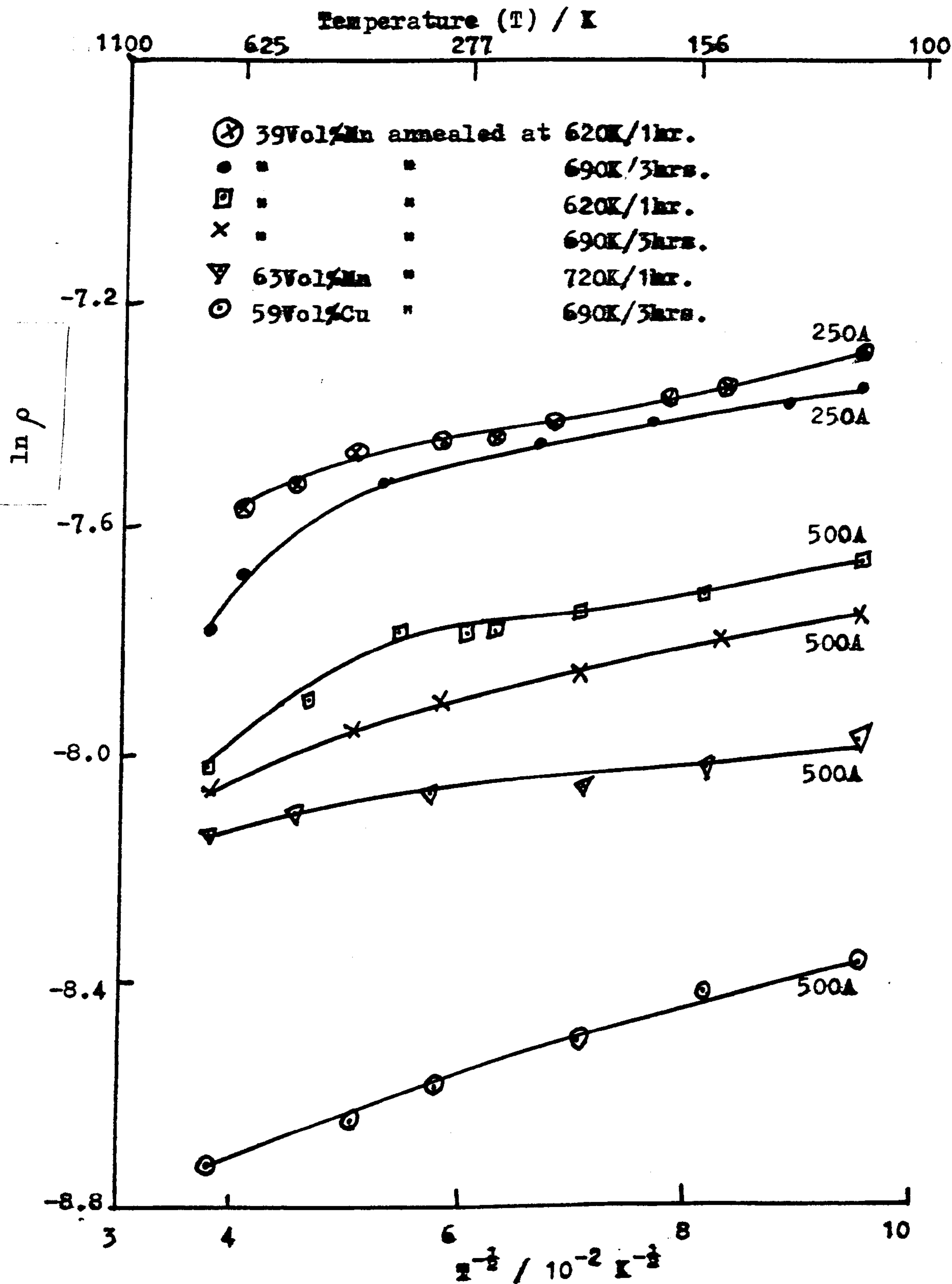

Fig.6.31 ln ρ Vs $T^{-\frac{1}{2}}$ for Metal/MgF_2 Cermets

do not occur by a single thermally - activated mechanism. The interesting feature of these graphs is that the activation energy of all 500A films have low values as have those within the low temperature region of the 250A cermets (0.80 to 5.80 meV).

It is interesting to note that a low activation energy of about 4 meV ($E \approx C$ [120]) was obtained (between 35 and 300K) by Abeles et al [63] for Au/Al_2O_3 cermet films containing 38 Vol % Au. This composition is also close to the transition composition (about 40 Vol % Au) for this cermet. According to these authors, conduction in the dielectric regime occurs by thermally - activated tunnelling with a charging energy E (see Section 3.4.3), and in the transition regime by percolation/thermally - activated tunnelling.

The electron micrographs of Mn/MgF_2 cermets in Figure 6.19 show that the films are composed of isolated Mn islands and a Mn metallic-maze structure. These films have a negative TCR which is contrary to the positive TCR obtained in the metallic regime but typical of those cermets in the transitional and dielectric regimes. (Hence the films are either in the dielectric or transitional regime).

Films in the dielectric regime are field dependent [63] ($\ln\rho \propto F^{-1}$, where F is the electric field strength) and frequency dependent [63, 118] ($\ln\rho \propto f^{-1}$, where f is the frequency). Also films in this region show a linear relationship between $\ln\rho$ and T^{-1} or $T^{-\frac{1}{2}}$.

Mn/MgF_2 cermets of 250 and 500A thickness and annealed at 620, 690 and 720K are ohmic, frequency independent (100 Hz to 18kHz) and $\ln\rho$ neither varies linearly with T^{-1} nor $T^{-\frac{1}{2}}$ in the temperature range (110 to 720K). Therefore these films probably lie within the transition regime.

At low temperature, electronic conduction in annealed Mn/MgF_2 cermets is primarily a percolation process and at high temperatures, the process is boosted by electron tunnelling between isolated Mn islands.

Figure 6.19 shows that the annealing causes the agglomeration of Mn islands in the film. Compared with the 250A thick films, it is likely that the 500A cermets contain a relatively larger number of Mn percolation paths than isolated Mn islands. The conduction process is dominated by electrons percolating along the maze structure at all temperatures from 110 to 720K. Such a mechanism could be responsible for the low values of the activation energy.

In the case of the 250A annealed cermets there are fewer percolation paths but the number of isolated Mn islands increases. In addition, in order for the cermet composition to remain fixed separation between Mn islands must increase. Therefore percolation conduction is reduced and thermally - activated tunnelling is enhamced at high temperatures. Then the 250A cermets should have a higher activation energy than the 500A, which is in agreement with experimental results.

At low temperature, due to the relatively large inter-island separations and the low thermal energies of the electrons, the percolation currents far exceed the tunnelling currents. In this region, the activation energy is low (~ 0.9 to 1.8 meV, Fig. 6.28). Thus giving further support to a percolation-dominated conduction process.

The activation energies for the high temperature region are higher (~ 18 to 45 meV) than those for the low temperature region. Here it is likely that the thermally - activated tunnelling process contributes significantly to the conduction mechanism.

The tunnelling process may occur in two stages owing to the relatively large inter-island spacings. An electron may tunnel firstly into a trap level in the dielectric MgF_2; tunnelling into the next metallic island from this trap level is not possible as there are no empty states at that level. The electron must hop into a higher trap level in MgF_2 where tunnelling into the next Mn island is possible. Transitions from isolated Mn islands into Mn metallic maze is also possible.

6.7.2.4 TEMPERATURE COEFFICIENT OF RESISTIVITY (TCR)

Figures 6.32 and 6.33 show the variation of TCR with Mn/MgF_2 cermet composition for both unannealed and annealed films deposited at 295K. The TCR was also measured at 295K.

Figure 6.32 for the unannealed films shows that the 100% Mn films of 1000A thickness have a positive TCR ~ + 500 ppm K^{-1} whereas the cermet films have a negative TCR.

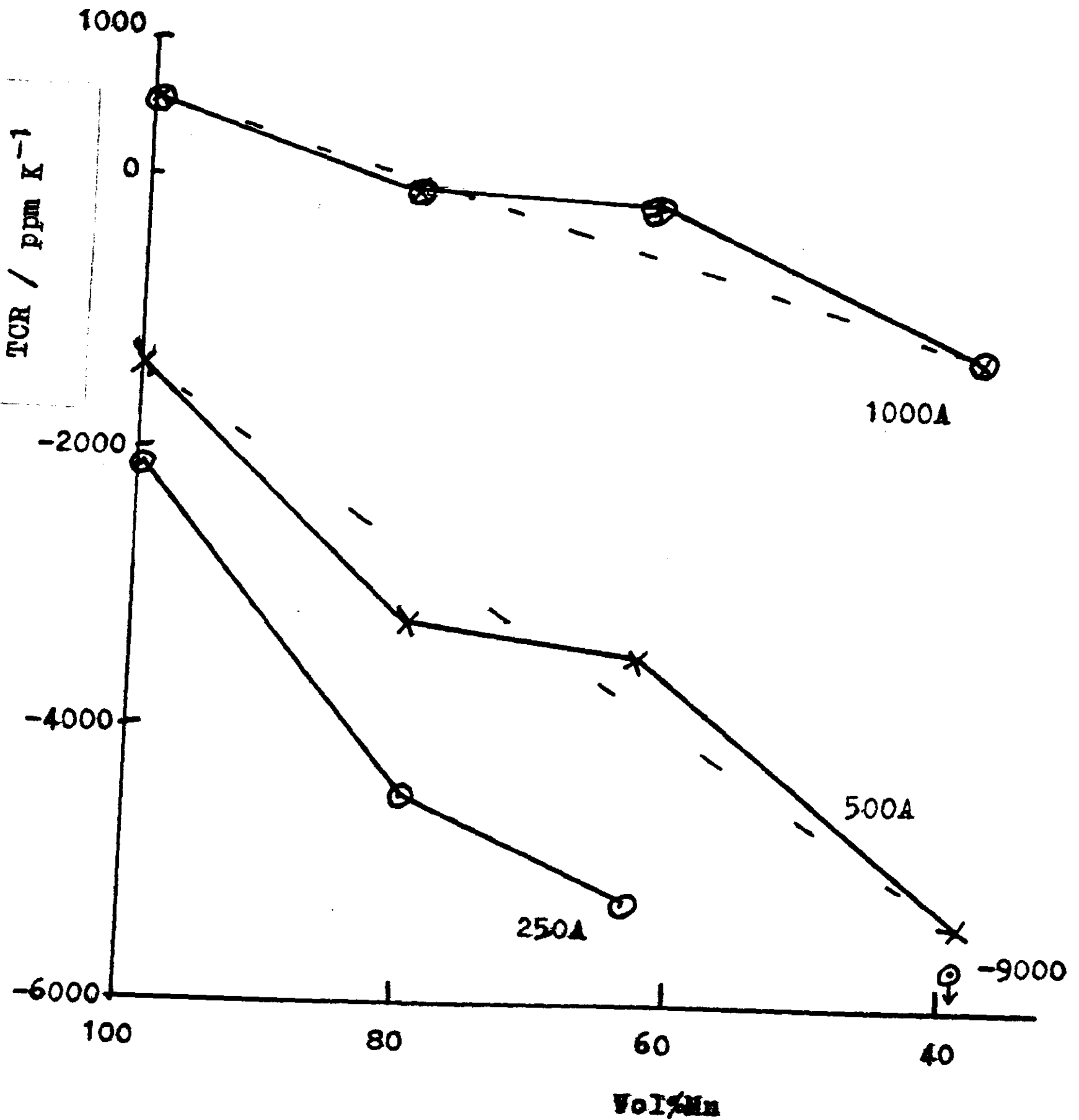

Fig.6.32 TCR Vs Mn/MgF_2 Cermet Composition measured at 295K for films deposited at 295K (unannealed)

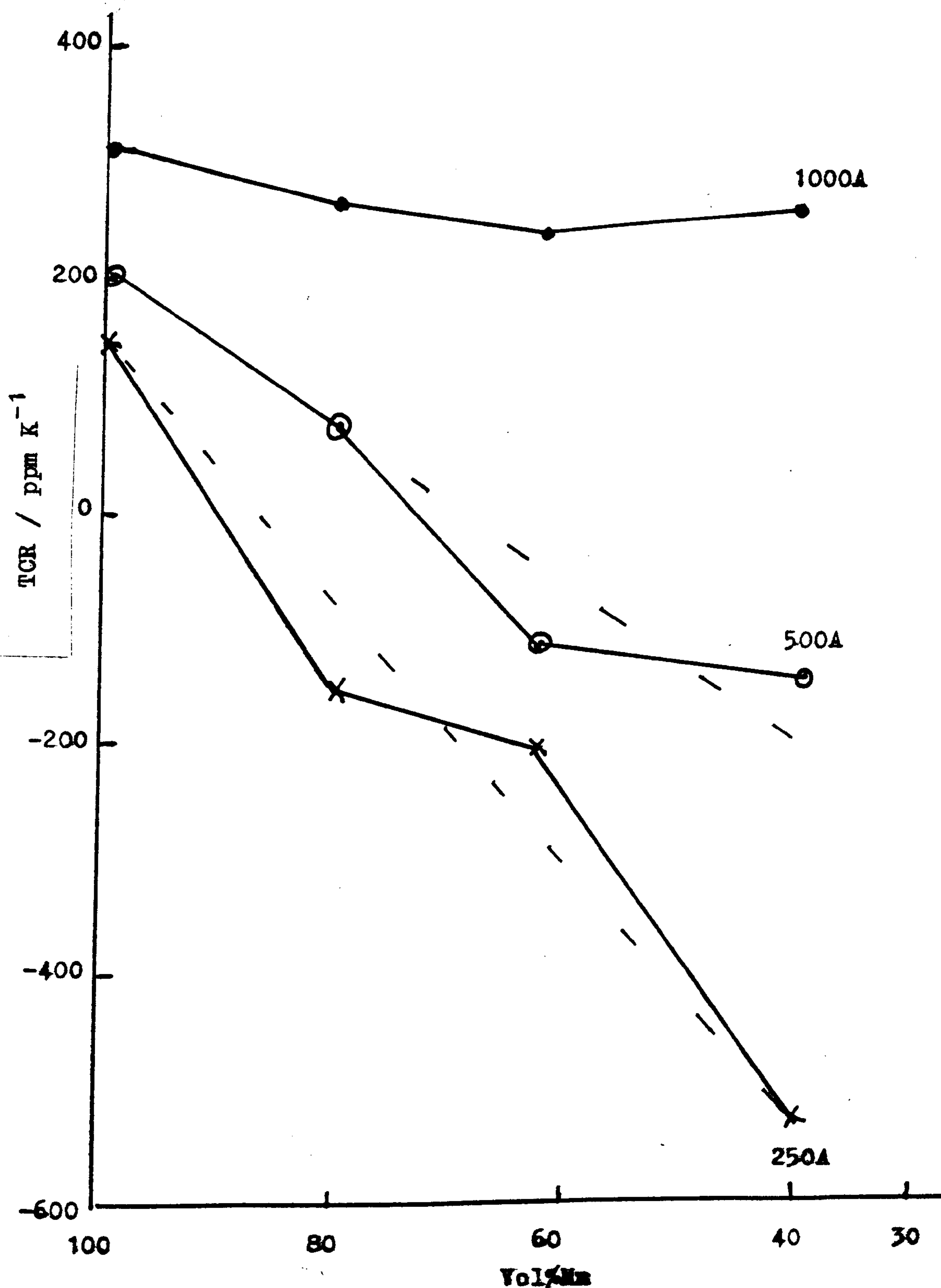

Fig. 6.33 TCR Vs Mn/MgF_2 Cermet Composition for Films deposited at 295K and annealed at 620K for 1hr.

For a given composition the TCR increases in a negative direction as film thickness decreases. It can be seen that only 1000A thick pure Mn and 60 to 90 Vol % Mn films have a TCR lying within the commercially acceptable range [57] of TCR's, viz: - 250 to + 250 ppmK^{-1}

Figure 6.33 shows the corresponding graphs for films deposited at 295K and then annealed at 620K for one hour. Figure 6.33 is similar to Figure 6.32 in that it also shows a negative increase in TCR with a fall in both film thickness and Vol % Mn. These properties imply that TCR increases with decrease in resistivity since an increase in the insulator content of a cermet film generally leads to an increase in its resistivity. Indeed a number of workers [57, 119, 121, 122] have found this to be the case.

Mn/MgF_2 cermets, 250A thick exhibit a small positive TCR for metal content > about 90 Vol % Mn. On increasing the thickness to 500A we find that the positive TCR region extends from 100 to about 72 Vol % Mn, whilst for thicknesses $\geq$ 1000A, the TCR is always positive, at least in the range 100 to 39 Vol % Mn.

It is interesting to note that most annealed films are either within the commercial range or very close to it except for the 250A films with Mn content less than 55 Vol %.

6.8. RELIABILITY OF Mn/MgF_2 CERMETS

The reliability of an electronic component is usually based on three criteria:

(i) performance;

(ii) stability; and

(iii) production cost.

Unfortunately, these three factors often interact with one another, thus making it difficult to assign a reliability rating to thin film resistors. Production cost is outside the scope of this thesis. Experimental results of the performance and stability of Mn and Mn/MgF_2 cermets are presented in the following sections.

6.8.1 PERFORMANCE

Figure 6.34 shows the current-voltage characteristics of Mn and Mn/MgF_2 cermets of 500A thickness. The films were deposited on Corning 7059 glass substrates held at 375K and they contained between 10 and 100 Vol % Mn. The electrical resistivity measurements were carried out in air at room temperature.

All the films investigated exhibit a linear current-voltage (I - V) characteristics up to the break-down point where the film burnt-out. The power handling ability, of the films is good, being $\sim 3kWm^{-2}$

A linear I - V relation was also obtained for measurements carried out in vacuo. The break-down voltage and the resistor handling power were of the same order of magnitude. However when the resistors were operated continuously at 75% of the break-down voltage (75% was chosen arbitrarily), it was found that their value increased very rapidly in air to within 2 to 3 times the initial value in 3 hours. Resistors in vacuo showed an increase in resistance of less than 25% in 48 hours.

SYMBOL	CERMET Vol% Mn	Maximum Power kWm^{-2}	Sheet Resistance Ω/□
×	100	30	22.7
⊙	63	30	52.1
▽	39	33	83.3
⊡	22	28	214.2
⊗	10	36	781.2

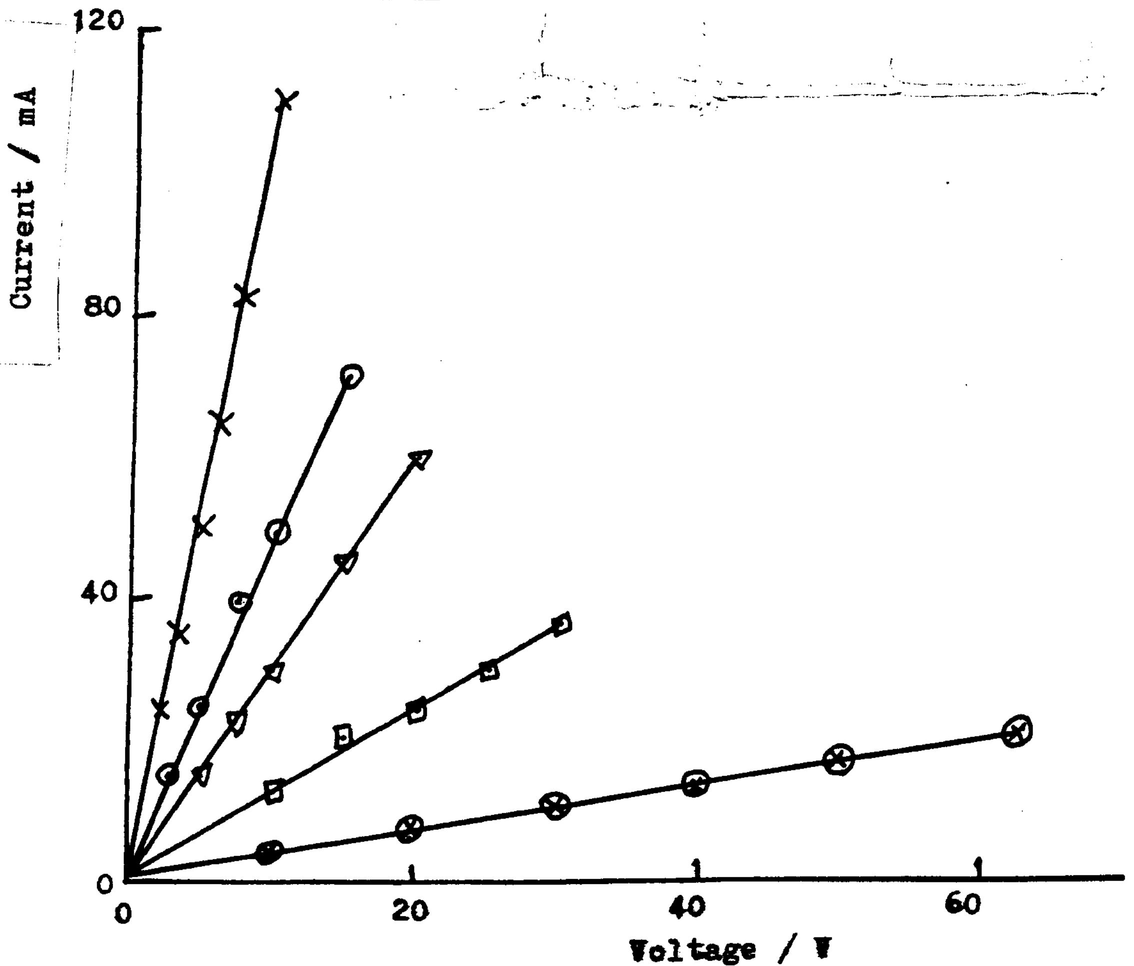

Fig.6.34 Current-Voltage characteristic of Mn/MgF_2 cermets measured in air. The Films were 250Å thick and were deposited at 375K

When the substrate temperature of the cermets in vacuo was raised to 375K, it was found that the break-down voltage decreased by ~20%. A possible explanation for the lower break-down voltage may be that the substrate acts as a heat sink and its effectiveness diminishes when its temperature was raised.

6.8.2 STABILITY

The stability of a resistor should be determined by the maximum drift in its value during its entire life when operated at certain specified conditions (such as operating temperature, power handling, relative humidity etc.) As this would involve tests lasting for many years and high costs, stability data are usually obtained from thermally accelerated aging processes. These processes usually involve subjecting a test resistor to a constant high temperature for about 1000 hours [93, 123]. In some cases a voltage is applied across the resistor during the aging process.

Unfortunately, there were no facilities for carrying out the thermally accelerated aging process. Instead some resistors were stored at room temperature and atmospheric pressure, and some at room temperature, and a residual air pressure ~ 1×10^{-1} torr. The film resistivities were measured at regular interval of time over a period of six months. The results are presented in Figure 6.35, for both annealed and unannealed cermet films of 250A containing 39 Vol % Mn.

Figure 6.35 shows that ρ varies almost linearly with logarithm of time for films stored at 1×10^{-1} torr; the change

100
80
60
40
20
0
$\frac{\Delta \rho}{\rho}$ %
10
10^2
10^3
10^4
Time/hrs
300
Annealed at 620K
Unannealed
Stored at room temperature and pressure
Annealed at 620K
Unannealed
stored at $1x10^{-1}$ torr

Fig.6.35 $\frac{\Delta \rho}{\rho}$ Vs Time for annealed and unannealed 39Vol% Mn Cermets stored at room Temperature/ $1x10^{-1}$ torr and at room Temperature/Pressure

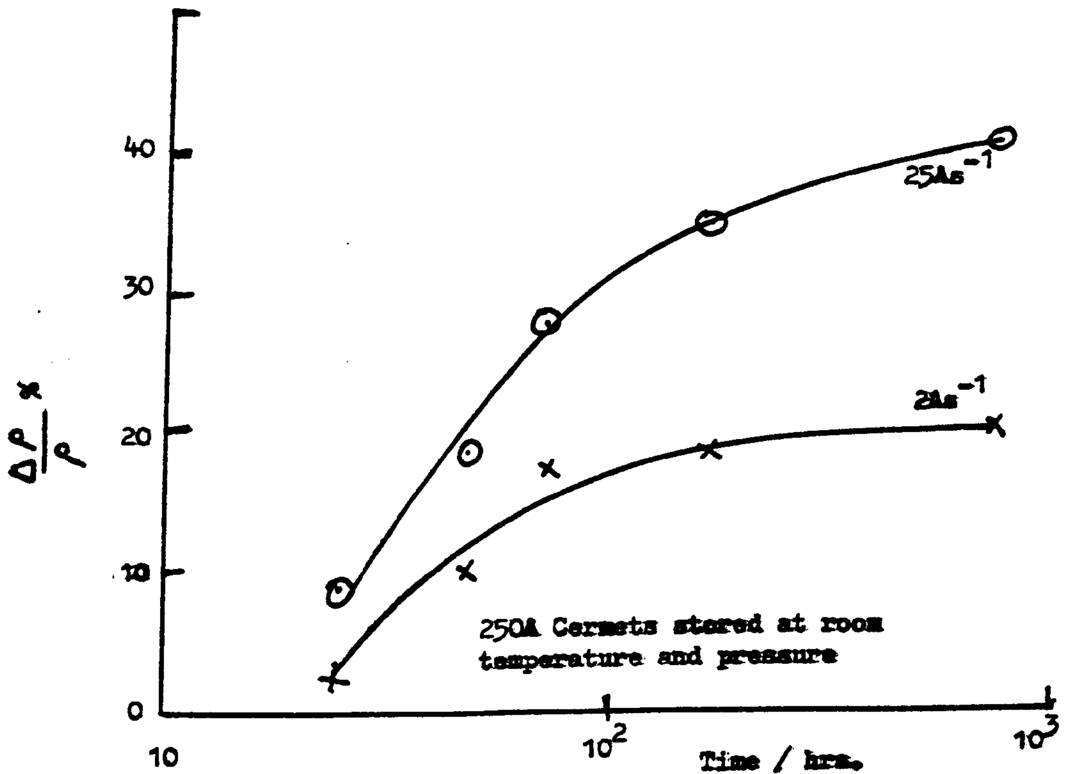

Fig.6.36 $\frac{\Delta \rho}{\rho}$ Vs Time for 39Vol% Mn Cermets with deposition rate as a parameter.

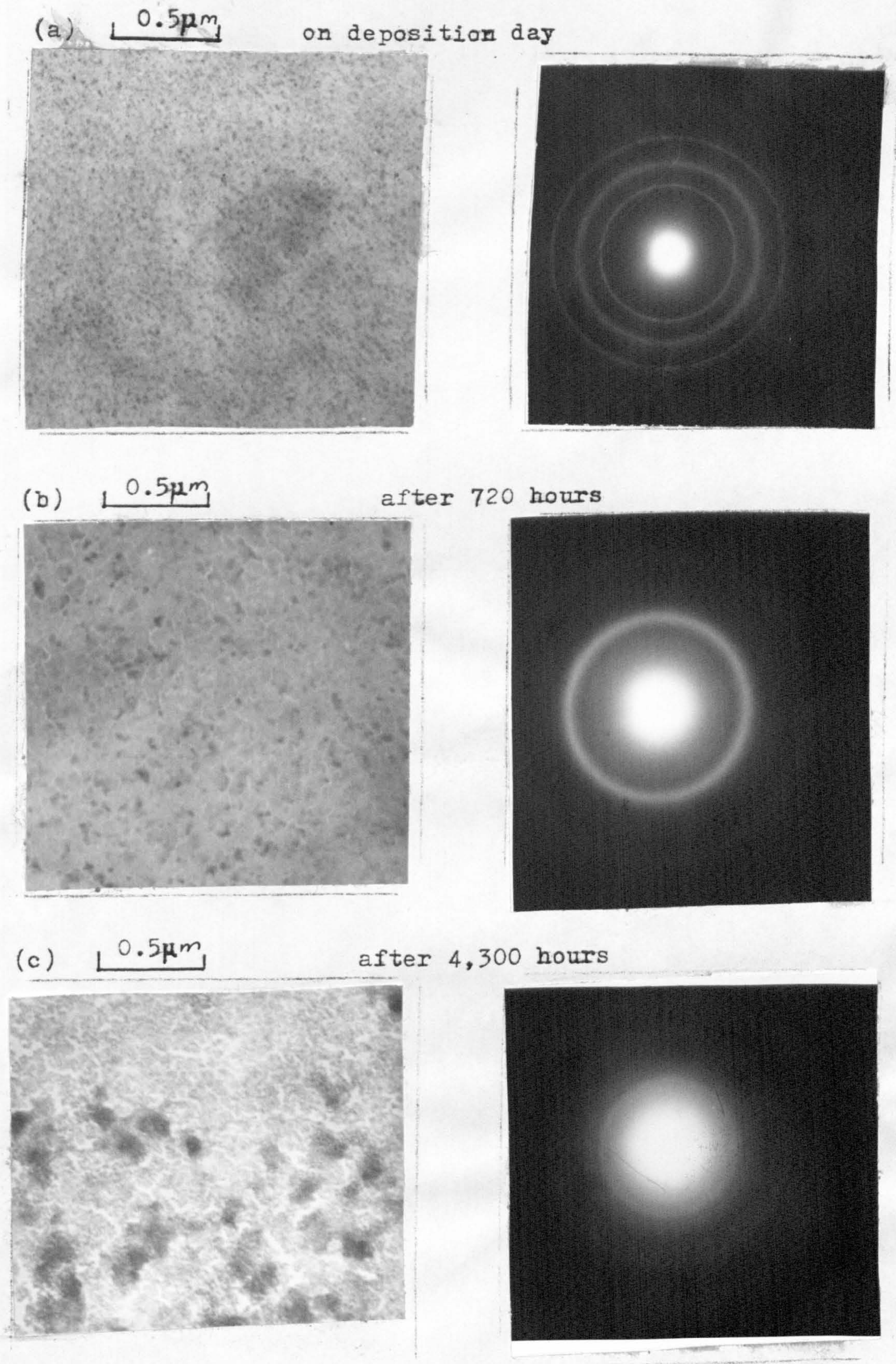

Fig.6.37 Electron Micrographs/Diffraction patterns for 39Vol.%Mn/MgF_2 film 250A thick stored at room temperature and pressure.

being from 0 to 20% and 0 to 14% respectively for the unannealed and annealed films in 4,300 hours. However when the films were stored in air over the same period of time, the corresponding rise in $\frac{\Delta \rho}{\rho}$ are 300% and 70% respectively.

Visual observations show that after about 1700 hours, a large number of randomly distributed transparent spots (~ 0.1 mm diameter) were visible in the films. These spots grew progressively larger in size, and new ones forming in the spaces between the larger spots until the whole film became transparent after about 6,500 hours and the film resistivity became infinite.

The electron micrographs of the unannealed, 39 Vol % Mn cermet films stored at room temperature and atmospheric pressure are shown in Figure 6.37. Figure 6.37(a) shows the structure of the film immediately after deposition, and Figures 6.37(b) and 6.37(c) the structure of the same film after 720 and 4,300 hours.

It can be seen (Fig. 6.37(b)) that after 720 hours in air, channels are present in the films. These channels are in fact regions of intensive oxidation (MnO_2 pyrolusite was identified). This tends to support the hypothesis [104, 105] that oxidation proceeds at particular nucleation sites. The channels grow larger and larger in size until they become inter-connected. This marks the beginning of the steep rise in $\frac{\Delta \rho}{\rho}$ graph of Figure 6.35. As the channels grow it appears that the unoxidized Mn in the film migrates thus leading to agglomeration and a higher concentration of Mn. The effect of this migration can be seen in Figure 6.37(c)

Figure 6.36 shows the variation of $\frac{\Delta\rho}{\rho}$ with time at two different deposition rates. The graphs show that $\frac{\Delta\rho}{\rho}$ of films deposited at 2Ås^{-1} are less affected by oxidation when compared with those deposited at 25Ås^{-1}. The percentage difference in resistivity between the two films being 5, 12 and 22% respectively after 24, 72, and 720 hours. A possible explanation of this difference may be due to the structural characteristics of the films. Films deposited at 25Ås^{-1} have a finer grain structure than a corresponding film deposited at 2Ås^{-1}. Hence Mn in the latter will have a smaller surface area exposed to oxidation and consequently a smaller rise in $\frac{\Delta\rho}{\rho}$ with time.

CHAPTER SEVEN

7. CONCLUSION

The resistivity of pure Mn and Mn/MgF_2 cermets of 250A to 1500A, and containing 100 to 22.5 Vol % Mn lies between 100 $\mu\Omega$ - cm and 10 mΩ - cm. This resistivity range is low when compared with other cermet systems in the same composition range - 100 $\mu\Omega$ - cm to 1 Ω - cm for Au/SiO and 700 $\mu\Omega$ - cm to 10 Ω - cm for Cr/SiO.

The resistivity of Mn and Mn/MgF_2 cermets increase non-linearly with decrease in film thickness and decrease in Mn content. For a given composition, there is little or no decrease in resistivity when the film thickness is greater than 800A (Fig 6.5)

Like film thickness and cermet composition, substrate temperature plays an important part in deciding the resistivity of the films. An increase in substrate temperature causes a relatively large fall in resistivity. The resistivity of 100% Mn films of 250A thickness, and deposited at 295K may fall to about one third its value when deposited at 430K. The cermet films also show a similar fall in resistivity with an increase in substrate temperature.

The effect of deposition rate on film resistivity is both thickness and composition dependent. The 100% Mn film of 250A thickness has a maximum fall in resistivity $\sim$ 14% as the deposition rate was increased from 2 to 25As $^{-1}$. On the contrary a maximum rise of 25 and 20% was observed in cermet films containing 63 and

39 Vol % Mn respectively. The rise or fall in resistivity with increase in deposition rate becomes less significant as film thickness increases being less than 5 and 13% respectively for the 100% Mn and the Mn/MgF_2 cermets of 1000A thickness. In all the films studied resistivity appears to be constant between 2 and $8As^{-1}$.

The resistivity of the film increases with increase in both argon and air pressures. Films deposited at air pressures have a higher resistivity than those deposited at corresponding argon pressures mainly due to oxidation. The resistivity of the film approaches a constant value for both air and argon pressures higher than $5x10^{-4}$ torr. The percentage increase in resistivity due to an increase in air pressure is higher for films of 250A than that of 500A thickness.

By increasing the annealing temperature from 295 to 620K, the resistivity of all Mn and Mn/MgF_2 cermets fall to between 30 and 50% of their value at 295K, with films of 250A having the largest fall and those of 1000A the least fall. The fall in resistivity is caused by a combination of mass diffusion leading to increased agglomeration and a reduction in the number of structural defects. The calculated values for the maximum lattice distortion energy $F_o(E)_{max}$ and the maximum decay energy E_{max} for Mn both decrease as the film thickness is increased. Further, $F_o(E)_{max}$ and E_{max} values for Mn are at least 50% lower than those for Au, C, and Cu films.

The activation energy of the unannealed films calculated from film geometry were of the same order of magnitude as those obtained

from resistivity measurements between 110 and 295K. Hence both calculations obey the Neugebauer and Webb theory, that is the electronic conduction mechanism in unannealed Mn and Mn/MgF_2 cermets is by thermal activated tunnelling.

Upon annealing at 620, 690 and 720K for one hour or more, all pure Mn films of 250 to 1000A were non-thermally activated. The cermet films of 250 and 500A show a spectrum of low activation energies in the temperature range 110 to 720K. The activation energies appear to be higher in the high temperature region than in the low temperature region.

The spectrum of activation energies of the annealed films may be due to a combination of two thermally-activated conduction processes - electron tunnelling between isolated Mn islands and electron percolation with the latter being dominant at low temperatures and the former making a significant contribution at high temperatures.

After deposition at 295K, all the films have a large negative TCR except for the 100% Mn film of 1000A thickness which was small and positive. On the contrary annealed Mn/MgF_2 cermets of 250 and 500A have a small TCR of about - 550 to + 300 $ppmK^{-1}$ which is almost entirely within the useful commercial range.

Aging experiments show that the drift in the electrical resistivity of Mn and Mn/MgF_2 may be reduced by:

(i) annealing the films;

(ii) condensing the films at low rates of 2 to 8 As^{-1}; and

(iii) by storing the films _in vacuo_.

7.1. PROPOSALS FOR FURTHER WORK

A further effort should be made to investigate:

(i) the electronic conduction processes in both annealed and unannealed Mn/MgF_2 cermets in the temperature range 4.2 to 110K;

(ii) the electro-magnetic properties of Mn and Mn/MgF_2 cermets;

(iii) the high and low field electrical characteristics of Mn - MgF_2 - Mn structures; and

(iv) investigate more fully the plateau regions in Mn and MgF_2 cermets annealed at 620K.

REFERENCES

1. CABRERA. N., Discussions Faraday Soc., 28 (1959) 16

2. ZWANZIG. R.W., J. Chem Phys., 32 (1960) 1173

3. EHLICH. G., in Structure and Properties of Thin Films, Eds Neugebauer CA, et al (1959) P. 423 Wiley

4. GOODMAN. F.O., Phys Chem Solids., 23 (1962) 1269 and 24 (1963) 1451

5. LENNARD - JONES. J.E., Proc. Roy. Soc., London A 163 (1937) 127

6. McCARROL. B. and EHRLICH G., J. Chem Phys, 38 (1963) 523

7. HOLMON. J.H. and TUNBULL. D., Prog. Metal Phys., 4 (1953) 333

8. SIGSBEE. R.A. and POUND. G.M., Advan. Coll. Interf. Sci., 1 (1967) 335

9. VOLMER. M. and WEBB. A., Z. Phys. Chem., 119 (1925) 277

10. BECKER. R. and DORING. W., Ann. Physik., 24 (1935) 719

11. HIRTH and POUND G.M. in Single Crystal Films Ed. Francombe and Sato (1964) Pargamon

12. CHOPRA. K.L., Thin Film Phenomena (1969) p.144, Mc. Graw Hill

13(a) WALTON. D., J. Chem. Phys., 37 (1962) 2182

13(b) WALTON. D., Phil. Mag. 7 (1962) 1671

14. RHODIN. T., and WALTON. D., Trans. 9th Am - Vac Soc., 3 (1962)3

15. LEWIS. B. and CAMPBELL D.S. J. Vac Sci. Technol 4 (1967)209

16. PASHLEY. D.W., STOWELL. M.J., JACOBS. M.H., and LAW. T.J. Phil Mag., 10 (1964) 127

17. KINGERY. W.D. and BERRY. M., J. Appl Phys. 26 (1955) 1205

18. NICHOLS. F.A., J. Appl. Phys., 37 (1966) 28

19. SEMENOFF. N.Z., Phys. Chem., B7 (1930) 741

20. PALATNIK. L.S., in Basic Problems in Thin Film Physics. Ed. Niedermayer and Mayer (1966) p. 92 Vandenhoeck and Ruprecht.

21. PALATNIK. L.S. FEDOROV. G.V., and BOGATOV., Soviet. Phys. Solid State (English translation) 7 (1966) 2141.

22. OSTWALD. W., Z. Physik Chem. 22 (1897) 289

23. BUCKEL. W., Proc. Confr Electromagnetic Properties Thin Metallic Layers (1961) p. 264 Lauvain.

24. DECKKAR. A.J., Solid State Physics (1969) McMilan

25. MEADEN. G.T., ELECTRICAL PROPERTIES OF METALS (1965) Heywood Books

26. MAISSEL. L.I. in Handbook of Thin Film Technology Eds. Maissel and Glang (1970) p. 13-2 Mc Graw Hill.

27. THOMSON. J.J., Proc. Camb. Phil Soc 11 (1901) 119

28. WILSON. A.H., The Theory of Metals (1965) Cambridge Univ. Press.

29. FUCHS.K., Proc. Camb. Phil. Soc. 34 (1938) 100

30. SONDHEIMER. E.H., Advan. Phys. 1 (1952) 1

31. LUCAS. M.S.P., Appl. Phys. Letters 4 (1964) 73

32. LUCAS. M.S.P., J. Appl. Phys., 36 (1965) 1632

33. CHOPRA. K.L. and RANDLETT. M.R., J. Appl. Phys., 38 (1967) 3144

34. DARMOIS. G., J. Phys. Rad., 17 (1956) 298

35. MOSTOVECH. N. and VODAR. B., Semiconducting Material (1951) p. 260 Butterworth.

36. MINN.S.S., J. Tech. CNRS., 51 (1960) 131

37. BLANK-LAPIERRE. A., and NIFFONTOFF. N., J. Phys. Rad., 17 (1956) 230

38. NEUGEBAUER. C.A. and WEBB. M.M., J. Appl. Phys., 33 (1962) 174

39. SWANSON. J.G., CAMPBELL. D.S. and ANDERSON. J.C., Thin Solid Films., 1 (1967/68) 325

40. WEITZENKAMP. L.A. and BASHARA. N.M., Trans. Met. Soc. AIME 236 (1966) 351

41. HARTMAN. T.E., J. Appl. Phys., 34 (1963) 943

42. HERMAN. D.S., and RHODIN. T.N., J. Appl. Phys., 37 (1966) 1594.

43. MILGRAM.A.A. and Lu. C., J. Appl. Phys., 37 (1966) 4773

44. ROSE. A., Phys. Rev., 97 (1955) 1538

45. van STEENSEL. K., Philip Res. Repts., 22 (1967) 246

46. SIMMONS. J.G., J. Appl. Phys., 34 (1963) 1793

47. GEPPERT. D.V., J. Appl. Phys., 34 (1963) 490

48. HILL. R.M., Proc. Roy. Soc., A 309 (1969) 377 and 397

49. HILL. R.M., Nature., 204 (1964) 35

50. NIFFONTOFF. N., Compt. Rend, 236 (1953) 1538, 2486 and 237 (1953) 24

51. COUTTS. T.J., Electrical Conduction in Thin Metal Films (1974) Elsvier Scientific Publications

52. BEYNON. J., Thin Solid Films, 37 (1976) L 71

53. PITT. K.E.G., Thin Solid Films, 1 (1967) 173

54. GLANG. R., HOLMWOOD. R.A. and HERD. S.R., J. Vac. Sci. Technol., 4 (1967) 163

55. BEYNON. J. and MILWAY. N.R.P., Thin Solid Films, 14 (1972) 387

56. MORRIS. J.E., Thin Solid Films, 11 (1972) 299

57. COUTTS. T.J., Thin Solid Films, 4 (1969) 429

58. DINGLE.R.B., Proc. Roy. Soc., A 201 (1950) 545

59. JEANS. J.H., Electricity and Magnetism (1923) Cambridge Univ. Press

60. CHRISTEN. T.E. and HEWITT. J.G., Proc. 20th Electronic Component Confr., (1970) p. 63

61. CHAMBERS. R.G., Proc. Roy. Soc., A 202 (1950) 378

62. MILLER. N.C. and SHIRN. G.A., Appl. Phys. Letters, 10 (1967) 86

63. ABELES. B., SHENG. P., COUTTS. M.D., and ARIE. Y., Advan. Phys., 24 (1975) 407

64. RAYL. M., WOJTOWICZ. P.J., ABRAHAMS. M.S., HARVEY. R.L., and RIOCCHI. C.J., Phys. Letters., A 36 (1971) 477

65. GITTLEMAN J.I., GOLDSTEIN. Y., and BOZOWSKI. S., Phys. Rev., 135 (1972) 3609

66. NEUGEBAUER C.A., Thin Solid Films, 6 (1970) 443

67. GASPERIC. J. and NAVINSEK. B., Thin Solid Films, 36 (1976) 353

68. KRUGER. F., British Patent 157, 909, (1919)

69. van ATTA. C.M., Vacuum Science and Engineering (1965) Mc Graw Hill

70. DUSHMAN. S., Scientific Foundation of Vacuum Technology (1962) Wiley

71. MARSTEN J., J. Proc. IRE., 50 (1962) 920

72. MacDONNALD. D.K., Thermoelectricity: an Introduction to the Principle (1962) Wiley

73. HAMPEL. C.A., Ed., Encyclopedia of Chemical Elements (1968) 390

74. POWERS. B.D., High Vacuum Pumping Equipment (1966) Chapman and Hall

75. HOLLAND. L., Vacuum Depostion of Thin Films (1956) Chapman and Hall

76. OSTRANDER. W.J., and Lewis. C.W., Trans 8th Am. Vac. Soc. 2 (1961) 881

77. GLANG. L., in Handbook of Thin Film Technology. Eds., Maissel and Glang (1970) p.1 - 107. Mc Graw Hill

78. INSTRUCTION MANUAL, Film Thickness Monitor, Model 1 Edward High Vacuum Ltd.

79. HALL. P.M., Appl. Phys. Letters, 12 (1968) 212

80. BROWN. R. in Handbook of Thin Film Technology. Eds. Maissel and Glang (1970) p. 6 - 30 Mc Graw Hill

81. BECKERMAN. M. and THUN. R.E., Trans. 8th Am Vac. Soc., 2 (1961) 905

82. BEYNON. J. and OLUMEKOR. L., to be published, Thin Solid Films.

83. MILGRAM. A.A. and Lu. C., J. Appl. Phys., 39 (1968) 4219

84. GUTHRIE. A. Vacuum Technology (1963) Wiley

85. STRATTON. R., J. Phys. Chem. Solids., 23 (1962) 1177

86. DEBYE. P., SHERRER. P., Z. Phys. 17 (1916) 277

87. HULL. A.W., Phys. Rev., 9 (1917) 84 and 564

88. WHITAKER. A., J. Sci. Instrument, 44 (1967) 1041

89. NEUGEBAUER. C.A., Physics of Thin Films, 2 (1964) 1

90. MADER. S., in Handbook of Thin Film Technology. Eds., Maissel and Glang (1970) p. 9 - 1 Mc Graw Hill

91. BEYNON. J. and OLUMEKOR. L., Thin Solid Films, 24 (1974) 530

92. BEYNON. J. and OLUMEKOR. L., Thin Solid Films, 41 (1977) 29

93. MAISSEL. L., in Handbook of Thin Film Technology. Eds. Maissel and Glang (1970) p. 18 - 3 Mc Graw Hill

94. THUN. R., Physics of Thin Films, 1 (1963) 187

95. SENNETT. R.S. and SCOTT G.D., J. Opt. Soc. Am. 40 (1950) 203

96. BASSETT. G.A., MENTHER. J.W. and PASHLEY. D.W., in Structural Properties of Thin Films. Eds., Neugebauer. C.A. et al (1959) p. 11 Wiley.

97. FRIDRICH. J. and KOHOUT. J., Thin Solid Films, 7 (1971) R 49

98. ADAMOV. M., PEROVIC. B., and NENADOVIC T., Thin Solid Films, 24 (1974) 89

99. HEAVENS. O.S., Thin Film Physics (1970) p. 128 Methuen.

100. CAMPBELL. D.S. in Basic Problems in Thin Film Physics. Eds. Niedermayer and Mayer (1966) p.113 Vandenhoeck and Ruprecht.

101. LEARN. A.J., and SPRIGGS. R.S., J. Appl. Phys., 34 (1963) 3012

102. NEUGEBAUER. C.A., in Handbook of Thin Film Technology. Eds. Maissel and Glang. (1970) p. 8 - 3 Mc Graw Hill

103. CHOPRA. K.L., and RANDLETT. M.R., J. Appl. Phys., 39 (1968) 1874

104. RHODIN T.N., Structure and Properties of Thin Films. (1959) p. 87 Wiley

105. GULBRANSEN. E.A. and COPAN, Disc. Faraday Soc., 28 (1959) 229

106. VAND. V., Proc. Phys. Soc., 55 (1943) 222

107. SHAH. V.V. and NAIK. Y.G., Indian J. Pure and Appl. Phys., 3 (1965) 20

108. DAMODARA-DAS. V. and JAGDEESH, Thin Solid Films, 24 (1974) 203

109. TOYODA. H., and NAGASHIMA M. J. Phys. Soc. Japan, 14 (1959) 274

110. WILKINSON. P.G. and BIRKS. L.S., J. Appl. Phys., 20 (1949) 1168

111. HOFFMAN. R.W., ANDERS. F.J., and CRITTENDEN C.C., J. Appl. Phys., 24 (1953) 231

112. McMASTER A.D., and FUSCHILLO. N., J. Non - Cryst. Solids, 2 (1970) 307

113. MADER. S., NOWICK. A.S., and WIDMER. H., ACTA. MET., 15 (1967) 203

114. MADER. S., J. Vac. Sci. Technol., 2 (1965) 35

115. FEINSTEN L.G. and HUTTEMANN R.D., Thin Solid Films, 20 (1974) 103

116. SASHITAL. S.R. and PAKSWER S. J. Vac. Sci. Technol., 9 (1972) 78

117. TICK. P.A. and FEHLNER F.P., J. Appl. Phys., 43 (1972) 362

118. POLLAK. M. and GEBALLE. T.H., Phys. Rev. 122 (1961) 1742

119. LOOD. D.E., J. Appl. Phys., 38 (1967) 5087

120. SHENG. P., and ABELES. B., Phys. Rev. Letters, 28 (1972) 34

121. WITTS. G.R., Thin Solid Films, 13 (1972) 109

122. HIEBER. K. and DITTMANN. R., Thin Solid Films, 36 (1976) 357

123. BEENSH-MARCHWICKA. G. et al, Thin Solid Films, 36 (1976) 361.